THESE / UNIVERSITE DE BREST
sous le sceau de l'Université européenne de Bretagne
pour obtenir le titre de
DOCTEUR DE l'UNIVERSITE DE BREST
Mention : Biologie Marine
Ecole Doctorale des Sciences de la Mer

Présentée par
Aurélie Jolivet
Préparée à l'Unité Mixte de recherche (n°6539)
Institut Universitaire Européen de la Mer
Laboratoire des Sciences de l'Environnement Marin

« Compréhension des mécanismes de Biominéralisation : quantification spatialisée des fractions minérale et organique et influence de facteurs environnementaux »

Thèse soutenue le 19 février 2009
devant le jury composé de :

Jean Laroche
Professeur, IUEM, Brest / *président*

Béatriz Morales-Nin
Professeur Directeur IMEDEA, Iles Baléares / *rapporteur*

Mireille Harmelin
Directeur de recherche CNRS, Marseille / *rapporteur*

Bruno Ernande
Chercheur, Ifremer, Port-en-Bessin / *examinateur*

Jean-François Bardeau
Chargé de recherche, CNRS, Le Mans / *membre invité*

Hélène de Pontual
Chercheur, Ifremer, Brest / *Co-directeur de thèse*

Ronan Fablet
Maître de conférence, Institut Télécom/Telecom Bretagne, Brest / *Co-directeur de thèse*

Yves-Marie Paulet
Professeur, IUEM, Brest / *Directeur de thèse*

UBO université de bretagne occidentale

Ifremer

REMERCIEMENTS

A tous ceux qui se reconnaîtront

Je remercie toutes les personnes qui ont de près ou de loin contribué à l'aboutissement de ce travail. En particulier, je remercie mes encadrants qui m'ont accompagné au cours de ces trois années : Yves-Marie Paulet, Hélène de Pontual, Ronan Fablet à qui j'associe Jean François Bardeau pour leur soutien, leur confiance et leurs nombreux conseils. J'ai vraiment apprécié de travailler avec vous et j'espère vous retrouver dans de nouveaux projets. Je remercie aussi les membres du jury qui ont accepté de juger mon travail malgré l'appel des vacances de Noël.

Ce travail a été réalisé au sein du LASAA où l'accueil et le soutien ont rendu ce travail si agréable. Merci à Maylis, Anne, les deux Eric, Jean Marie, Louis et tout particulièrement à François et André, mon petit personnel, qui ont été de toutes les expérimentations et des pauses café rythmées au son des comptines pour enfants et des musiques d'ascenseur.

Je ne pourrai continuer ses remerciements sans évoquer Stéphane et Magali qui ont toujours été là.

Ce travail n'aurait pu se faire sans toutes les personnes rencontrées au cours des expérimentations : les campagnes sur le Gwen Drez, les élevages au mole ou en salle larvaire, les manips Raman. Je remercie ces personnes des labos pêche, ARN et du LPEC au MANS pour leur accueil, leur soutien et surtout leur sympathie.

Enfin je ne pourrai conclure sans remercier mes amis, Esther, Maria, Flo, Céline, Anatole, Hilaire, Youen, Alex, Erika, Tristan, Julie, … et ma famille pour leur présence.

Pour conclure, un petit merci à tous nos merlus, qui bien qu'on ne sache pas encore bien s'occuper d'eux, m'ont permis d'obtenir de jolis résultats.

Tables des matières

Introduction générale

Introduction générale

Contexte général et problématique de la thèse

Les otolithes sont des concrétions calcaires présentes dans l'oreille interne des poissons osteichtyens correspondant aux organes de l'ouïe et de l'équilibre. Leur croissance accrétionnelle résulte d'un contrôle strict de l'organisme sous l'influence des paramètres du milieu dans lequel il vit (Pannella 1971; Panfili *et al.* 2002a). Ainsi des paramètres exogènes (salinité, température) et endogènes (métamorphose, état reproducteur, âge) influent sur le processus de biominéralisation de l'otolithe. Ce processus d'accrétion couche par couche produit généralement des marques successives sur l'otolithe dont la rythmicité peut aller de l'ultradien au circannuel. L'otolithe restant généralement stable dans le temps, l'analyse de ces couches offre un potentiel de reconstruction des conditions environnementales et/ou physiologiques au moment de leur dépôt. L'otolithe apparaît alors comme une véritable archive biologique utilisée tant à l'échelle individuelle pour la reconstruction des traits de vie du poisson (croissance, migration, âge) qu'à l'échelle populationnelle (structure en âge, dynamique spatio-temporelle) (Campana and Thorrold 2001).

L'analyse de l'otolithe en tant que source d'informations est largement reconnue et utilisée aussi bien pour la gestion des stocks avec près d'un million d'otolithes interprétés chaque année pour la formation des clés taille-âge (Campana and Thorrold 2001), que pour la traduction des traits de vie individuels par l'identification de lien entre la signature chimique lue sur l'otolithe et les paramètres environnementaux et/ou métaboliques. Ainsi, le rapport isotopique du carbone $\delta^{13}C$ de l'otolithe a pu être utilisé comme proxy du métabolisme (Wurster and Patterson 2003), le rapport isotopique de l'oxygène $\delta^{18}O$ comme proxy de la température (Høie *et al.* 2004) ou encore les éléments et/ou leurs rapports, Strontium/Calcium, Manganèse/Calcium, Magnésium/Calcium et Baryum/Calcium, comme

marqueurs de l'origine natale des poissons par l'identification des stocks et la caractérisation des nurseries (Campana 1999; Thresher 1999; de Pontual *et al.* 2000). Cependant dans de nombreux cas, l'information structurelle ou chimique lue sur l'otolithe reste indéchiffrable. C'est le cas des otolithes de merlu pour lesquels les critères d'estimation d'âge à partir de l'interprétation des otolithes, bien qu'agréés au niveau international (Piñeiro and Sainza 2003), n'ont pas été validés et pour lesquels une surestimation importante de l'âge a été démontrée (de Pontual *et al.* 2006). De même, l'utilisation du rapport Sr/Ca pour la reconstruction de la température a conduit dans de nombreuses études à des résultats contradictoires (Gallahar and Kingsford 1996; Clarke and Friedland 2004; Rooker *et al.* 2004). Cette difficulté à comprendre les signaux de l'otolithe est essentiellement due à une méconnaissance des processus de formation de l'otolithe. Par conséquent, l'intégration des signatures environnementales et/ou métaboliques dans l'otolithe est très peu connue. Ces cas mettent en évidence la nécessité d'une meilleure compréhension de l'archive « otolithe » et la calibration de son utilisation.

En tant que biominéral, l'otolithe est constitué de carbonate de calcium principalement sous forme d'aragonite représentant plus de 90% de la masse et d'une matrice organique (Murayama *et al.* 2000; Murayama *et al.* 2002; Borelli *et al.* 2003b). Son processus de formation est peu connu et les études se sont, jusqu'à présent, principalement intéressées à la chimie de l'endolymphe, le milieu dans lequel se forme l'otolithe, et la caractérisation de la matière organique (Payan *et al.* 2004a). La croissance de l'otolithe est un processus d'incrémentation s'effectuant couche par couche induisant une alternance de zones opaques et translucides. Ce degré d'opacité peut être le résultat de variations quantitatives des fractions minérale et organique mais aussi de leurs natures et de leurs propriétés physiques (taille des cristaux, orientation…) (Morales-Nin 1987). Les informations relatives à la chimie de l'otolithe portent essentiellement sur les compositions élémentaires et les isotopes par des

techniques d'analyses ponctuelles (Spectrométrie à longueur d'onde dispersive WDS, Spectrométrie de masse à torche à plasma inductif par ablation laser LA-ICPMS…..) ou globale (Spectrométrie de masse à torche à plasma inductif ICPMS, Spectrométrie de masse des rapports isotopiques IRMS…). La matière organique de l'otolithe, du fait de sa faible quantité (quelques pourcents de la masse de l'otolithe) a été essentiellement étudiée à l'aide d'analyses globales sous forme de poudre ne permettant pas une analyse spatiale de ses caractéristiques. L'analyse conjointe des fractions organique et minérale au niveau des structures des otolithes n'est à notre connaissance pas documentée et l'influence de leurs propriétés qualitatives et quantitatives sur l'opacité observée méconnue.

Cette thèse s'inscrit donc dans cette problématique d'amélioration de la compréhension de la formation de l'otolithe et de sa calibration en fonction des paramètres environnementaux et physiologiques en vue d'optimiser son utilisation. Elle s'articule autour de deux axes principaux :

1) la mise en relation d'informations structurelles (opacité) avec des propriétés physico-chimiques (fractions minérale et organique) au niveau des structures de l'otolithe;

2) la relation avec les facteurs environnementaux et physiologiques influençant la formation et le dépôt de ces deux fractions minérale et organique sur l'otolithe.

Concernant l'extraction de l'information structurelle et chimique de l'otolithe, l'utilisation de techniques d'analyses « fines » s'avère indispensable pour accéder à une caractérisation quantitative de la matière organique à la fois au niveau des macrostructures et des microstructures dont les largeurs caractéristiques respectives sont de l'ordre de quelques centaines de microns et quelques microns (Wright *et al.* 2002b). La micro-spectrométrie Raman répond à ces critères. Cette technique, non destructive, consiste à analyser la réponse de la matière, sous forme de spectres vibrationnels, à un rayonnement lumineux

monochromatique. Elle permet à une résolution de l'ordre du micron de discriminer de manière quantitative des signatures de composés organiques et minéraux. Cette technique a auparavant permis de distinguer les différents morphes de carbonates de calcium présents sur l'otolithe (aragonite, vatérite et calcite) (Gauldie *et al.* 1997; Tomás and Geffen 2003; Melancon *et al.* 2005; Tzeng *et al.* 2007) mais sans exploitation de la signature de la fraction organique présente sur ces spectres et analysée sur d'autres biominéraux : coraux, bivalves (Kaczorowska *et al.* 2003; Hedegaard *et al.* 2006; Perrin and Smith 2007).

L'étude de la relation entre les signatures extraites des otolithes et les facteurs environnementaux et/ ou métaboliques est difficile sur des échantillons issus du milieu naturel du fait de l'interaction des facteurs. Une approche en milieu contrôlé permet de manipuler les facteurs d'intérêts tout en limitant ces interactions. De plus, l'expérimentation permet l'obtention d'une calibration temporelle des événements par le marquage des otolithes à des pas de temps déterminés, à l'aide d'injection d'oxytétracycline permettant le dépôt d'une marque fluorescente sur l'otolithe. Le modèle biologique choisi pour cette étude est le merlu européen (*Merluccius merluccius*), d'une part pour ses otolithes de grande taille présentant des macro- et microstructures bien caractérisées et d'autre part pour améliorer les connaissances sur la biologie de l'espèce et en corollaire la gestion de la ressource. Depuis les années 60, les débarquements de merlu n'ont cessé de décroître passant de 120 000 tonnes dans les années 60 à 40 000 tonnes dans les années 2000, niveau auquel les captures semblent actuellement se stabiliser (ICES 2007). En 2002, le CIEM diagnostique un état inquiétant du stock Nord, conséquence probable d'une surpêche de cette espèce. Un plan visant à reconstituer le stock de merlu a donc été promulgué par la Commission Européenne en 2004. L'obtention des clés taille-âge à partir des otolithes est essentielle pour la gestion des stocks et reste problématique pour le merlu. En effet, l'otolithe de merlu est reconnu pour être difficile à interpréter (Morales-Nin *et al.* 1998) et bien que les critères d'estimation de l'âge à partir de

l'interprétation de ces otolithes aient été agréés au niveau international, ils ne sont pas validés (Piñeiro and Sainza 2003; de Pontual *et al.* 2006). De récentes campagnes de marquage-recapture menées par l'Ifremer (de Pontual *et al.* 2003a) ont remis en cause ces schémas de lecture et mis en évidence une sous-estimation de la croissance du merlu de l'ordre d'un facteur deux, liée à une surestimation de l'âge (de Pontual *et al.* 2006). Cette surestimation de l'âge est due à la formation de structures secondaires, comparables à des marques saisonnières. Ainsi la problématique de caractérisation des structures en fonction de leur composition et des conditions environnementales et métaboliques paraît de premier ordre pour les otolithes de merlu afin d'améliorer leur interprétation.

Etat des connaissances sur le processus de Biominéralisation

Cette synthèse des connaissances du processus de biominéralisation a été construite et actualisée à partir de la publication d'Allemand *et al.* (2007). L'otolithe est une structure métaboliquement inerte incluse dans l'otosac et baignant dans un fluide, l'endolymphe (Figure 1). Il est constitué de carbonate de calcium $CaCO_3$ sous forme d'aragonite représentant plus de 90% du poids de l'otolithe et d'une matrice organique. La connaissance du processus de biominéralisation de l'otolithe, et en particulier le rôle de la matrice organique, reste parcellaire (Payan *et al.* 2004a). Il est toutefois admis que cette matière organique joue un rôle prépondérant dans le contrôle de la formation de l'otolithe (Murayama *et al.* 2002; Söllner *et al.* 2003) et doit être sous influence des conditions environnementales prévalant au moment du dépôt. Jusqu'à présent, les recherches dans le domaine de la biominéralisation ont principalement porté sur la chimie de l'endolymphe et la caractérisation de la composition de la matrice organique de l'otolithe.

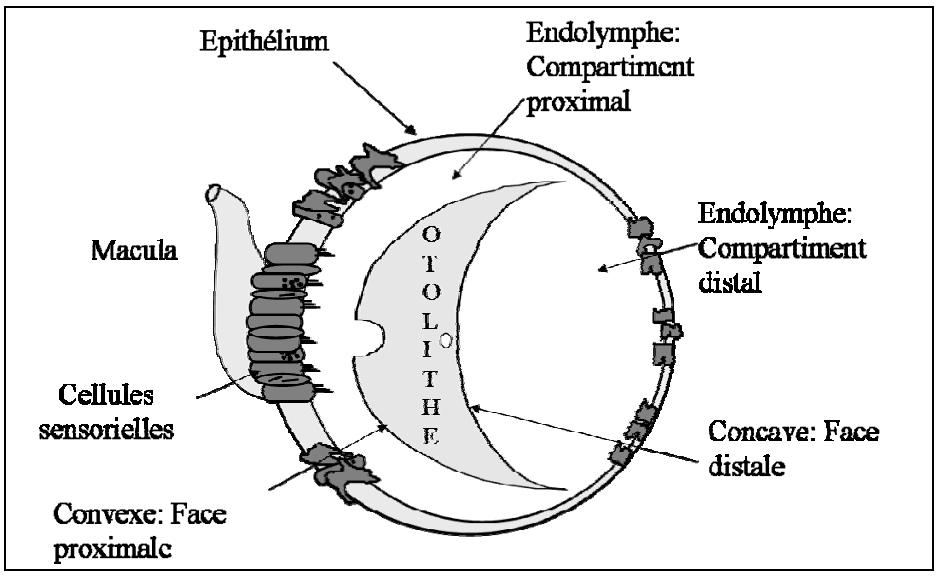

Figure 1 : Représentation schématique du complexe otolithe-otosac tirée d'Allemand *et al.* (2007).

Le processus de biominéralisation sera présenté autour de cinq points : 1) le principe de la calcification, 2) l'importance de la matière organique, 3) l'hétérogénéité spatiale de la composition de l'endolymphe, 4) les variations nycthémérales observées dans l'endolymphe et 5) l'impact des facteurs environnementaux.

Le principe de la calcification

La précipitation du carbonate de calcium dépend d'un point de vue ionique de 3 ions majeurs : le calcium Ca^{2+}, le couple bicarbonate / carbonate HCO_3^- / CO_3^{2-} et les ions hydrogène H^+. Elle est gouvernée par la réaction :

$$Ca^{2+} + HCO_3^- \rightarrow CaCO_3 + H^+$$

caractérisée par un coefficient de saturation $Sa^2 = [Ca^{2+}]\ [HCO_3^-] / K_S$ avec K_S le produit de solubilité. Cette précipitation ne peut avoir lieu que si le coefficient de saturation est supérieur à 1. Les ions H^+ produits lors de la formation du carbonate de calcium influent sur le pH de l'endolymphe et doivent être éliminés afin d'éviter que la calcification ne s'arrête par acidose. Le coefficient de saturation et le pH apparaissent donc comme des facteurs de régulation du processus de calcification. Selon les études et la méthodologie utilisée : séparation des fractions distale et proximale de l'endolymphe ou mesure globale, le coefficient de saturation serait toujours supérieur à 1 dans l'endolymphe (Takagi *et al.* 2005) ou suivrait un rythme nycthéméral et ne serait atteint qu'en fin de nuit dans la zone proximale de l'endolymphe (Payan *et al.* 2004a). Des expériences menées in vitro ont montré que les paramètres de cette précipitation de carbonate de calcium dépendaient de la température (Romanek and Gauldie 1996) et qu'elle pouvait être régulée par un composé de l'endolymphe, le FRC ou Factor Retarding Crystallization (Wright 1991a; Borelli *et al.* 2001; Guibbolini *et al.* 2006).

Rôle de la matrice organique

Le carbonate de calcium synthétisé est associé à un faible pourcentage de matière organique principalement constituée de lipides, glycoprotéines et protéines. Cette matière organique est essentielle et interviendrait principalement dans la nucléation, l'orientation, le contrôle, la croissance et la forme de l'otolithe (Pisam *et al.* 2002; Söllner *et al.* 2003; Falini *et al.* 2005). Elle subirait une maturation pour former une trame en 3D où s'intercaleraient les cristaux de carbonate de calcium. Elle est régulièrement décrite comme constituée de deux fractions soluble et insoluble dont la caractérisation dépend des protocoles d'extraction (acide éthylène-diamine-tétraacétique EDTA, acide acétique) (Borelli *et al.* 2001). Ces deux fractions ont cependant été démontrées comme différemment secrétées par les cellules de l'endolymphe vers le site de minéralisation (Asano and Mugiya 1993; Sasagawa and Mugiya 1996; Takagi and Takahashi 1999; Murayama and Takagi 2004; Payan *et al.* 2004a) La fraction insoluble à l'EDTA semble former les bases structurelles pour la croissance du minéral limitant la vitesse de calcification par le nombre de sites de nucléation produits. Cette matrice est aussi un facteur significatif contrôlant la forme de l'otolithe (Murayama *et al.* 2005; Tohse *et al.* 2008). La fraction soluble à l'EDTA associée à des polysaccharides est directement liée à la fraction minérale et dirigerait la croissance du minéral en régulant le taux de dépôt du minéral. Les capacités de régulation des protéines solubles sont dues à leurs propriétés de fixation du calcium (Asano and Mugiya 1993; Borelli *et al.* 2001; Murayama *et al.* 2005). Ces propriétés sont applicables aux fractions solubles à l'acide acétique (Wright 1991a; Sasagawa and Mugiya 1996; Borelli *et al.* 2003b)

Hétérogénéité spatiale de l'endolymphe

L'hétérogénéité de l'endolymphe a été mise en évidence par Payan *et al.* (1999). Cette disparité résulte particulièrement de la structure de l'épithélium et des propriétés de l'endolymphe (Mayer-Gostan *et al.* 1997; Pisam *et al.* 1998). L'endolymphe est caractérisée par une forte concentration en ion potassium K^+ permettant une dépolarisation des cellules sensorielles quand elles sont activées par le déplacement des otolithes ; et par un pH plus alcalin que le sang. L'épithélium transporte à la fois passivement et activement les ions (Na^+, K^+, Cl^-, Ca^{2+}, HCO_3^-) (Payan *et al.* 1997; Tohse and Mugiya 2001) dans l'endolymphe et sécrète les composés organiques. Ces composés ioniques et organiques apparaissent compartimentés avec des concentrations différentes suivant les zones proximale et distale de l'endolymphe (Figure 2). Ceci s'applique en particulier pour les paramètres intervenant dans la calcification : $Ca_{tot,}$ CO_{2tot}, pH, protéines collagènes et non-collagènes, protéoglycans et le facteur de régulation de la cristallisation (FRC) (Borelli *et al.* 2001; Borelli *et al.* 2003a; Guibbolini *et al.* 2006). Ainsi le côté proximal apparaît comme le lieu principal de la biominéralisation contenant les plus fortes concentrations des ions de la calcification (Mugiya 1974) et des protéines intervenant dans ce processus (Payan *et al.* 1999; Takagi and Takahashi 1999). Cette disparité spatiale déterminerait les axes de croissance de l'otolithe expliquant sa croissance dissymétrique.

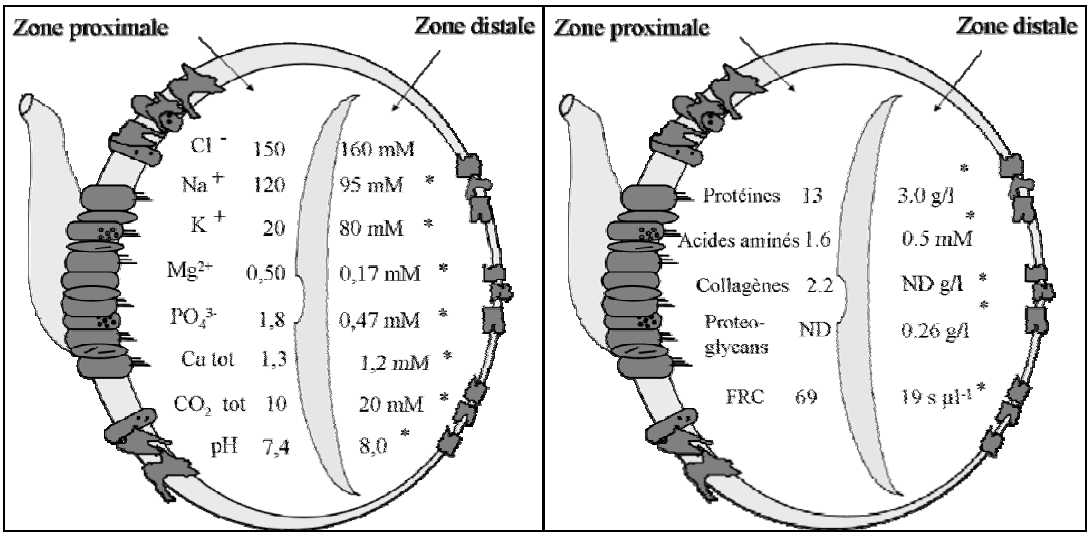

Figure 2 : Hétérogénéité spatiale des composés de l'endolymphe : à gauche : les composés ioniques, à droite : les composés organiques. Les * indiquent que les différences entre côtés proximal et distal sont significatives. Tiré de Allemand *et al.* 2007 (Payan *et al.* 1999; Borelli *et al.* 2001; Payan *et al.* 2004a; Guibbolini *et al.* 2006)

Variations nycthémérales

La composition de l'endolymphe est continuellement renouvelée et son analyse permet d'évaluer les besoins en constituants élémentaires pour le dépôt journalier de $CaCO_3$ et de matrice organique associée. La précipitation du carbonate de calcium nécessite jusqu'à sept fois les quantités de précurseurs présentes dans l'endolymphe ce qui nécessite un fort renouvellement estimé à hauteur de 17 fois par jour pour les ions HCO_3^- et à 12 fois par jour pour le Ca^{2+} (Payan *et al.* 2002). D'autre part les quantités en protéines collagènes et non-collagènes sont 1000 fois supérieures aux besoins journaliers de l'otolithe et ne constituent donc pas un élément limitant. Des variations nycthémérales des concentrations des principaux composés de la calcification ont aussi été démontrées dans le compartiment proximal de l'endolymphe (Figure 3). Ainsi les composés protéiques et collagènes montrent une

concentration maximale pendant le jour alors que les ions HCO_3^- présente des concentrations maximales pendant la nuit. La quantité en ion libre Ca^{2+} a été estimée à partir du Ca_{tot} et de la quantité en protéine et supposée maximale pendant la nuit (Edeyer *et al.* 2000; Borelli *et al.* 2001).

Dans l'endolymphe proximale, la saturation de l'endolymphe serait atteinte en fin de nuit permettant la précipitation de $CaCO_3$ sur la matrice organique formée le jour quand la concentration en précurseurs protéiques est maximale (Payan *et al.* 2004a). Pendant la nuit, une forte concentration en otolin-1, protéine surtout présente dans la fraction insoluble à l'EDTA de la matrice organique, impliquerait sa participation dans le contrôle de la précipitation du carbonate de calcium (Takagi *et al.* 2005). Néanmoins, les variations de la composition de l'endolymphe et les effets sur la composition de l'otolithe ne sont pas encore clairement établis. Les données disponibles concernent essentiellement le calcium et les ions mineurs (Kalish 1991; Payan *et al.* 1999; Tohse and Mugiya 2008).

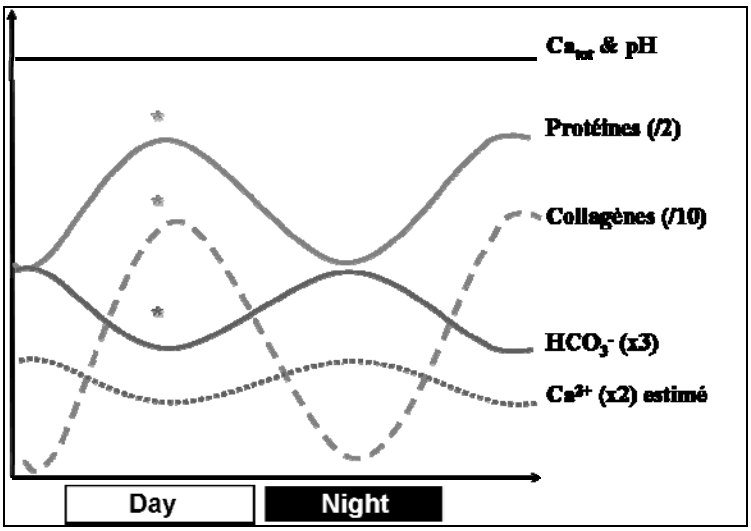

Figure 3 : Variations journalières des principaux constituants de l'endolymphe intervenant dans la calcification. Adapté de Borelli *et al.* (2001).

Impact des facteurs environnementaux sur les composés de l'endolymphe

L'incorporation d'un signal environnemental, relatif en particulier à la composition de l'eau, dans l'otolithe doit passer par deux barrières biologiques : le passage de l'environnement au plasma à travers les branchies et la paroi intestinale et celui du plasma à l'endolymphe à travers l'épithélium sacculaire. Certaines études se sont basées sur la caractérisation de composés dans l'endolymphe suivant des variations de salinité, de température (Edeyer 1999), de jeun ou de stress (Payan *et al.* 1997; Guibbolini *et al.* 2006) tout en considérant les effets sur la croissance de l'otolithe. Ainsi les composés intervenant dans la calcification ne varient pas de façon significative dans le cas d'une augmentation de température ou de baisse de salinité (par exposition à une eau chlorée) bien que la croissance de l'otolithe augmente. Par contre un stress induit la formation d'un check sur l'otolithe, (discontinuité structurale à l'échelle des microstructures), ainsi qu'une baisse de la concentration en CO_2 total dans l'endolymphe distal et une augmentation de la concentration en protéines (Payan *et al.* 2004b). A l'inverse une période de jeun diminue le taux de croissance observé sur l'otolithe et entraîne une baisse des concentrations en CO_2 total et du pH dans l'endolymphe distal (Payan *et al.* 2004b).

Des questions sans réponse

Cette synthèse permet de mettre en avant les nombreux points d'interrogation existant sur le processus de biominéralisation :

- les concentrations ioniques de l'endolymphe semblent influencer la calcification cependant cette relation de cause à effet entre ces deux variables restent à définir.
- Les composés de la matrice organique (protéines collagènes, non-collagènes, glycoprotéines, protéoglycans) doivent être caractérisés ainsi que leur rôle dans la formation de l'otolithe.
- Les effets des perturbations environnementales sur les concentrations ioniques et les composés organiques ne sont pas quantifiés.

Utilisation et caractérisation des structures de l'otolithe

Rythme d'accrétion

En raison de sa croissance accrétionnelle, l'otolithe présente des couches dont la rythmicité est variable allant d'accroissements annuels, les bandes saisonnières, à des fréquences ultradiennes. Les mécanismes associés de régulation et de contrôle par les paramètres environnementaux sont méconnus (Campana and Neilson 1985; Panfili *et al.* 2002a). L'alternance des zones opaques et translucides (Figure 4) est présumée résulter de variations des caractéristiques physico-chimiques : la largeur des accroissements primaires contenus, la taille et l'orientation des cristaux d'aragonite, les variations des quantités relatives de carbonate de calcium et de matière organique, la quantité d'éléments traces (Wright *et al.* 2002b).

Près d'un million d'otolithes sont lus chaque année pour l'interprétation des structures saisonnières ou annuelles. Ces structures mesurent jusqu'à quelques centaines de microns et permettent la construction de clé taille-âge pour l'estimation de la structure démographique d'une population et l'évaluation des stocks (Panfili *et al.* 2002a). Outre ces marques périodiques, des zones de croissance secondaires peuvent apparaître. Elles correspondent à des zones non saisonnières caractérisant par exemple des événements ontogéniques ou des stress environnementaux. La caractérisation de ces zones de croissance secondaires sont d'importance car considérées comme une source d'erreur importante lors de l'interprétation des otolithes. Le merlu en est un bon exemple.

Quelles sont marqueurs physico-chimiques permettant de distinguer les structures saisonnières des structures secondaires de croissance ?

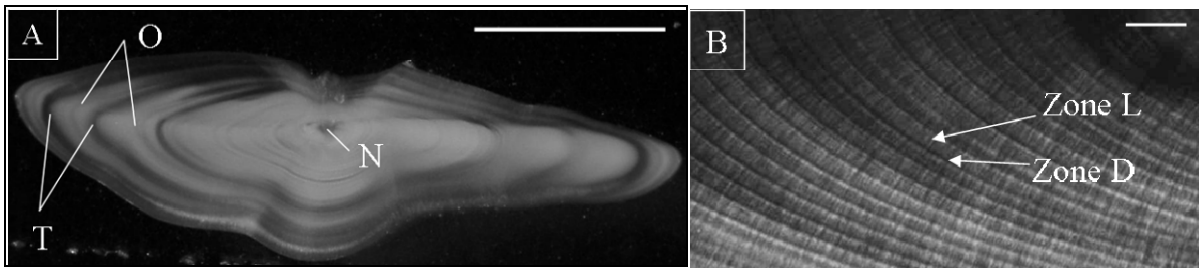

Figure 4 : Structures de l'otolithe aux échelles macro- et microscopiques. A) Section transversale d'otolithe de merlu observée en lumière réfléchie présentant des zones translucides (T) et opaques (O). Le noyau (N) correspond à la zone comprenant le primordium, structure initiale de l'otolithe. Echelle : 1 mm. B) Section transversale fine de l'otolithe de merlu observée en lumière transmise. Les accroissements primaires sont composés des zones L et D. Echelle : 20µm.

Caractérisation de l'opacité des macrostructures

A l'échelle saisonnière ou annuelle deux types de structures sont observables dites translucide et opaque. Les zones translucides sont définies comme des zones absorbant moins de lumière que les zones opaques. Elles apparaissent claires en lumière transmise et sombres en lumière réfléchie. A l'inverse les zones opaques apparaissent sombres en lumière transmise et lumineuses en lumière réfléchie. Les causes de variations de l'opacité des macrostructures sont mal comprises. Des facteurs associés à la saisonnalité tels que la température, la photopériode, le régime alimentaire ont été corrélés aux changements d'opacité (Beckman and Wilson 1995). Le jeûne alimentaire induit la formation de zone translucide sur des otolithes de saumon (*Oncorhyncus tsawytscha*) (Neilson and Geen 1985) ainsi que sur des otolithes de morue (*Gadus morhua*) (Hüssy and Mosegaard 2004; Hüssy *et al.* 2004; Høie *et al.* 2008). Une température supérieure à l'optimal thermique affecte aussi l'opacité avec la formation d'une zone plus translucide sur les otolithes de morue (Mosegaard and Titus 1987; Volk *et al.* 1990; Weidman and Millner 2000; Høie and Folkvord 2006). Cependant en

l'absence de fluctuations de température, les otolithes du poisson Utah chub (*Gila autraria*, Girard) et de nombreux poissons profonds présentent toujours des structures translucides et opaques (Johnson and Belk 2004). La température ne pouvant expliquer de telles variations, l'alimentation mais aussi des changements physiologiques tels que la reproduction ou des processus endogènes ont alors été supposés comme facteur de régulation (Johnson and Belk 2004). Ainsi la formation de zone translucide a été mise en corrélation avec des périodes de faible croissance somatique (Hüssy *et al.* 2004; Høie *et al.* 2008) ou de changement physiologique tel que le développement des gonades (Beckman and Wilson 1995; Høie and Folkvord 2006). De même l'âge du poisson influe sur l'opacité : ainsi des zones opaques proches du bord seront plus claires que des zones opaques proches du noyau (Mina 1968; Hoff and Fuiman 1993; Høie and Folkvord 2006).

De nombreux facteurs peuvent donc être à l'origine des variations d'opacité observées sur l'otolithe et intervenir à l'échelle des macrostructures ainsi qu'à l'échelle des microstructures (Wright *et al.* 2002b). Les effets de ces facteurs restent cependant à définir à travers deux questions majeures :

- quelles sont les importances relatives des différents facteurs environnementaux et métaboliques sur l'opacité ?
- quelles sont les effets des interactions entre ces facteurs sur l'opacité?

Relation opacité-composition de l'otolithe

1- Composition ionique

Les informations relatives à la composition de l'otolithe concernent essentiellement sa composition élémentaire. En plus des éléments C, O et Ca dominant la composition de

l'otolithe, une trentaine d'éléments ont également été mesurés à l'état d'éléments mineurs (> 100 ppm, Na, Sr, K, S, N, Cl) ou de traces (< 100 ppm). Les techniques de mesures utilisées peuvent être globales telles que la spectrométrie de masse ICP-MS, nécessitant une dissolution dans l'acide soit des otolithes entiers intégrant alors l'ensemble de la vie de poisson, soit de poudre prélevée au micromill sur l'ensemble d'une zone de l'otolithe correspondant alors à une période donnée de la vie du poisson. D'autres part des techniques ponctuelles peuvent être utilisées telle que la microsonde WDS ou la spectrométrie de masse par ablation laser LA-ICP-MS. Ces méthodes permettent de coupler une haute résolution spatiale, zones de prélèvement de quelques microns, à une détection chimique précise sur de faibles quantités. Certains de ces éléments ou leur rapport au calcium peuvent être définis comme des proxys des facteurs environnementaux prévalant lors de leur dépôt : tels que le Sr/Ca pour la salinité (Secor *et al.* 2001; Tzeng *et al.* 2003; Bath Martin *et al.* 2004), Ba/Ca et Mg/Ca pour la température (Eldson and Gillanders 2002).

L'analyse de la composition chimique des marques de croissance (zones translucides et opaques) de l'otolithe peut mettre en évidence des différences chimiques aidant à la compréhension du processus de formation. Ainsi une variabilité spatiale des ions strontium, calcium et sodium ainsi que le ratio Sr/Ca a été décrite sur les otolithes de nombreuses espèces telles que le vivaneau bourgeois (*Lutjanus sebae*) (Seyama *et al.* 1991), la limande sole (*Microstromus pacificus*) (Toole *et al.* 1993) et plus récemment le merlu (*Merluccius merluccius*) (Tomás *et al.* 2006). Ces études montrent des zones translucides plus riches en strontium et calcium mais plus pauvres en sodium que les zones opaques. Tomás *et al.* (2006) démontrent que ces variations en ions ne permettent pas de distinguer les zones translucides saisonnières des structures secondaires. Ces variations pourraient être associées à des paramètres environnementaux ou physiologiques tels que la maturation et la métamorphose (Kalish 1991; Arai *et al.* 1997). Elles pourraient également être associées à des différences en

structure cristalline des zones translucides et opaques. Tomás *et al.* (2006) posent l'hypothèse que l'accumulation de Sr/Ca décrirait une zone à forte densité cristalline résultant d'un arrangement compact des cristaux alors que la présence en sodium serait révélatrice d'une zone présentant de nombreuses irrégularités cristalline.

L'analyse de la composition ionique des otolithes permet ainsi l'identification de proxys de facteurs environnementaux et/ou métaboliques et une probable caractérisation des différences de cristallisation entre les structures. Cependant dans de nombreux cas, ces signatures restent indéchiffrables nécessitant : 1) la caractérisation du processus d'intégration de ces éléments sur l'otolithe, 2) la caractérisation des effets dus aux interactions entre facteurs environnementaux et métaboliques sur ce processus.

2- Composition organique

Les variations quantitatives de la matière organique et son rapport à la fraction minérale sont des critères supposés comme expliquant les degrés d'opacité observés sur l'otolithe. A l'échelle macroscopique, la quantification de la matière organique a été effectuée par Dannevig (1956) puis par Mugiya (1965), utilisant respectivement des techniques de brulage et de dosage de l'azote. Ils concluent que les zones opaques sont plus riches en matière organique que les zones translucides. A l'échelle microscopique, le protocole d'analyse consistait surtout en une attaque acide suivie d'observations au Microscope Electronique à Balayage, MEB (Dunkelberger *et al.* 1980; Morales-Nin 1987; Mugiya 1987). Ces observations conduisaient à la définition d'une zone L majoritairement constituée de fraction minérale et d'une zone D majoritairement constituée de fraction organique (Panfili *et al.* 2002b). Ces études ont cependant leurs limites : l'utilisation de l'attaque acide pour

l'analyse des microstructures altérant la surface d'étude et la composition des structures observées, la séparation des zones translucides et opaques dans l'étude de Mugiya (1965) à l'aide d'une lame diamantée questionnant sur la précision. Ces quantifications sont contraintes par la faible quantité de matière organique présente sur l'otolithe. Le développement de techniques d'analyses fines serait alors indispensable pour valider ces hypothèses permettant soit une analyse in situ, soit des techniques de micro-forage au niveau des macrostructures couplées à des dosages de matière organique.

Concernant la caractérisation de la fraction organique de l'otolithe, la littérature distingue souvent les fractions solubles et fraction insolubles (Baba *et al.* 1991; Asano and Mugiya 1993; Sasagawa and Mugiya 1996; Hüssy *et al.* 2004) et évoque leur influence sur l'opacité. Cette distinction entre fractions soluble et insoluble n'est pas intrinsèque mais dépend essentiellement du mode d'extraction : EDTA ou acide acétique (Borelli *et al.* 2001). Le ratio fraction soluble/insoluble à l'EDTA a été évalué à 15 :85% sur un pool d'otolithes d'espèces différentes (Baba *et al.* 1991) alors qu'Asano et Mugiya (1993) le mesurèrent à 45 :47%. Par séparation à l'acide hydrochlorique, Hüssy *et al.* (2004) montrèrent que ce ratio variait entre 75 :19% et 68 :26% lors d'une augmentation de température. D'après une étude sur le hareng (*Clupea harengus*), Tomás *et al.* (2004) ont confronté la composition organique d'otolithes dits « normaux » constitués d'aragonite avec celle d'otolithes vatéritiques correspondant à des otolithes nettement plus translucides. Ils ont déduis que seule la quantité en fraction insoluble et les différences de propriétés physiques des protéines affecteraient l'opacité. Cependant, cette étude se base sur des otolithes vatéritiques considérés comme « anormaux » (Gauldie 1986), nécessitant donc une validation entre zones translucides et opaques d'otolithes aragonitiques correspondant à un mécanisme « normal » de formation de l'otolithe.

De nombreuses études ont analysé la composition en acides aminées de la fraction soluble (Baba *et al.* 1991; Asano and Mugiya 1993; Sasagawa and Mugiya 1996) et de la fraction insoluble (Degens *et al.* 1969; Davis *et al.* 1995) et de la matrice protéique totale (Morales-Nin 1986a; b). Les seules études investiguant la composition et les variations du contenu protéique en fonction de l'âge du poisson sont celles de Morales Nin (1986a; 1986b) et de Hüssy *et al.* (2004). Ainsi Hüssy *et al*. (2004) démontrèrent un effet négatif de la taille du poisson entraînant une baisse de l'incorporation en protéine totale, une augmentation de la part en fraction insoluble à l'acide hydrochlorique et une modification en acides aminés (augmentation des concentrations en aspartate, glutamate et proline et une baisse en leucine) confirmant les résultats de Morales-Nin (1986b). De même, une augmentation de la température entraînerait une baisse de l'incorporation en protéines totale et une augmentation de la part en fraction soluble à l'acide hydrochlorique (Hüssy *et al.* 2004).

La caractérisation de la matrice organique à travers la distinction des fractions solubles et insolubles ne semble pas être pertinente du fait de la variabilité induite par le protocole d'extraction utilisé. Ainsi pour aborder le mécanisme de biominéralisation, il est nécessaire de développer des méthodes analytiques permettant l'analyse des composés organiques et ainsi d'étudier :

- 1) quelles sont les caractéristiques quantitatives et qualitatives (nature, propriétés) de ces composés qui interviennent dans l'opacité ?
- 2) quels sont les mécanismes intervenant dans la formation des macro- et microstructures ?

3- Caractérisation des composés de la matrice organique

Jusqu'à présent, quatre protéines de l'otolithe ont été identifiées :

- otolin-1, de poids moléculaire 100 kDa, correspondant à une protéine de type collagène ayant une fonction structurelle (Murayama *et al.* 2002) dont la sécrétion suit un cycle nycthéméral (Takagi *et al.* 2005).
- Starmaker, de poids moléculaire 66 kDa, protéine intervenant dans le polymorphisme du carbonate de calcium des otolithes de zebrafish en contrôlant la taille et la forme des dépôts cristallins. Des expériences in vitro ont montré qu'en absence de Starmaker la calcite remplaçait l'aragonite (Söllner *et al.* 2003).
- OMP-1, de poids moléculaire 55 kDa, glycoprotéine nécessaire à la déposition de l'otolin-1 (Murayama *et al.* 2000; Murayama *et al.* 2005).
- OMM-64, de poids moléculaire 64 kDa, présente une structure et un ADN proche de celui de starmaker, protéine présentant une activité de ligand avec le calcium, se lie à otolin-1 et formerait un complexe contrôlant la morphologie des cristaux (Tohse *et al.* 2008).

Du fait de la taille des structures et de la faible quantité de matière organique dans les otolithes, des techniques d'analyses fines ont du être développées afin d'analyser la distribution spatiale des fractions minérale et organique. L'identification des protéines de l'otolithe a ainsi conduit à la mise au point d'immuno-marquage permettant de quantifier la présence d'OMP-1 et otolin-1 sur les microstructures d'otolithes de truites (*Oncorhynchus mykiss*) et les sites de sécrétion au niveau de l'épithélium (Murayama and Takagi 2004).

La micro-spectrométrie Raman consiste à analyser la réponse de la matière, sous forme de spectres vibrationnels, à un rayonnement lumineux monochromatique. Ses principales propriétés sont les suivantes :

- non destructive : évitant ainsi la formation de cratères à la surface de l'otolithe,
- ne nécessite aucun mode de préparation particulier : évitant ainsi l'utilisation d'attaque acide,
- très haute résolution spatiale de l'ordre du micron permettant d'analyser les structures les plus fines de l'otolithe telles que les zones,
- permet l'analyse ponctuelle ou par cartographie (mapping),
- permet d'analyser la fraction minérale de l'otolithe et de distinguer les différents morphes de carbonates de calcium : aragonite, vatérite, calcite (Gauldie *et al.* 1997; Tomás and Geffen 2003; Melancon *et al.* 2005; Tzeng *et al.* 2007),
- permet aussi d'analyser la matière organique à la fois de façon quantitative (réponse proportionnelle à la concentration) et qualitative (caractérisation de liaisons chimiques) comme précédemment démontré sur d'autres biominéraux : analyse de la fraction organique des coraux (Kaczorowska *et al.* 2003), le squelette corallien et la dégradation des matrices organiques (Perrin and Smith 2007) et les pigments des coquilles de mollusques (Barnard and de Waal 2006; Hedegaard *et al.* 2006).

De par ses propriétés, elle apparaît donc comme une technique permettant l'extraction d'informations quantitatives et qualitatives des fractions minérale et organique de façon simultanée sur l'otolithe. Récemment, l'utilisation de la micro-spectrométrie Raman sur les otolithes s'est intéressée à l'analyse de la fraction organique particulièrement au niveau du noyau (Zhang *et al.* 2008).

Le modèle choisi : le merlu européen (Merluccius merluccius)

Généralités

Le merlu (*Merluccius merluccius*, Liné 1758) (Figure 5) est une espèce démersale dont la répartition géographique s'étend de la Norvège à la Mauritanie jusqu'en Méditerranée. Il vit principalement à des profondeurs comprises entre 70 et 400 m et plus largement entre 30 et 1000 m (Casey and Pereiro 1995).

Figure 5 : Photo sous-marine d'un merlu marqué et relâché au cours des campagnes dans le golfe de Gascogne (photo IFREMER Brest)

Les populations d'Atlantique et de Méditerranée sont séparées par le détroit de Gibraltar et reconnues comme distinctes par des études génétiques (Roldan *et al.* 1998; Lundy *et al.* 2000; Castillo *et al.* 2004; Cimmaruta *et al.* 2005) ainsi que par la composition chimique des otolithes (Swan *et al.* 2006). Bien que l'existence de plusieurs populations n'ait pas été clairement mise en évidence en Atlantique, deux stocks sont considérés pour la gestion communautaire de la ressource par le CIEM, séparés par le Cap Breton : le stock Nord réparti

de la Norvège au golfe de Gascogne et le stock Sud correspondant aux côtes espagnoles et portugaises (Figure 6) (ICES 2007).

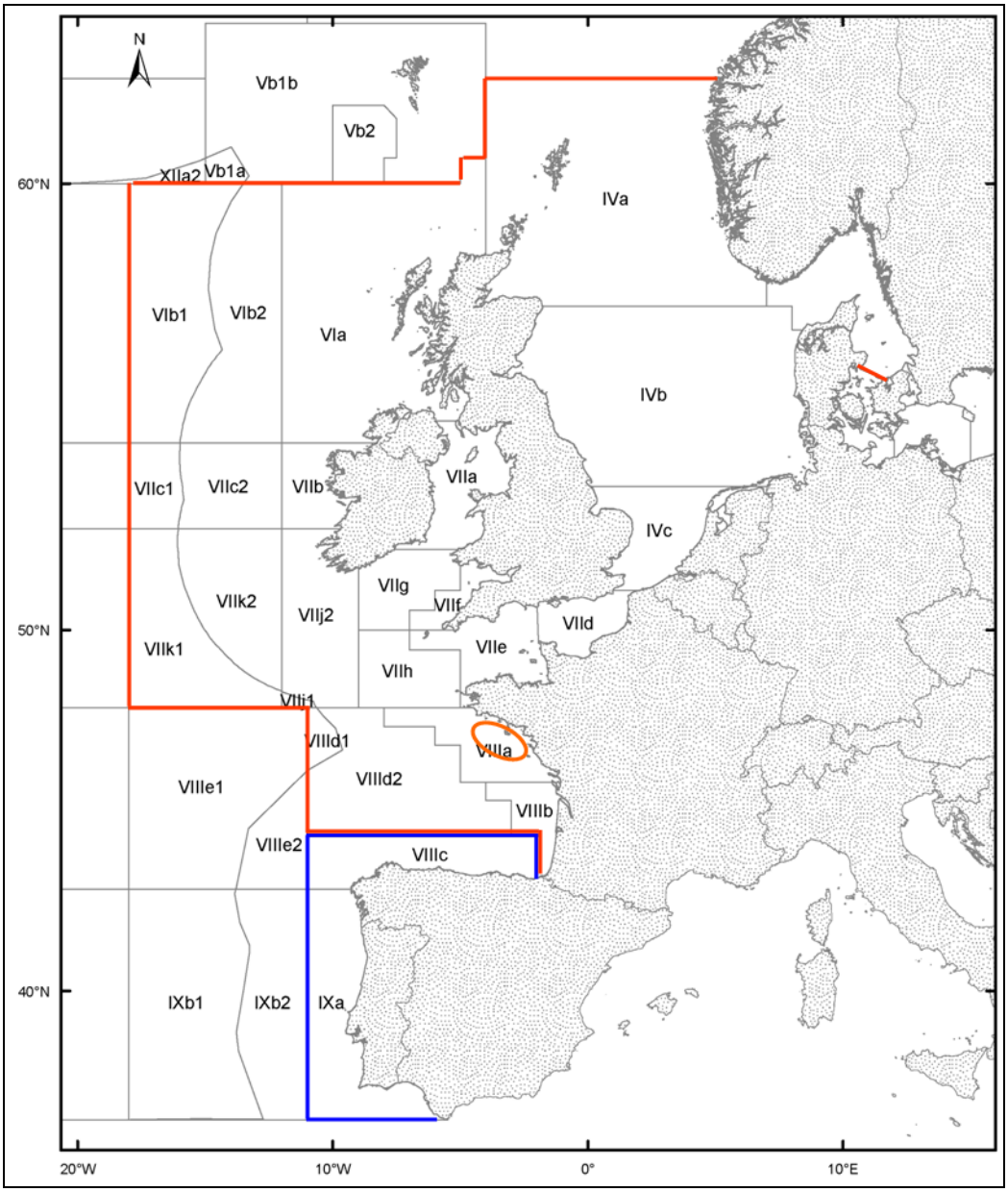

Figure 5 : Sous-divisions définies par le CIEM pour les stocks Nord (rouge) et sud (bleu) et localisation de la Grande Vasière (orange)

Le stock Nord représente une forte valeur économique en Europe et est principalement exploité par l'Espagne, la France, et le Royaume-Uni représentant respectivement 59, 26 et 6% des débarquements (ICES 2007). Les débarquements totaux ont diminués depuis les

années 60 passant de 120 000t à 40 000t au début des années 2000 et semblent se stabiliser. En 2002, Le stock Nord a été reconnu dans un état inquiétant basé sur des estimations en biomasse féconde inférieure à la biomasse féconde minimale supportable par la population et une estimation de la pression de pêche supérieure à la pression de pêche maximale supportable par la population. Ce diagnostic entraîna la mise en place d'un plan de restauration en 2004 par la Commission Européenne (EC Regulation n°811/2004). Le stock sud a aussi été diagnostiqué dans un étant inquiétant et un plan de restauration a été mis en place en 2006 (CE 2166/2005).

La fiabilité du diagnostic repose sur une bonne connaissance de la biologie de l'espèce et en particulier la croissance, l'âge de première maturité et les migrations. Comme nous le précisons dans la suite, ces conditions ne sont pas réunies pour le merlu, ce qui constitue une des motivations du choix de ce modèle biologique.

Biologie de l'espèce :

1- Alimentation

Le merlu est une espèce vivant essentiellement proche du fond le jour et se nourrissant à mi-hauteur de la colonne d'eau voire à la surface de l'eau la nuit impliquant des migrations verticales (Alheit and Pitcher 1995). Les juvéniles de merlu se nourrissent essentiellement de crustacés et de petits poissons tels que les gobies. Adulte, le merlu est piscivore et se nourrit surtout, dans le Golfe de Gascogne, de merlan bleu (*Microsmesistius poutassou*), chinchard (*Trachurus trachurus*) et maquereau (*Scomber scombrus*) (Guichet 1995; Du Buit 1996). Le cannibalisme des juvéniles est reconnu et démontré dans le nord du Golfe de Gascogne et en

Mer Celtique (Guichet 1995; Mahe *et al.* 2007). Son importance dépend de l'abondance en juvéniles et de la séparation des aires de distribution des juvéniles et des adultes.

2- Migrations

Les migrations du merlu ont été étudiées de façon indirecte par la distribution saisonnière des captures en Mer Celtique et dans le golfe de Gascogne. Ainsi les jeunes merlus sont principalement localisés le long des côtes et dans la Grande Vasière (Dardignac 1988; Bez *et al.* 1995). Les individus adultes occupent tout le plateau continental et sont observés en Mer Celtique d'avril à novembre. Les plus vieux individus migrent plus à l'ouest et sont principalement capturés le long des marges continentales de février à avril/ mai (Poulard 2001; Woillez *et al.* 2007).

Les migrations verticales sont principalement motivées par la recherche de proies. Ce comportement a souvent été mis en avant pour expliquer la baisse des captures la nuit pour des gadidés tels que la morue et le merlu (Beamish 1966; Bowman and Bowman 1980). Bien que les migrations verticales soient connues, les facteurs contrôlant ces mouvements et leurs caractéristiques sont peu documentés en Atlantique Est (Hickling 1927).

3- Reproduction

L'ogive de maturité proposée par Martin (1991) et confirmée par Lucio et al. (2000) estime que la taille de première maturité sexuelle (L_{50}) se situe à 39 cm pour les mâles et 47 cm pour les femelles. Le merlu présente une période de ponte étendue avec des femelles matures toutes l'année (Murua and Motos 2006). Dans le golfe de Gascogne, la principale période est entre janvier et mai avec un pic en février/ mars (Martin 1991; Alvarez *et al.* 2004;

Murua and Motos 2006). La ponte est séquentielle et plusieurs pontes peuvent se succéder au cours d'une même saison (Murua and Motos 2006). La reproduction a surtout lieu le long de la marge du plateau continental (Alvarez *et al.* 2001) à une température optimale pour la survie et le développement des œufs de 10.5 à 12°C (Valencia *et al.* 1989). Les larves sont ensuite transportées près des côtes du golfe de Gascogne et en Mer Celtique vers les zones de nourricerie : la Grande Vasière et le nord ouest de la Mer Celtique (Kacher and Amara 2005).

Croissance et estimation de l'âge

1- Croissance somatique

Le merlu européen présente une taille maximale de 1.40 m et une taille commune variant entre 30 cm et 1.10 m (Quero and Vayne 1997). Depuis les années 30, deux hypothèses de croissance s'affrontent : une à croissance rapide présentée par Belloc (1935) qui mesura un taux de croissance de 16.7 cm/an sur un merlu marqué ayant passé 9 mois de liberté dans le milieu ; et une hypothèse de croissance lente présentée par Hickling (1933) qui, à partir de l'interprétation des otolithes, estima la croissance du merlu à 8.9 cm/ an. Depuis, de nombreuses études proposèrent différentes estimations de la croissance dans les différentes aires de distribution du merlu : entre l'Irlande et les îles britanniques (Bagenal 1954; Guichet *et al.* 1973), au Maroc (Goni 1983), le golfe de Gascogne (Descamps and Labastie 1978; ICES 1993; Lucio *et al.* 2000) et le long de la péninsule Ibérique (Robles *et al.* 1975; Iglesia and Dery 1981; Goni and Pineiro 1988; Piñeiro and Sainza 2003). Malgré ces confrontations, c'est l'hypothèse de croissance lente qui est utilisée pour l'élaboration des clés taille-âge dans les groupes de travail du CIEM.

Depuis 2002, des campagnes de marquages-recaptures ont été menées par l'Ifremer dans le golfe de Gascogne pour une validation directe de la croissance somatique (de Pontual *et al.* 2003a; de Pontual *et al.* 2006). Les premiers résultats issus de la campagne de 2002 se rapportent à des merlus ayant passés entre 101 et 1066 jours de liberté dans le milieu. Ils mettent en évidence un taux de croissance de 0.052 ± 0.009 cm/jour. Ce taux de croissance est supérieur d'un facteur 2 aux estimations précédentes et implique un modèle de croissance aboutissant à des tailles de 25, 45 et 60 cm la première, deuxième et troisième année au lieu des 20, 29 et 37 cm estimées à partir du schéma de lecture des otolithes agréé au niveau international (Figure 7) (Piñeiro and Sainza 2003). Ces résultats confirmèrent l'hypothèse de croissance rapide proposée précédemment par Bagenal (1954) qui utilisait la lecture des otolithes in toto, ainsi que celles de Pineiro et Pereiro (1993) et Alemany et Oliver (1995) qui examinèrent les modes de progression des fréquences en taille. Ces résultats ont été confirmés en Méditerranée (Mellon *et al.* submitted) ainsi que sur le stock Sud par des campagnes comparables de marquages-recaptures montrant un taux de croissance du merlu à 0.052 ± 0.003 cm/jour calculé à partir de merlus ayant passé entre 347 et 466 jours de liberté dans le milieu (Piñeiro *et al.* 2007).

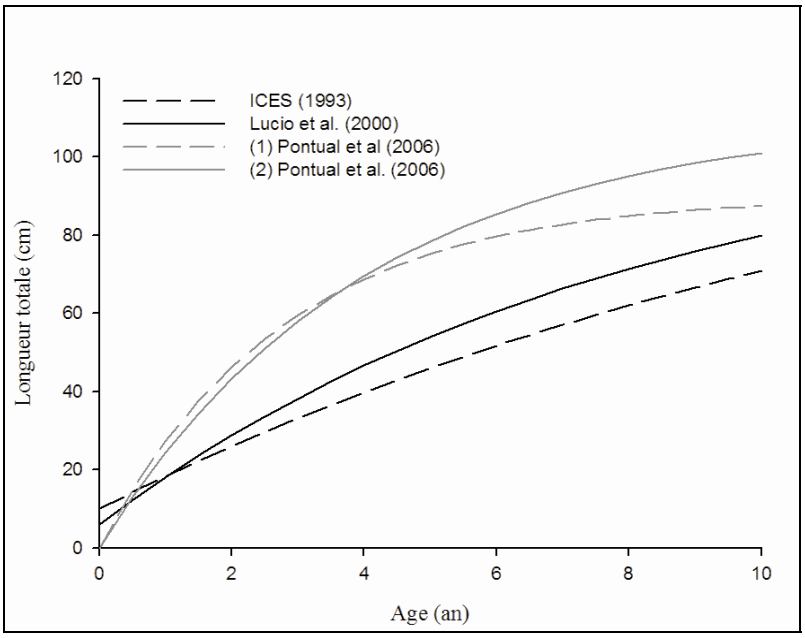

Figure 7 : Modèle de croissance de Von Bertallanffy estimé par les différentes études. Pour le modèle (1) les paramètres L∞ et K ont été estimés à partir des recaptures alors que pour le modèle (2) le paramètre L∞ a été fixé. D'après de Pontual et al. (2006)

2- Croissance de l'otolithe et estimation de l'âge

Des otolithes issus de la campagne Ifremer 2002 ont été lus en aveugle par deux experts du groupe de travail du CIEM selon les critères d'interprétation agréés au niveau international (Piñeiro and Sainza 2003) (Figure 8). Cette analyse a mis en évidence que la sous-estimation de la croissance résultait d'une surestimation de l'âge du merlu (de Pontual *et al.* 2006).

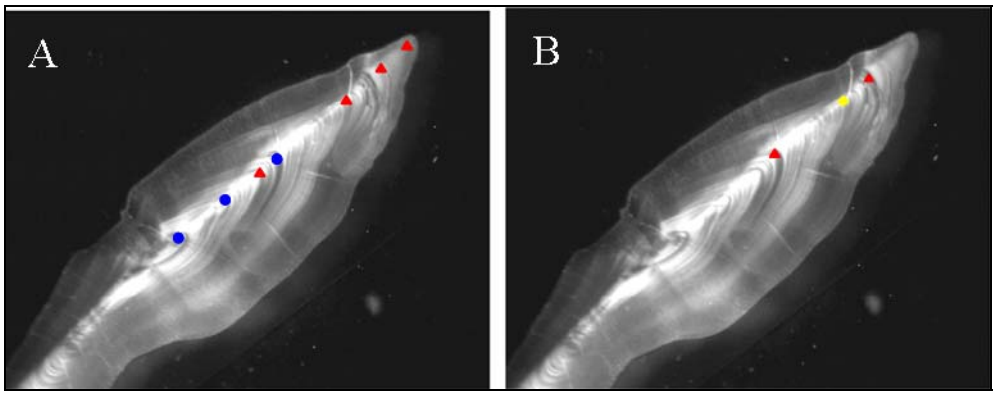

Figure 8 : Coupe transversale de merlu marqué observé en lumière réfléchie. (A) Lecture en aveugle, âge = +4 ans, (B) nouvelle interprétation, âge = +2 ans. En bleu sont indiqués les faux anneaux décrits par Pineiro and Sainza (2003), en rouge les anneaux d'hiver et en jaune la marque de tétracycline. Le poisson mesurait 30 cm à la capture et 49 cm à la recapture, 301 jours plus tard. D'après de Pontual et al. (2006)

Cette surestimation de l'âge s'explique par la complexité des otolithes de merlus présentant des structures secondaires pouvant être interprétées comme des structures saisonnières (Morales-Nin *et al.* 1998). Les critères d'estimations de l'âge bien qu'agréés au niveau international pour les trois premières années de la vie du merlu, restent cependant non validés (Pineiro *et al.* 2004). Suite à ces résultats, depuis 2003, le groupe de travail du CIEM élabore 2 diagnostics pour la gestion du stock de merlu sur la base des 2 hypothèses de croissance lente et de croissance rapide (ICES 2006). L'hypothèse de croissance rapide modifie les estimations de mortalité par pêche, de recrutement du stock et de biomasse féconde. Les tendances restent cependant les mêmes pour la mortalité par pêche et le recrutement. Les simulations avec la croissance rapide mettent surtout en évidence une capacité de reconstitution rapide du stock en cas de baisse de la pêche (Bertignac and de Pontual 2007).

De nombreuses études se sont aussi intéressées à la croissance des juvéniles via la lecture des microstructures. Ces études concernent les différentes aires de distribution du merlu : la Méditerranée (Morales-Nin and Aldebert 1997; Morales-Nin *et al.* 1998; Arneri and

Morales-Nin 2000; Morales-Nin and Moranta 2004; Belcari *et al.* 2006), le stock Nord Atlantique (Kacher and Amara 2005) ; le stock sud Atlantique (Piñeiro *et al.* 2008) (Tableau 1). Cette analyse des microstructures présente des difficultés de par l'apparition de centres secondaires de croissances à la fin de la phase pélagique des juvéniles. Cependant, le dépôt journalier des incréments a été validé de façon indirecte par retrocalcul sur des otolithes de juvéniles de merlu pêchés en Mer Adriatique (Arneri and Morales-Nin 2000) et en Méditerranée (Belcari *et al.* 2006) et de façon directe à partir d'élevage larvaire en Norvège durant lequel une larve a survécu pendant 245 jours (Morales-Nin *et al.* 2005). Les incréments journaliers ont été utilisés pour estimer le taux de croissance et la distribution des dates d'éclosion sur des juvéniles (Morales-Nin and Moranta 2004; Piñeiro *et al.* 2008) et sur des larves (Palomera *et al.* 2005). Les études résumées dans le tableau 1 divergent dans l'estimation du taux de croissance pendant la phase juvénile et par conséquent sur la taille atteinte par le merlu au bout de la première année, en particulier entre les merlus d'Atlantique et de Méditerranée. Ces croissances différentes peuvent être expliquées par différentes approches méthodologiques mais aussi par des différences génétiques et de conditions environnementales entre les deux zones.

Auteur	GR	LT	Echantillonnage	Zone détude
Morales-Nin and Aldebert (1997)	1,15 cm/mois	16	81 10,5-20,7 cm	Golfe du Lion
Arneri and Morales-Nin (2000)	1,1-1,6 cm/mois	15	145 1,6-16,4 cm	Adriatique centrale
Morales-Nin and Moranta (2004)	1,2-2,5 cm/mois	-	153 2,5-25 cm	Méditerranée
Kacher and Amara (2005)	0,72-0,74 mm/jour	23,8	107 6-22 cm	Golfe de Gascogne et Mer Celtique
Palomera et al (2005)	0,15-0,19 mm/jour	-	71 2,5-9,1 mm *	Méditerranée
Alvarez and Cotano (2005)	0,15-0,17 mm/jour	-	40 2-12 mm *	Golfe de Gascogne
Bjelland and Skiftesvik (2006)	1,8 cm/mois	-	1 13,5 cm	Elevage larvaire
Belcari et al (2006)	1,3-1,7 cm/mois	18,3	579 4-20 cm	Mer Tyrrhénienne
Pineiro et al (2008)	0,66 ± 0,06 mm/jour (moyenne ± SD)	25,2	103 3-25 cm	Atlantique, NW de l'Espagne

Tableau 1 : Résumé des données de croissance journalière obtenues dans les différentes zones d'études : taux de croissance (GR), taille moyenne estimée à un an (Longueur totale LT en cm), échantillonnage et gamme de taille (LT en cm sauf * Longueur Standard en cm) et zone d'étude. D'après Pineiro et al. (2008).

Maintien du merlu en captivité

La compréhension des otolithes permettant la calibration des informations structurelles et chimiques est indispensable et doit passer par des expérimentations en milieu contrôlé. Ces expérimentations permettent aussi une meilleure compréhension de la biologie et de la croissance du merlu. L'élevage du merlu est loin d'être maîtrisé du fait de sa grande sensibilité à la manipulation et à la capture (Hickling 1933; Belloc 1935). Jusqu'à présent les observations faites sur le merlu sont issues de données provenant du milieu naturel. Seule une étude de la croissance des juvéniles de merlu propose des résultats issus d'un élevage larvaire mené en Norvège mais au cours duquel seule une larve a survécu jusqu'au 245ème jour

(Bjelland and Skiftesvik 2006). La capture des merlus a sensiblement été améliorée par la mise au point d'un cul-piscine optimisant la survie du poisson à la capture pour les campagnes de marquages (de Pontual *et al.* 2003a). Jusqu'à la fin 2007, seuls deux élevages de merlus étaient connus et conduits par l'Ifremer en France et par l'Université de Bergen en Norvège. La difficulté de maintenir le merlu en bassin porte sur différents domaines dont le manque de connaissances zootechniques et les difficultés de récupération de la pêche. Dans ces deux élevages, des pontes naturelles ont été observées à partir de 2007 et les tentatives d'élevage larvaire effectuées en Norvège à partir de ces pontes ont échoué au bout de 30 jours essentiellement dû à des difficultés de premier nourrissage des larves. De nombreux essais d'élevage larvaire à partir d'œufs issus du milieu naturel ont été effectués par ces deux instituts et seule la tentative de Bjelland entre 1997 et 1999 (Bjelland and Skiftesvik 2006) réussit à dépasser la période du premier mois.

Cet intérêt pour la mise au point des techniques d'élevage a non seulement un objectif halieutique mais aussi une perspective en aquaculture. En effet, de par sa forte croissance somatique et l'importance économique de cette espèce, le merlu semble être un bon candidat pour l'aquaculture des gadidés et apporterait une diversification dans un domaine où l'élevage de la morue prédomine (Quémener *et al.* 2002). Ce constat a été renforcé par l'apparition d'études sur d'autres espèces de merlus. Ainsi, au Chili, *Merluccius australis* est élevé dans un site avec une production annuelle de 15 000 juvéniles (données 2004) avec un objectif de production de 3 à 5000 tonnes en 2010 (Rosenlund and Skretting 2006; Bustos *et al.* 2007). De même un stock de géniteurs sauvages de *Merluccius bilinearis* a pu être est maintenu en captivité et effectuer des pontes naturelles aux Etats-Unis (Buckley *et al.* 1993).

Objectifs et plan du mémoire

L'otolithe est une source d'informations extrêmement riche pour l'identification des traits de vie individuels. Cependant dans de nombreux cas cette information reste indéchiffrable soit par la présence de structures secondaires de croissance compliquant les schémas d'interprétations des otolithes, soit par la difficulté à associer une signature chimique à un facteur environnemental ou métabolique. Ces difficultés sont principalement dues à une connaissance parcellaire de la formation des otolithes et donc de l'intégration des informations chimiques et structurelles en fonction des facteurs environnementaux et/ou métaboliques. Afin d'améliorer le décryptage des otolithes et de ses signatures, une calibration de cet outil et en particulier une calibration temporelle par l'analyse des structures des otolithes est indispensable. L'état des connaissances a mis en évidence de nombreux points de questionnements sur l'extraction, la caractérisation et la compréhension des signatures structurelles et physico-chimiques de l'otolithe. Deux axes d'étude principaux ont été choisis pour répondre à cette problématique :

1) la mise en relation d'informations structurelles (opacité) avec des propriétés physico-chimiques (fractions minérale et organique) via l'utilisation de la micro-spectrométrie Raman au niveau des structures de l'otolithe à l'échelle macroscopique et microscopique;

2) la relation avec les facteurs environnementaux et physiologiques influençant la formation de ces structures sur l'otolithe.

La calibration des informations extraites sur les otolithes ne pouvant être fait en milieu naturel, elle nécessite dans un premier temps l'expérimentation en milieu contrôlé permettant

de dissocier les facteurs et leurs interactions. Le modèle choisi pour cette étude est le merlu européen (*Merluccius merluccius*) tant pour les propriétés de ses otolithes (grande taille, macrostructures et microstructures visibles) que pour répondre à une problématique halieutique due à un manque de connaissance sur sa biologie (croisance, migrations) et à la difficulté d'interprétation de ces otolithes.

Les résultats de cette étude s'articuleront en deux parties : 1) l'acquisition de connaissances nécessaires à l'utilisation du modèle biologique, 2) la caractérisation de l'information structurelle des otolithes.

Le premier axe s'inscrit dans une stratégie portant à la fois sur 1) l'amélioration des connaissances sur la biologie de l'espèce et 2) la compréhension des processus de biominéralisation nécessitant des expérimentations en milieu contrôlé et en milieu naturel. Les résultats obtenus au cours des expérimentations en milieu contrôlé s'articule en deux axes :

- l'étude du marquage sur la survie et la croissance en milieu contrôlé (Chapitre 1)
- l'évaluation de la croissance en milieu contrôlé sous des effets de température et d'alimentation. (Chapitre 2).

La deuxième partie expose les travaux et les résultats sur le modèle otolithe à travers trois aspects :

- l'etude de l'opacité de l'otolithe en fonction du taux de croissance, du métabolisme et de la température (Chapitre 3)

- la caractérisation des microstructures, les zones L et D et du noyau à l'aide de la micro-spectrométrie Raman (Chapitre 4)
- l'analyse des relations entre l'opacité de l'otolithe et des distributions spatiales des fractions minérales et organiques à l'aide de la micro-spectrométrie Raman. (Chapitre 5)

Chapitre 1 :

Effets du marquage par spaghettis et capteurs électroniques sur la survie et la croissance du merlu européen

Chapitre 1 :

Effets du marquage par spaghettis et capteurs électroniques sur la survie et la croissance du merlu européen

L'individualisation des poissons est une étape essentielle pour le suivi de la croissance lors des campagnes de marquage-recapture et les expérimentations en milieu contrôlé. Cette pratique peut néanmoins avoir des effets sur les poissons : stress et dommages physiques dus à la manipulation et l'implantation de la marque. Ces effets peuvent affecter la survie et la croissance des poissons étudiés et donc influencer les résultats issus de ces expériences. Une évaluation quantitative préalable de ces effets est par conséquent indispensable mais ne peut se faire en milieu naturel et nécessite un suivi en milieu contrôlé.

Au cours des campagnes menées par l'Ifremer, les merlus sont usuellement marqués à l'aide de marques externes dites « spaghettis ». Par la suite, l'implantation de marques électroniques a été envisagée afin d'enrichir les données de croissance par des enregistrements de température et de profondeur apportant des informations complémentaires sur le comportement du merlu. L'utilisation de marques électroniques représente un coût important et implique une manipulation supplémentaire pour l'implantation chirurgicale de la marque dans la cavité abdominale. Le merlu étant reconnu comme une espèce sensible à la manipulation, l'évaluation de l'effet du marquage est indispensable avant d'envisager son exploitation lors de campagnes. L'objectif de cette étude était par conséquent double : 1) évaluer l'effet du marquage dit « conventionnel » effectué à l'aide des marques externes

« spaghetti » sur la survie et la croissance du merlu ; 2) estimer la faisabilité du marquage électronique en fonction de ses effets sur la survie et la croissance.

Une expérimentation en milieu contrôlé a été menée sur deux lots de 30 merlus de taille distincte : un groupe de petits individus nommés SF (longueur totale moyenne ± écart type : 29.9 cm ± 2.2 cm) et un lot de grands individus nommé LF (longueur totale moyenne : 36.4 cm ± 2.5 cm). Pour chaque classe de taille, trois traitements furent appliqués de façon aléatoire. Un premier lot fut conservé en tant que témoin et n'a subit que l'anesthésie. Un second a été marqué de façon conventionnelle à l'aide d'une marque spaghetti. Enfin le troisième a été marqué à la fois par le marquage conventionnel ainsi que par l'implantation d'une pseudo-marque électronique, ne différant que par l'absence des capteurs.

Après 4 mois, le taux de survie global était de 35%. Les deux classes de tailles ont répondu différemment au marquage. Le lot des SF a moins réagi au stress induit par la manipulation, l'anesthésie et le marquage avec un taux de survie équivalant pour le marquage conventionnel et le marquage électronique à hauteur de 30%. Le lot des LF a montré à l'inverse un taux de survie nul au marquage électronique et très faible pour le marquage conventionnel (10%). En termes de croissance, le traitement des données était difficile du fait de la forte variabilité individuelle et du peu d'individus ayant survécu à chaque traitement. Néanmoins, aucune différence significative n'a été mise en évidence entre les témoins et les poissons marqués.

Cette expérience a ainsi permis de mettre en évidence : 1) que le marquage conventionnel influait sur le taux de survie ; 2) que le marquage électronique était envisageable sur des individus de 30 à 35 cm avec un taux de survie comparable au marquage conventionnel.

Effects of T-bar and DST tagging on survival and growth of European hake

Aurélie Jolivet, Hélène de Pontual, François Garren, Marie-Laure Bégout

Accepté dans **Reviews: Methods and technologies in Fish Biology and Fisheries**

Abstract:

Controlled experiments were conducted to assess the effects of T-bar and DST tagging on post-release survival and growth of European hake. In this study, two groups of each 30 hake were considered: small fish (SF, average total length: 29.9 cm ± 2.2 cm) and large fish (LF, average total length: 36.4 cm ± 2.5 cm). Within each size group, fish were randomly assigned to one of 3 treatment groups: control (C), T-bar tagging referred as conventional tagging (CT) and DST tagging (DST) with dummy tags. After 4 months, the overall survival rate was 35%. Smaller fish were less impacted by the stress induced by handling, anaesthesia and tagging and in the SF group, the survival rates were similar (30%) for CT or DST. Specific growth rates were highly variable and no significant difference could be observed between control and tagged fish. Our results demonstrate that 1) conventional tagging affects fish survival rates and 2) DST tagging is feasible in the field on "small fish" with expected survival rate and recapture probability close to that of conventional tagging.

Introduction

European hake, *Merluccius merluccius*, is a demersal fish widely distributed from the west coast of Norway, south to the coast of Mauritania, and eastwards into the Mediterranean Sea. It is a major demersal resource in the North East Atlantic, which has been heavily exploited by fisheries. Total landings of *M. merluccius* have decreased from 120000t in the early 1960s to 50000t in recent years. Although there is no evidence that multiple populations

exist, the northern stock (ICES areas IIIa, IV, VI and VII and VIIIa, b, d) and the southern stock (ICES areas VIIIc and IXa) are managed separately (ICES 2005).

Recent mark-recapture experiments (de Pontual *et al.* 2003a; Piñeiro *et al.* 2007) have provided evidences of growth underestimation of the species due to a bias in the age estimation method internationally agreed and routinely used for the species (de Pontual *et al.* 2006). Simulations have estimated a significant associated impact on assessment (*e.g.* higher F, lower SSB) and management advices (Bertignac and de Pontual 2007). Besides growth, directed movements and fishing mortality are other key information that can be gained from mark-recapture experiments (Beverton and Holt 1957). To estimate fishing mortality, it is necessary to estimate post release mortality due to the stress of capture, handling and tagging on the fish (Brattey and Cadigan 2004). Estimating post-release mortality is difficult and requires experiments that compare the survival of tagged fish *vs.* control fish held in captivity (Rutecki and Meyers 1992; Millner et al. 1993; Pierce and Tomcko 1993). Furthermore, it is now well recognized that fish tagged with archival tags (also called Data Storage Tags, DST) provide important information about fish movements, behaviour and their environmental conditions (Thorsteinsson 2002). As such internal tagging is more invasive and expensive than external T-bar tagging (referred below as conventional tagging), a feasibility study needed to be conducted before the start of a DST tagging experiment in the field on European hake.

The main challenge to study the effects of conventional tagging on mortality rates in European hake is that this species is not commercially farmed. One reason for this might well be that the species has long been regarded as especially sensitive to capture- and handling-related damages. A pioneering study on larval rearing experiment (Bjelland and Skiftesvik 2006) provided some basic information on egg incubation to weaned larvae. Here we report a study carried out on wild-caught fish kept in captivity. The main objectives were to estimate

the effects of conventional and DST tagging on fish survival and growth. The information gained from these research objectives will help determine the feasibility of DST tagging studies at sea.

Methods

Fish origin

Fish were caught in the Bay of Biscay in July 2005 using the capture method developed by de Pontual et al. (2003a) for mark-recapture experiments. To acclimatize the fish, individuals were kept in captivity for 7 months in 15 m^3 tanks. These tanks were supplied with seawater flow at ambient temperature (from 7.9°C to 13.7°C), flushed with a daily water renewal rate of 20%, and illuminated following the natural photoperiod. Fish were fed ad libitum on inert preys (sprat, herring and mackerel).

Tagging Protocol

Prior to tagging the experimental group of fish (average total length: 31.2 cm ± 2.3 cm and average weight: 190.1 g ± 52 g), we determined the best anaesthesia protocol suitable for further experiments onboard research vessels. Our protocol criteria were the following: low toxicity for both operator and fish, short induction time, short recovery time, small secondary effects, and no withdrawal period. After testing several protocols, we choose Benzocaïne (ethyl *p*-aminobenzoate) at a concentration of 100 mg l^{-1} at a sea water temperature of 9.3°C. The tagging experiment started on February 7, 2006 and ended on June 15, 2006 (128 day duration). Two size groups were selected: small fish (SF, average total length TL ± standard deviation SD: 29.9 cm ± 2.17 cm, N= 30) and large fish (LF, average total length TL 36.4 cm

± 2.5 cm, N=30). Within each size group, fish were randomly assigned to 3 treatment groups: control (C), conventional tagging (CT) and DST tagging (DST).

All fish were anaesthetised, measured (total length TL_0) and weighed (W_0) prior to subsequent treatment. SF individuals were exposed to a 100 mg l^{-1} benzocaïne solution, a concentration which was increased to 120 mg l^{-1} for the LF group. Total exposure time to benzocaïne did not vary between groups and was set at 15 min to allow for the time needed to insert DST tags (5 min). Individual fish behaviour such as loss of reaction to external stimuli and loss of equilibrium was followed during the anaesthesia steps. Conventional tagging (CT group) was carried out according to the method developed by de Pontual et al. (2003a) for mark recapture experiment. Briefly, a T-bar tag was inserted at the base and in front of the second dorsal fin and the fish was injected with a solution of oxytetracycline at a dose of 60 mg kg^{-1} of fish. This antibiotic is used to mark calcified structures for age validation (de Pontual *et al.* 2006a). In addition, the DST fish group had Star-Oddi DST micro dummy tags (8.3 mm diameter x 25.4 mm length, 3.7 g in air), inserted in the peritoneal cavity. This surgerical procedure consisted of 1) 1 cm cut through the ventral muscle at 1 cm in front of the anus, 2) pushing the tag gently inside the peritoneal cavity and 3) suturing the wound by 2-3 stitches with polyamide monofilament (Bégout Anras et al. 2003). After treatment, fish were transferred to two 15 m^3 indoor tanks, one for the SF group (thus including 3 groups: SF-C, SF-CT, SF-DST) and the second for the LF group (LF-C, LF-CT, LF-DST). At the end of the experiment fish were killed with an overdose of anaesthetic and measured (total length TL_f), weighed (W_f) and sexed. Euthanized and fish dead during the course of the experiment were deep frozen prior subsequent treatment.

Data analyses

The condition factor of individual fish was calculated as (Wege and Anderson 1978; Jobling et al. 2001):

$$K_t = W_t/W_e x100 \quad \text{(Eqn 1)}$$

where W_t is the weight of the fish at time t and W_e is the theoretical weight calculated from the length-weight relationship derived from the field: W_e (g) = 0.00513 $L^{3.074}$ (Dorel 1986). Specific Growth Rate (SGR % day^{-1}) was calculated as:

$$SGR = (e^g-1)\ x100 \quad \text{(Eqn 2)}$$

where $g = [\ln(W_{tf})-\ln(W_{t0})]/(t_f-t_0)\ ]$ and W_{tf} and W_{t0} are the wet body weight (g) at death or experimental end (t_f) and tagging (t_0) time respectively (Houde and Schekter 1981; Nordgarden et al. 2003). Estimates of individual growth rate were not available for the control groups (SF_C, LF_C) as, by definition, fish could not be tagged. We addressed the later issue by considering average SGRs for both SF_C and LF_C groups estimated from the total mass growth with respect to the total survival time. For the 20 fish that had DST implantations, we analysed the impact of insertion on mean survival. The tag to fish weight ratio (R) was calculated as:

$$R = W_{DST}/W_0*100 \quad \text{(Eqn 3)}$$

where W_{DST} is the DST weight in air and W_0 the fish wet weight. Two groups were considered: R1 with R <2% and R2 with R $\geq$ 2% (Winter 1983).

Measurements of length, weight and SGR expressed as average ± standard deviation (SD), were compared using ANOVA or t-tests with treatments and group size as factors after data had been tested for normality. Estimates of condition factors were compared using Kruskal-Wallis test (KW). Survival analysis was conducted using Kaplan-Meier analysis with respect to treatment and group size. However, as the initial condition (K_0) impacts fish survival, we also applied Cox regression analysis with K_0 as covariable. Spearman's rank correlation was used to test the relationship between an individual's initial condition factor and survival rate. Statistical analyses were performed using SPSS 14.0. (SPSS, USA) and the significance level was set at $P < 0.05$.

Results

Analysis of initial fish characteristics according to treatment and group size

At the end of the acclimation period, 68% of fish had an initial condition factor (Kt0) greater than 100%. Thus, we considered that acclimazation to rearing conditions had been achieved for most individuals after 7 months. At the beginning of the experiment, Kt0 ranged from 71% to 127% and three Kt0 classes (<80%, 80-100% and >100%) were considered for each group and treatment (Table 1). The initial condition factor did not differ (a) between groups (Table 1, KW Test: df = 1, P= 0.906), or b) between treatments (Table 1, KW Test: df = 2, P= 0.400).

			Group		Total
			Small fish	Large fish	
Treatment	control	Kt0 < 80%	0	20	10
		Kt0 80-100%	10	20	15
		Kt0 >100%	90	60	75
		Total	**100**	**100**	**100**
		Average Kt0 ± SD	105.2 (± 6.7)	100.3 (±15.5)	102.7 (±11.9)
	CT	Kt0 < 80%	10	30	20
		Kt0 80-100%	30	10	20
		Kt0 >100%	60	60	60
		Total	**100**	**100**	**100**
		Average Kt0 ± SD	99.2 (± 11.9)	96.1 (± 16.7)	97.7 (± 14.2)
	DST	Kt0 < 80%	20	10	15
		Kt0 80-100%	10	20	15
		Kt0 >100%	70	70	70
		Total	**100**	**100**	**100**
		Average Kt0 ± SD	100.3 (± 15.2)	102.9 (± 14.7)	101.6 (± 14.6)
		Average Kt0 ± SD	101.6 ± 11.7	99.7 (± 15.4)	

Table 1: Percentage of fish with an initial condition factor (Kt0) in each size group and the average value of Kt_0 (%) (± standard deviation SD %) with respect to each size group (SF and LF) and treatment group (C: control, CT: conventional tag, DST: data storage tag).

Effect of tagging on survival

Out of the initial 60 fish, 21 were survived until the end of the experiment (day 128), which corresponds to an overall survival rate of 35%. Kaplan-Meier survival functions with respect to treatments (C, CT and DST) and size groups (SF and LF) showed that, regardless of fish size, tagging (CT or DST) severely decreased survival probability compared to the control group (Figure 1). Mortality was observed 50 days after tagging and after this time period mortality stabilized in at least the SF group. It is worth noting that, for both SF and LF groups, survival proportion did not differ significantly between CT and DST groups (Log

Rank tests: SF: $P_{C/CT}$=0.017, $P_{C/DST}$=0.07, $P_{CT/DST}$=0.777; LF: $P_{C/CT}$=0.021, $P_{C/DST}$=0.003, $P_{CT/DST}$=0.705). Moreover, it is worth noting that no mortality has been observed in anaesthetized groups during the preliminary experiment after 24 days.

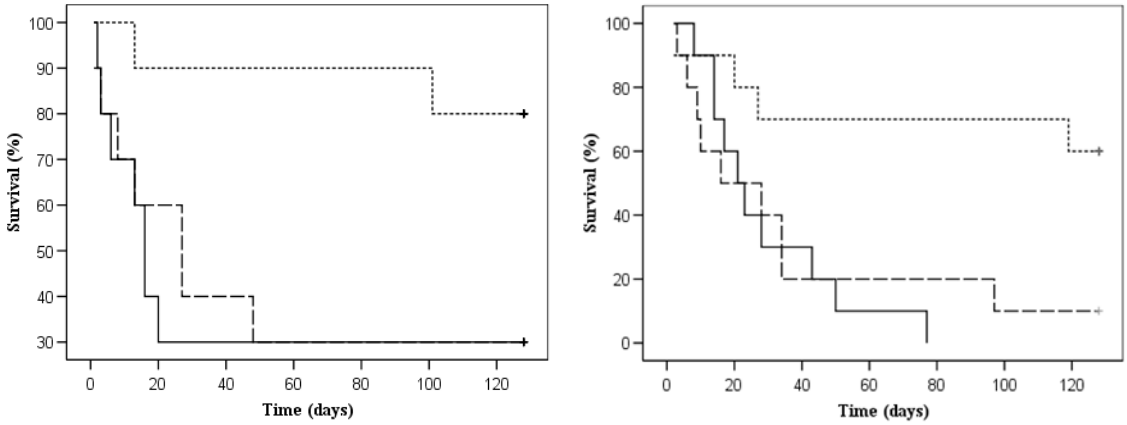

Figure 1: Kaplan Meier survival functions for (A) small fish (SF) and (B) large fish (LF). Control (dotted line), Conventional tagging (dashed line), DST tagging (solid line).

The initial condition Kt0 had a clear effect on the survival rate of fish. The seven tagged fish that had a Kt0<80, all died within the first 28 days. The correlation between survival time and Kt0 was significant when all tagged fish were considered (Spearman correlation test, N = 40, P= 0.006), whereas no significant correlation was observed if fish with a Kt0≤80 were removed from the statistical analysis. Cox regression analysis (Figure 2) indicated that DST tagging may slightly decrease the survival probability compared to conventional tagging.

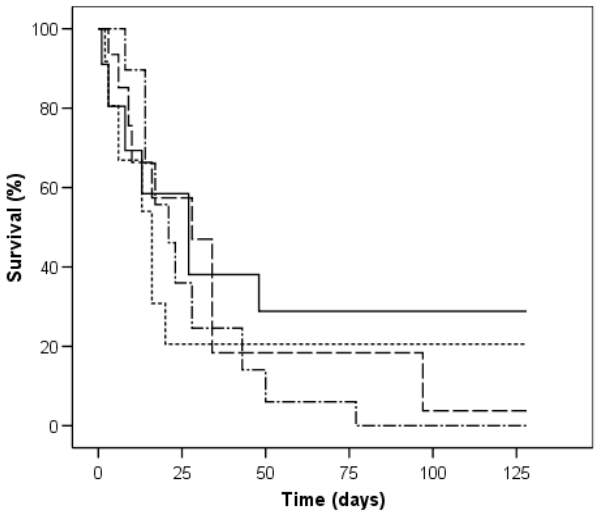

Figure 2: Survival functions with respect to fish size and tagging method derived from the Cox regression with initial condition factor as a covariate. Small Fish – Conventional Tagging (SF-CT, solid line), Small Fish – DST Tagging (SF-DST, dotted line), Large Fish – Conventional Tagging (LF-CT, dashed line), Large Fish – DST Tagging (LF-DST, dash-dotted line).

The R ratio also affected survival rate. Survival differed significantly between R1 and R2 (Log Rank tests: $P_{R1/R2}$=0.023) and actually, all fish with R>2% died rapidly after tagging (Figure 3).

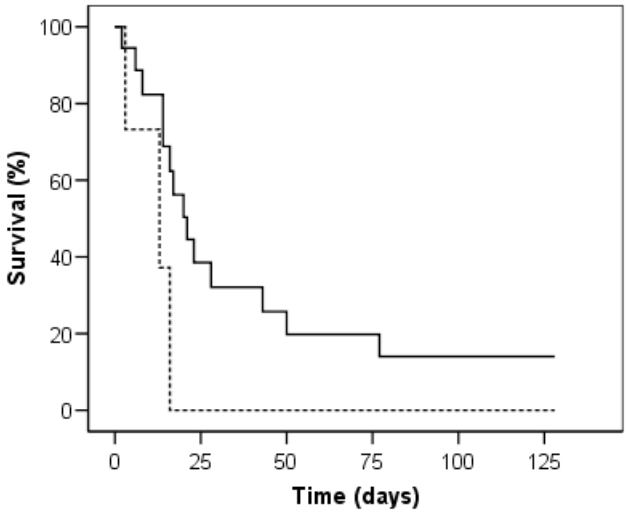

Figure 3: Survival functions of DST tagged fish for different tag to fish weight ratios (R) derived from Cox regression with initial condition factor as covariate. R<2% (solid line), R≥2% (dotted line).

Effect of tagging on growth

Determining the effects of tagging on fish growth was limited by two factors. First, survival at the end of the experiment was low for tagged groups (CT, DST), especially for the LF group (Figure 1). Second, the control fish were not tagged. The total masses of SF_C group were 1804.5 g and 2813.0 g at the start and the end of experiment, respectively. The survival time for this group was 1138 days and the SGR was estimated at 0.039 % day^{-1}. The corresponding data for the LF_C group was respectively 3428 g, 4066 g and 936 days resulting in a SRG of 0.018 % day^{-1}.

Group _ treatment		SGR	W_{t0}	W_{tf}
SF_CT	N	10	10	10
	Mean	-1.7	174.6	181.9
	Standard deviation	1.1	11.6	12.9
	Minimum	-9.7	95	129
	Maximum	0.8	240	248
SF_DST	N	10	10	10
	Mean	-0.7	195	214.6
	Standard deviation	0.5	13.9	28.8
	Minimum	-4.1	110	97
	Maximum	0.7	256	443
LF_CT	N	10	10	10
	Mean	-0.3	314.7	304.2
	Standard deviation	0.3	21	23.8
	Minimum	-2.6	212	196
	Maximum	0.2	423	415
LF_DST	N	10	10	10
	Mean	-0.1	325.1	320.7
	Standard deviation	0.1	27.8	32.3
	Minimum	-0.6	196	190
	Maximum	0.2	503	520
Total	N	40	40	40
	Mean	-0.7	252.4	255.4
	Standard deviation	0.3	14.4	15.4
	Minimum	-9.7	95	97
	Maximum	0.8	503	520

Table 2: Growth characteristics with respect to size group (SF and LF) and treatment group (CT: conventional tag, DST: data storage tag). SGR: specific growth rate (in % $days^{-1}$), W_{t0}: initial weight (g) and W_{tf}: final weight (g).

Statistical analysis of the tagged groups revealed relatively high individual growth variability regardless of the size and treatment group (Table 2). Negative SGR were observed for fish that had a very poor initial condition and died rapidly after tagging (Figure 4). It is worth noting that one fish in poor initial condition survived until the end of the experiment (Figure

4). Comparisons of SGR between control and treatment fish showed that tagging did not significantly affect the SGR (t-tests, df = 9, P_{SF_CT} =0.145, P_{SF_DST} =0.117, P_{LF_CT} =0.197, P_{LF_DST} =0.346).

Progressive feeding resumption occurred after 7 days post tagging. It started at a low level (0.5 prey day^{-1} per fish) and then increased to 1 prey day^{-1} per fish. The first week post tagging could thus be considered as a critical period characterized by fasting and death of fish that had poor initial condition.

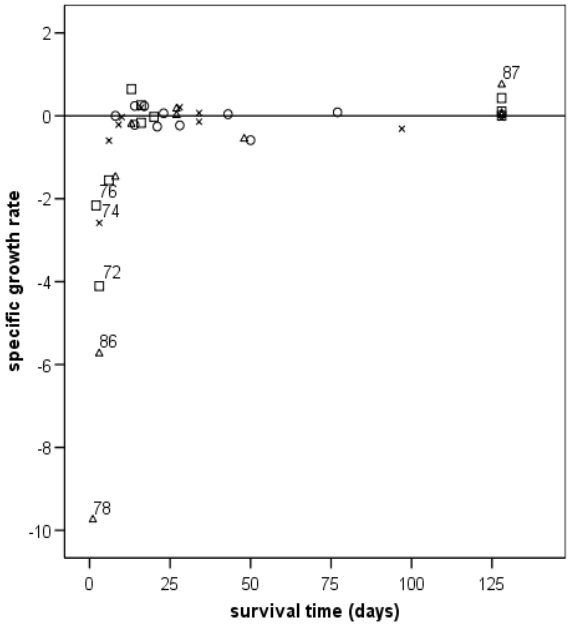

Figure 4: Time distribution of Specific Growth Rates (SGR) estimated at fish death for different fish size and tagging methods: Small Fish – Conventional Tagging (SF-CT, Δ), Small Fish – DST Tagging (SF-DST, □), Large Fish – Conventional Tagging (LF-CT, ×), Large Fish – DST Tagging (LF-DST, ○). SGR individual values are specified for fish that had a particularly poor initial condition.

Discussion

Effect of tagging on survival

Anaesthetics doses applied to European hake during our experiments (100-120 mg l^{-1}), correspond to the upper limit of those reported for other species (Soivio et al. 1977; Iwama et al. 1989; Iversen et al. 2003). Considering the required doses and deep anaesthesia induction time, hake seems to be relatively resistant to anaesthesia.

The first fact to be considered is that handling and anaesthesia might well be more harmful than expected from the short term (24 days) preliminary experiment as the mortality rate reached 30% in control group. The different mortality rates observed in the LF and SF groups also suggests that the former is more sensitive (40% against 20% for LF and SF respectively). We hypothesize that poor initial condition is a factor limiting survival for some fish, although direct evidence is missing because control fish were not individualized. The low ambient temperature (9°C) at the beginning of the experiment may have also been partly responsible for difficult recovery. Actually subsequent pilot tests have demonstrated that winter is not the best period for supplying experimental facilities with wild hake (de Pontual et al. unpublished data).

In terms of conventional tagging, survival rate was 30% for small tagged fish against 70% for the control group. These results confirm the observations made on controls regarding the higher ability of small fish to resist to physical stress. These results also indicate that, the CT tagging process has a strong effect on survival probability. This could be explained both by species-specific response and a sub-optimal tagging protocols. However, several studies have demonstrated negative effects of tag application to wild and hatchery fish on survival, in particular on salmon (Saunders and Allen 1967; Isaksson and Bergman 1978; Hansen 1988; Moffett et al. 1997; Crozier and Kennedy 2002). Another important consideration is the duration of the experiment. Two periods can be distinguished in terms of the fish mortality

rates. The first mortality phase extended to about 50 days post tagging (handling and tagging effects), whereas the second phase occurred at the end of the experiment (fish probably died due to nutritional stress because of unsuccessful feeding resumption, see below). Such a result questions the reliability of short term experiments, which may well provide biased estimations of mortality. This is the case for very short term (2-5 days) experiments held on research vessel during tagging surveys (*e.g.* de Pontual et al. 2003a for European hake). This issue has also been emphasised for short term (5-10 days) experiments in submersible enclosures (Brattey and Cadigan 2004). To best estimate port-release mortality rates for tagged fish, individual fish must be observed for longer periods of time.

A higher mortality rate in DST tagged fish than CT fish could result from the invasive surgery. Surprisingly survival probabilities in DST and CT fish were similar at least in small fish. The removal of a probable Kt_0 effect only slightly decreased the survival probability. However, the tag to body weight ratio (R) has an effect on hake survival. This is in accordance with earlier work showing higher mortality and/or reduced swimming performance in DST-tagged fish (Marty and Summerfelt 1986; Greenstreet and Morgan 1989; Peake et al. 1997; Adams et al. 1998). Our results confirm that this ratio should not be greater than 2% (Stasko and Pincock 1977; Winter 1983) even if the question is challenged (Jepsen et al. 2005). Based on the hake length-weight relationship (Dorel 1986), Star-Oddi DST micro tags should not be placed on a body wet weight less than 180 g, which corresponds to a total length of approximately 30 cm.

Effect of tagging on growth

Food resumption started only 7 days post-tagging and progressively increased after this period. Food consumption remained low relative to fish in other stocking tanks until c.a. 100 days post tagging. Consequently, we can hypothesize that fish first experienced a weight

loss phase due to fasting. This assumption is supported by a strong negative SGR of fish that died early in the experiment. The recovery process may have been longer than in nature as mark-recapture results indicated that fish stopped growing for 20-50 days after release (de Pontual *et al.* 2006). This might relate to upset feeding behaviour as hake acclimation on inert preys had proved to be a challenging process. It may also explain the difference observed in the growth rates estimated in this study (0.013 ± 0.016 cm d^{-1}) and estimates obtained from field experiment (up to 0.054 ± 0.004 cm d^{-1} for fish which had one year or more at liberty; de Pontual et al. 2006). An important outcome of the present work is that growth did not differ significantly between control and tagged fish. This result corroborates the findings of previous works on species such as European sea bass (Bégout Anras et al. 2003), juvenile cod (Jensen 1967; Tranquilli and Childers 1982; Svåsand et al. 1990; Cote et al. 1999), and adult cod (Righton et al. 2006). The latter concluded that tagging had no long term effect on growth except on the gonads mass, where tags could potentially occupy the space for gonad growth (Righton et al. 2006).

Conclusion

In this study, the first estimates of post tagging mortality were established and these results suggest mortality after tagging might be high in field experiments. They have to be refined before mark-recapture data can be used to estimate exploitation rates and population sizes. Our results also suggest that improvements in tag implantation could increase post tagging survival rate. Contrary to initial predictions, similar survival rates were observed for fish tagged with DST and conventional tags. Recovery rate close to that of conventional tagging can reasonably be expected. Results also emphasize the need for a thorough fish selection prior to DST tagging based on fish size and initial condition. Small fish with a high initial condition would be the most suitable for future tagging studies in the field. Actually,

criteria derived from this experiment have provided suitable basis for a successful field pilot study which analysis is ongoing (de Pontual et al. unpublished data).

Acknowledgements

The authors are thankful to M. Suquet for his help during experiment and fruitful discussion on hake rearing. Furthermore, we thank H. Arrizabalaga, N. Jepsen, I. Quincoces and an anonymous referee for their reviews and B. Graham for improving the language. This study was conducted under the approval of the Animal Care Committee of France under the official licence of M.L. Bégout (17-010).

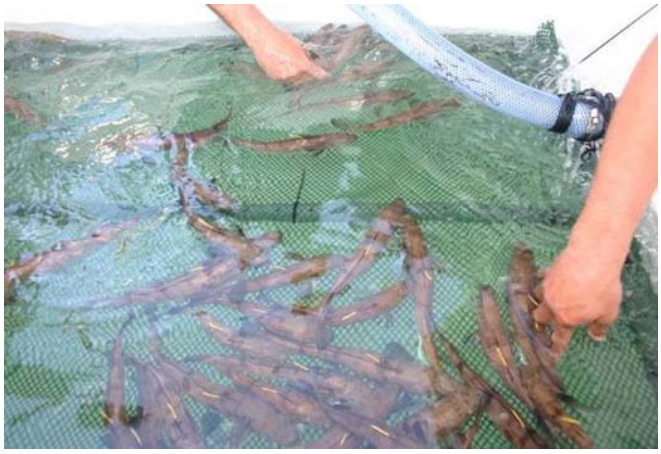

Chapitre 2 :

Vers une domestication du merlu européen : croissance en fonction de l’alimentation et de la température

Chapitre 2 :

Vers une domestication du merlu européen : croissance en fonction de l'alimentation et de la température

Les données sur la croissance du merlu proviennent essentiellement des expérimentations en milieu naturel confirmant l'hypothèse de croissance rapide. En milieu contrôlé, aucune étude à notre connaissance ne porte sur la croissance du merlu adulte et seuls les résultats d'un essai d'élevage larvaire ont été publiés. La difficulté à maintenir le merlu en captivité résulte de sa grande sensibilité à la manipulation et de la difficulté à le maintenir en bassin.

Une expérience en milieu contrôlé a été menée à partir de merlus pêchés en milieu naturel en juillet 2006 et acclimatés en bassin de $15m^3$. Deux classes de tailles distinctes sont considérées : un lot d'individus de petite taille, nommé SF (longueur totale moyenne ± écart type : 28.5 cm ± 1.4) et un lot d'individus de grande taille, nommé LF (longueur totale moyenne : 33.6 cm ± 2.3). L'expérimentation s'est divisée en deux périodes de 4 mois. La première a débuté par un marquage des poissons suivi par des phases d'acclimatation et de récupération en bassin de $15m^3$. Pendant la seconde période, les poissons sont maintenus en bassins de $2m^3$ où ils ont subis deux traitements de température à 9 ou 13°C.

Les premiers résultats de cette étude mettent en évidence une forte mortalité lors de la période d'acclimatation confirmant la grande sensibilité du merlu à la manipulation et au marquage et le manque de connaissances sur les conditions adéquates pour l'élevage du merlu. Ce manque de connaissance concerne en particulier les conditions de nourrissage.

L'inadéquation de trop faibles densités en proies et en merlus dans les bassins est démontrée pour le lot des petits individus SF qui étaient sous-alimentés.

La température a montré des effets diverses suivant les classes de taille. Ainsi les individus de petite taille ont été capables de récupérer des conditions de sous-alimentation de la première période et ont montré des taux de croissance supérieurs à ceux des plus grands individus lors de la deuxième période dans les deux conditions de température testées. Ceci a pu être associé soit à un mécanisme de compensation soit à la capacité de forte croissance des jeunes individus. Les plus grands individus ont semblé s'acclimater plus facilement aux conditions d'élevage et ont montré des taux de croissance et une prise alimentaire journalière corrélés à la température.

Bien que les conditions d'élevage n'aient pas paru optimales du fait du caractère innovant de cette expérience, certains poissons ont montré de forte croissance et ont été capable de doubler leur poids en 4 mois. Ces données confirment les résultats issus des campagnes de marquages. Ils mettent aussi en exergue le fort potentiel de croissance de cette espèce, qui pour un objectif d'aquaculture s'avère comparable à celui de la morue.

Towards domestication of European hake: relationships of growth with dietary and temperature

Aurélie Jolivet, Hélène de Pontual, Magali Hervy, Yves-Marie Paulet, Ronan Fablet

Soumis à Aquaculture

Abstract

Controlled experiments were conducted to assess the effects of temperature and feeding conditions on growth of European hake. Two size groups of wild-caught hake were considered: small fish (SF, average total length ± standard deviation: 28.5 cm ± 1.4) and large fish (LF, average total length ± standard deviation: 33.6 cm ± 2.3). The study was divided into two successive 4 month periods: a period of acclimatisation where fish were kept at 12 °C in 15 m^3 tanks, followed by a temperature experiment where fish were kept at 9 °C or 13 °C in 2 m^3 tanks. Relatively high mortality was observed during the acclimatisation period reflecting both the sensitivity of hake to handling and tagging (pit tags) and the lack of knowledge regarding appropriate rearing conditions for this species. In particular, feeding conditions (low prey density) proved to be inappropriate for the smaller fish, some of which probably starved. The subsequent effect of temperature in the experiment differed with respect to size groups. The smaller fish were able to recover from adverse conditions and actually presented higher growth rates than the larger fish, whatever the temperature treatment. This could be due to a compensation mechanism and/or to the higher growth rate of younger fish. The larger fish were well acclimated to rearing conditions and showed growth rates and daily food intake correlated with temperature. Although the rearing conditions were probably suboptimal, as this study is one of the first on this species, some fish were nevertheless able to double their weight in less than 4 months. This growth potential is comparable to that of Atlantic cod, a result with important implications both for fish aquaculture diversification and fisheries management.

Introduction

European hake, *Merluccius merluccius*, is a demersal fish with a wide natural distribution spreading from the west coast of Norway southwards to the coast of Mauritania and eastwards into the Mediterranean Sea. Bathymetric distribution of this species ranges from a few metres in coastal areas to more than 500 m depth (Casey and Pereiro 1995). Hake is among the major, most heavily exploited demersal resources in the North East Atlantic, and total landings have decreased from 120 000 t in the early 1960s to 50 000 t in recent years (ICES 2005). It was recently demonstrated that hake is a fast growing species, both in the Atlantic (de Pontual *et al.* 2006; Piñeiro *et al.* 2007; Piñeiro *et al.* 2008) and the Mediterranean Sea (Belcari *et al.* 2006; Mellon *et al.* submitted). Our knowledge about this species is thus being re-examined, especially regarding basic life history traits such as age and growth and their variation in relation to environmental factors such as temperature. These issues are of key importance for the sustainable exploitation of this marine resource (Bertignac and de Pontual 2007).

Moreover, it has been reported that hake can reach 140 cm total length and 15 kg weight (Cohen *et al.* 1990). Combined with their high growth rate, this potential makes hake an interesting candidate species for gadiform aquaculture diversification (Quémener *et al.* 2002), currently focused on Atlantic cod (Gadus morhua). Growth rate of cod is highly determined by temperature (Jobling 1988; Brander 1994; Björnsson *et al.* 2001) and optimal temperature has been found to decrease with increasing weight (Björnsson *et al.* 2001). It would therefore be of great interest to evaluate the effects of temperature on growth in hake.

Our knowledge about the biology of Atlantic hake, from early stages to adulthood, is scarce and relies mostly on analysis of biological material from the wild (Casey and Pereiro 1995; Alvarez and Cotano 2005; Kacher and Amara 2005; de Pontual *et al.* 2006; Murua *et*

al. 2006; Murua and Motos 2006). Very few experiments have been conducted on hake under controlled conditions as the species is sensitive to capture and handling. Basic information on stages from egg incubation to weaned larvae was provided by Bjelland and Skiftesvik (2006), while Jolivet et al. (in press) reported the first experiment carried out on juvenile and adult hake in captivity.

The present study was carried out on wild-caught fish acclimatized to captivity for 7 months at 12 °C and then observed at two rearing temperature conditions: 9 and 13 °C. We had four objectives for the overall study, of which the first two are the focus of the present paper:

- 1) Analysis of the effect of temperature on growth, in the range 9-13 °C commonly observed in the field (sea bottom temperature).
- 2) Analysis of the relationship between food intake and temperature.
- 3) Marking of otoliths at defined dates under known rearing conditions in order to subsequently analyze the relationship between otolith opacity and temperature. Such knowledge is required for a better understanding of the complex otolith macrostructure pattern in this species (de Pontual *et al.* 2006a).
- 4) Providing validated data for the calibration of a bioenergetic model (DEB) of hake growth, subsequently used for the characterization and modelling of the PCB bioaccumulation process in Mediterranean hake (Bodiguel *et al.* submitted).

The experimentation described here therefore concentrated on the effects of temperature, food intake and their interaction on somatic growth of European hake. As the species is not yet farmed, and as it is known to be sensitive to stress from handling and tagging (Jolivet *et al.* in press), survival results were recorded for both the acclimatisation period and the temperature experiment. Results are discussed and compared with observations

made on hake in the wild using tag recapture experiments (de Pontual *et al.* 2006), and with growth performances of reared cod.

Material and Methods

Acclimatisation period

Fish were caught in the Bay of Biscay in mid-July 2006 using a method developed for mark-recapture experiments by de Pontual et al. (2003a). To acclimatize the fish to rearing conditions, individuals were first sorted by size range to avoid cannibalism and kept in 15 m^3 circular tanks. These tanks were supplied through-flowing seawater at a controlled temperature (12 °C ± 0.5). The daily water renewal was about 20 %, and the light regime followed the natural photoperiod. Fish were fed *ad libitum* on forage fish. Between mid-October and mid-December 2006, all fish were tagged individually. The tagging procedure consisted of: 1) sedation in the 15 m^3 tank with benzocaine at a concentration of 10 mg l^{-1} for 20 min; 2) anaesthesia in a 100 l tank with benzocaine at a concentration of 80 mg l^{-1}; 3) measurement of total length (TL_0 in mm) and weight (W_0 in g); 4) insertion of a pit tag (Réseaumatique ©: 11.5 mm x 2.1 mm, 95 mg in air) at the base and in front of the second dorsal fin using a gauge hypodermic needle and syringe; and 5) injection with a veterinary solution of oxytetracycline at a dose of 60 mg kg^{-1} body weight. This antibiotic is commonly used to mark otoliths for validating ageing methodology (Wright *et al.* 2002a). Fish sorted by size range were then transferred in two 15 m^3 tanks: tank A for small fish and tank B for large ones (Fig.1). Conditions of sedation and anaesthesia were designed based on previous pilot experiments at 9 °C (Jolivet *et al.* in press), corrected for use at 12°C. Temperature in tanks A and B was 12 °C ± 0.5. Hereafter, we will refer to the pit-tagging date as T_0.

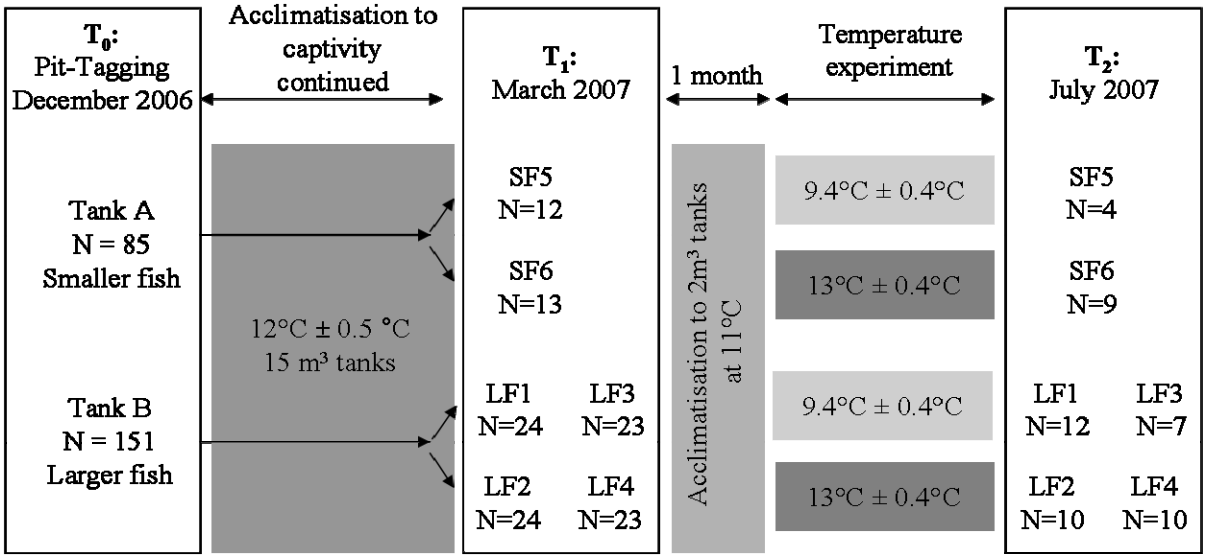

Figure 1: Diagram showing the time course of the experimental stages: acclimatisation and temperature experiment, with the corresponding rearing conditions. Note that the acclimatisation process actually started five months earlier since fish were caught in July 2006.

Temperature experiment

The temperature experiment started on February 27th, 2007 (hereafter referred to as T_1) and lasted until July 5th, 2007 (T_2). At T_1, fish were sedated before transfer to a 100 l tank for anaesthesia as described above. Total length (TL_1, mm) and weight (W_1, g) were recorded and fish were again tagged with oxytetracycline. The fish of the two groups then were divided among new experimental tanks of 2 m^3. Their average total length and weight ± standard deviation at T_1 were as follows: SF (tank A) TL_1= 29 cm ± 1.5 and W_1 = 151.2 g ± 29.8, N = 25; LF (tank B) TL_1= 36.4 cm ± 3.4 and W_1 = 368.3 g ± 138.8, N = 96. Within each size group, fish were randomly assigned to two temperature treatments (9 and 13 °C). The available number of fish allowed us to have two replicates per temperature for the LF group

but only one for the SF group (Fig. 1). Replicates were homogenous in size and weight (ANOVA $P > 0.05$). The experiment itself was conducted four weeks later in six 2 m^3 tanks under natural photoperiod, but water temperature was first maintained at 11°C until April 1st 2007 to acclimate fish to their new rearing conditions (2 m^3 tanks). After this date, the temperature was gradually changed to the test conditions. Temperature did not vary significantly with time or between tanks during the experiment. It averaged respectively 9.4 °C ± 0.4 and 13 °C ± 0.4 despite two thermal disturbances of 24 hours that caused a drop of 2.5 °C in the 13 °C tanks in May and an increase of 2 °C in the 9°C tanks in June, due to a pipe rupture. Dissolved oxygen was recorded daily and remained above 94 % saturation. Fish were fed *ad libitum* on forage fish and the consumption was estimated daily for each tank, based on the number and weight of the preys provided and the number left unconsumed. At the end of the experiment fish were killed with an overdose of anaesthetic, and were then measured (TL_2 and W_2) and sexed. Maturity was assessed based on macroscopic observations. Immature fish were assigned to stage I and fish showing gonadal development to stage II. Livers were weighed and muscle samples were taken for future bioenergetics analyses. The sacrificed fish were deep frozen as were those that died during the course of the experiment.

Parameters analysed

For each tank, Daily Food Intake (DFI) was calculated as the ratio between the estimated weight of food (g) consumed daily and the number of hake in the tank. The daily biomass in each tank (g m^{-3}) was estimated from initial weight, final weight and mortality data. The Feed Conversion ratio (FC) was calculated for each period, temperature treatment

and tank, as was the ratio between total food intake and biomass increase. This estimation, expressed in g of prey per g of fish biomass, only took into account surviving fish only. The condition index of individual fish was calculated as in Wege and Anderson (1978) and in Jobling et al. (2001):

$KT_t = W_t/W_e x100$ (Eqn 1)

where W_t is the weight of the fish at time t and W_e is the theoretical weight calculated from the length-weight relationship derived from field measurements: W_e (g) = 0.00513 $L^{3.074}$ (Dorel 1986). Individual growth rate GR (cm day^{-1}) was determined as:

$GR = (TL_{tf} - TL_{ti})/(t_f - t_i)$ (Eqn 2)

and the Specific Growth Rate SGR (% day^{-1}) was calculated as (Houde and Schekter 1981; Nordgarden *et al.* 2003):

$SGR = (e^g - 1)\ x100$ (Eqn 3)

where $g = [\ln(W_{tf})-\ln(W_{ti})]/(t_f-t_i)$]. W_{tf} and W_{ti} respectively denote the wet body weight (g) at t_f (end of a given period, T_1 or T_2, or date of fish death) and t_i (beginning of the corresponding period, i.e. T_0 or T_1), and TL_{tf} and TL_i denote the associated total lengths (cm).

Data analysis

Fish data, namely total length (TL), weight (W) and condition index (KT) are expressed hereafter as average ± standard deviation SD. These parameters were indexed 0, 1 or 2 depending on the reference time considered i.e. Pit-tagging (T_0), beginning of the temperature experiment (T_1) or end of the experiment (T_2). Data reported here only refer to

survivors at the end of each period. Statistical analyses were carried out with ANOVA and T-tests if homogeneity of variances was demonstrated by a Levene-test, otherwise data were analyzed with Kruskal-Wallis tests. For the temperature experiment, a Kaplan-Meier analysis was performed to compare survival probabilities between the groups of small and larger fish, and temperature treatments. Cox regression analyses (CRM) were performed using three successive covariables, namely initial condition index, initial size and sex. It is worth noting that these models permit the inclusion of censured data, for instance fish that accidentally died during the course of the experiment. This was the case for some fish that jumped out of tanks, which are subsequently referred to as "suicides".

Results

Period of acclimatisation to captivity (12 °C)

1. Survival

The first tagging, referred to as T_0, was carried out in three different sessions during the period from October and December, resulting in intervals from T_0 to T_1 of 125, 105 or 76 days. A survival time of 76 days post T_0 was used as a reference. After 76 days, 15 % and 38.4 % of the hake in tanks A and B had survived, respectively. Survival was not affected by initial condition or gender (CRM: $P>0.05$).

2. Growth and condition

At T_0, fish size and weight (Table 1) were significantly different between tanks A and B ($P < 0.001$). During acclimatisation, the averaged biomass of tank B (2429.4 g m^{-3} ± 183.5) was significantly higher than that of tank A (430.7 g m^{-3} ± 142.1, $P<0.001$). Feeding behaviour differed significantly between the two tanks, as indicated by DFI: estimated at 0.474 g day^{-1} $fish^{-1}$ and 3.078 g day^{-1} $fish^{-1}$ in tanks A and B, respectively.

Growth rates (GR and SGR) also differed significantly between tank A (small fish) and B (large fish) with greater growth rates in the latter. Moreover condition of the fish in tank A decreased by 5.5 % whereas it increased by 6 % in tank B. During this acclimatisation period, no significant difference between males and females was detected in the two size groups. Interestingly, the maximum individual growth rate observed during acclimatisation was 0.101 cm day^{-1}, corresponding to a SGR of 1.14 % day^{-1}, for a fish from tank B. This particular fish measured 33.3 cm for 243 g at T_0 and 41 cm for 577 g at T_1, 76 days later.

Tanks	time	N	TL	W	KT	GR	GR max	SGR	DFI	FC	BIOMASS
A	T_0	25	28.5 ± 1.5	149.6 ± 21.6	97.8 ± 7.7				0.474 ± 1.356	43.2	430.7 ± 142.1
	T_1	25	29 ± 1.5	151.2 ± 29.8	94.1 ± 14.2	0.005 ± 0.008	0.026	0.0012 ± 0.20			
B	T_0	94	33.7 ± 2.1	260 ± 54.6	100.9 ± 7.6				3.078 ± 4.137	2.8	2429.4 ± 183.5
	T_1	94	36.4 ± 3.4	367.8 ± 139.2	109.1 ± 13.3	0.024 ± 0.2	0.101	0.283 ± 0.27			

Table 1: Overall characteristics (average ± SD) of hake before, after and during the acclimatisation period at 12 °C, given for fish that survived throughout study in size groups SF (tank A) and LF (tank B) at T_0 (pit tagging) and T_1 (beginning of the temperature experiment): number of individuals (N), total length (TL: cm), weight (W: g), condition index (KT: %), growth rate (GR: cm day $^{-1}$), specific growth rate (SGR: % day^{-1}). Daily food intake (DFI), the food conversion (FC) and the biomass (g m^{-3}) correspond to the average values over the acclimatisation period.

Temperature Experiment

1- Survival

Out of an initial 94 large fish and 25 small fish at T_1, 39 (41.5 %) and 13 (52 %), respectively, survived to the end of the experiment (day 128). Seven of the fish that died during the experiment were 'suicides': 2 in tank LF1 (8 %), 1 in LF2 (4 %) and 4 in SF5 (33 %). Five of these suicides occurred because of a pipe rupture that reduced the water level. Kaplan-Meier survival functions did not show any significant differences between size groups (SF and LF) or between tanks within each size group (Fig. 2).

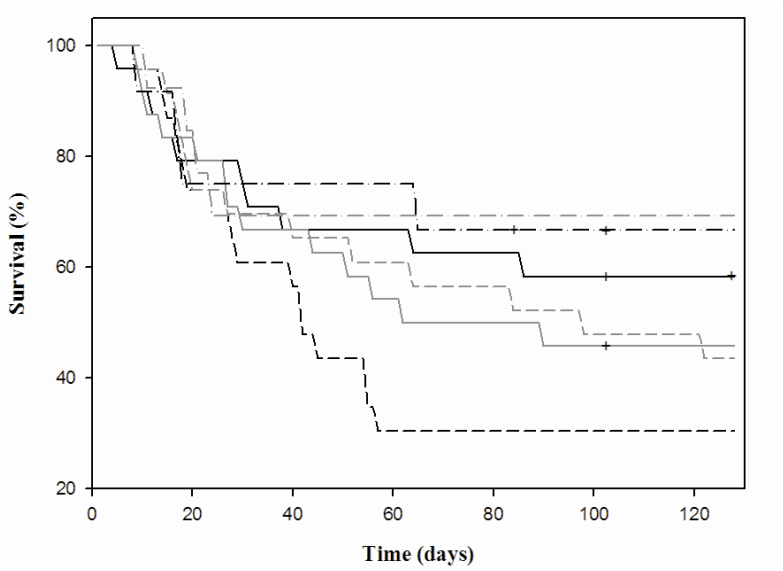

Figure 2: Kaplan-Meier survival functions during the temperature experiment with respect to tanks: LF1 (dark solid line), LF2 (grey solid line), LF3 (dark dashed line), LF4 (grey dashed line), SF5 (dark dash-dotted line), SF6 (grey dash-dotted line). Suicides are indicated by a cross.

However, one of the tanks of large fish (LF3) showed a particularly low survival rate due to the death of seven fish during April. A period of mortality occurred during the first 60

days of the temperature experiment. after which this stabilized in both size groups. At the beginning of the temperature experiment, condition index KT_1 ranged from 71 % to 132 % and three KT_1 classes (< 80 %, 80-100 % and >100 %) were considered for each size group and temperature treatment (Table 2).

		KT_1 classes				
		KT_1<80%	KT_1 80-100%	KT_1>100%	Total	Average KT_1 ± SD
Large Fish	LF1	0	12.5	87.5	100	111.7 ± 10.5
	LF2	8.3	25	66.7	100	107.1 ± 16.5
	LF3	4.3	17.4	78.3	100	107.8 ± 13.8
	LF4	0	21.7	78.3	100	109.6 ± 12.3
	Total	**3.2**	**19.1**	**77.7**	**100**	**109 ± 13.3**
Small Fish	SF5	33.3	33.3	33.4	100	92.1 ± 15.1
	SF6	7.7	61.5	30.8	100	96 ± 13.5
	Total	**20**	**48**	**32**	**100**	**94.1 ± 14.2**

Table 2: Distribution of fish between condition index classes at the beginning of the temperature experiment (T_1) with respect to size group (SF and LF group) and tank (LF1, LF3 and SF5 at 9 °C; LF2, LF4 and SF6 at 13 °C).

The proportion of fish with a KT_1 below 80 % differed between tanks and significantly affected survival ($P < 0.05$, Fig. 3). Tank SF5 had a greater survival rate than tank SF6, and tank LF3 had a significantly lower survival than the other groups. Sex and temperature, however, did not affect survival rates.

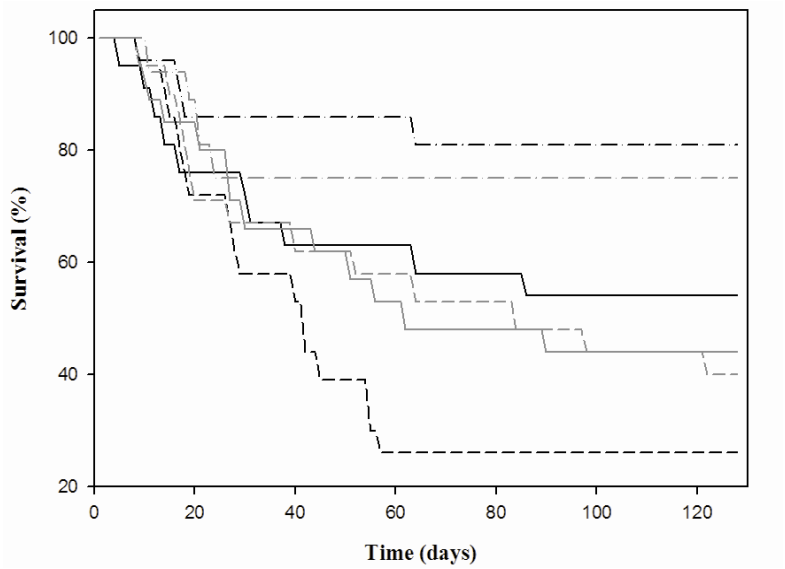

Figure 3: Survival functions derived from Cox regression analysis with the initial condition index as covariate: LF1 (dark solid line), LF2 (grey solid line), LF3 (dark dashed line), LF4 (grey dashed line), SF5 (dark dash-dotted line), SF6 (grey dash-dotted line).

2- Feeding

Food intake resumed four days after T_1 regardless of the temperature treatment. In the SF group, the DFI did not depend on the temperature and was significantly higher during the temperature experiment than it had been during the acclimatisation period. However, the feed conversion ratio at 9 °C was lower than at 13 °C (Table 3). In the LF group, in contrast, this ratio was significantly higher at 9 °C than at 13 °C (Table 3), although temperature had no effect on daily food intake.

Tanks	Temp °C	time	N	TL	W	KT	GR	GR max	SGR	DFI	FC	BIOMASS
LF1	9	T_1	12	38.1 ± 3.9	449.3 ± 164.5	115.8 ± 11.1				2.622 ± 3.456	15.6	3632.4 ± 544.8
		T_2	12	40.2 ± 3.8	470.9 ± 145.6	104.4 ± 5.6	0.016 ± 0.01	0.045	0.051 ± 0.12			
LF2	13	T_1	10	36.1 ± 3.8	363.3 ± 162.4	108.8 ± 15.9				2.477 ± 3.769	3.9	2882.7 ± 572.5
		T_2	10	40.1 ± 5.3	485.2 ± 219.6	104.7 ± 10.5	0.031 ± 0.02	0.07	0.22 ± 0.25			
LF3	9	T_1	7	36.4 ± 2.9	377.3 ± 102.5	114.1 ± 9.8				3.678 ± 4.409	15.7	2067.3 ± 869.7
		T_2	7	38.5 ± 2.6	397.6 ± 70.9	102.7 ± 9	0.017 ± 0.012	0.036	0.055 ± 0.17			
LF4	13	T_1	10	36.5 ± 3.1	370.1 ± 97.9	111.3 ± 11.4				2.938 ± 3.596	3.5	2963.2 ± 525.6
		T_2	10	40 ± 4.1	479.1 ± 174.6	107.5 ± 6.5	0.027 ± 0.017	0.065	0.19 ± 0.17			
LF	9	T_1	19	37.5 ± 3.6	422.7 ± 146	115.2 ± 10.4				2.546 ± 3.172	15.6	5699.7 ± 1397.9
		T_2	19	39.6 ± 3.4	443.9 ± 126.3	103.8 ± 6.8	0.016 ± 0.011	0.045	0.052 ± 0.14			
LF	13	T_1	20	36.3 ± 3.4	366.7 ± 130.6	110.1 ± 13.5				3.309 ± 3.757	3.7	5845.9 ± 1085.4
		T_2	20	40 ± 4.6	482.2 ± 193.1	106.1 ± 8.6	0.029 ± 0.02	0.07	0.20 ± 0.21			
SF5	9	T_1	4	30.3 ± 1.3	171.3 ± 26	93.3 ± 7.7				2.479 ± 3.792	1.6	874.8 ± 86.7
		T_2	4	36.3 ± 2.8	366.5 ± 96.5	112.7 ± 5.1	0.047 ± 0.012	0.063	0.58 ± 0.14			
SF6	13	T_1	9	28.6 ± 1.5	149.9 ± 20.3	97.9 ± 15.5				2.494 ± 3.24	2.4	1044.9 ± 134.2
		T_2	9	33.1 ± 3.2	285.4 ± 109.6	114.2 ± 12.5	0.035 ± 0.02	0.068	0.47 ± 0.22			

Table 3: Characteristics (average ± SD) of hake before (T_1), after (T_2) and during the temperature experiment given for fish that survived throughout study with respect to size group (LF and SF), rearing temperature (°C) and tank: number of individuals (N), total length (TL: cm), weight (W: g), condition index (KT: %), growth rate (GR: cm day $^{-1}$), specific growth rate (SGR: % day^{-1}). The daily food intake (DFI), the food conversion (FC) and the biomass (g m^{-3}) correspond to the average values over the temperature experiment period.

3- Growth rates, condition index and reproductive development

For the LF group, averaged condition index KT_2 was lower than the condition index at the beginning of the experiment but not significantly different. However, some differences were observed when sex and temperature were considered. At 9 °C, females showed a significant drop of 14 % in their KT compared with 2.2 % at 13 °C, while no such shift was observed for males ($P > 0.05$). Conversely, a major increase in condition index was observed in the SF group with 21 % at 9 °C and 17 % at 13 °C. There was no effect of temperature or sex on condition in this group.

During the temperature experiment, somatic growth rate increased strongly in the SF group relative to during the acclimatisation period, but decreased in the LF group (Fig. 4, $P < 0.001$). Most of fish that had very poor initial condition ($KT_1 < 80$ %) died rapidly after T_1 (63 % during the first 20 days) and showed negative SGR. However, it is worth noting that one fish that was in poor initial condition (76.3 %) survived to the end of the experiment and had a relatively high somatic growth rate (0.29 % day^{-1}, Fig.4). On the other hand, a few fish that were in good conditions initially ($KT_1 > 100$ %) did not recover from the handling and tagging process at T_1 and died rapidly, with negative SGR (Fig. 4). Therefore, the somatic growth of the LF group was negatively correlated with condition index KT_1 ($C_{SGR/KT1} = -0.434$, $P = 0.006$). This result contrasts with the SF group for which the somatic growth was independent of condition index KT_1. Most of the 'suicide' fish had shown positive somatic growth rates (Fig. 4).

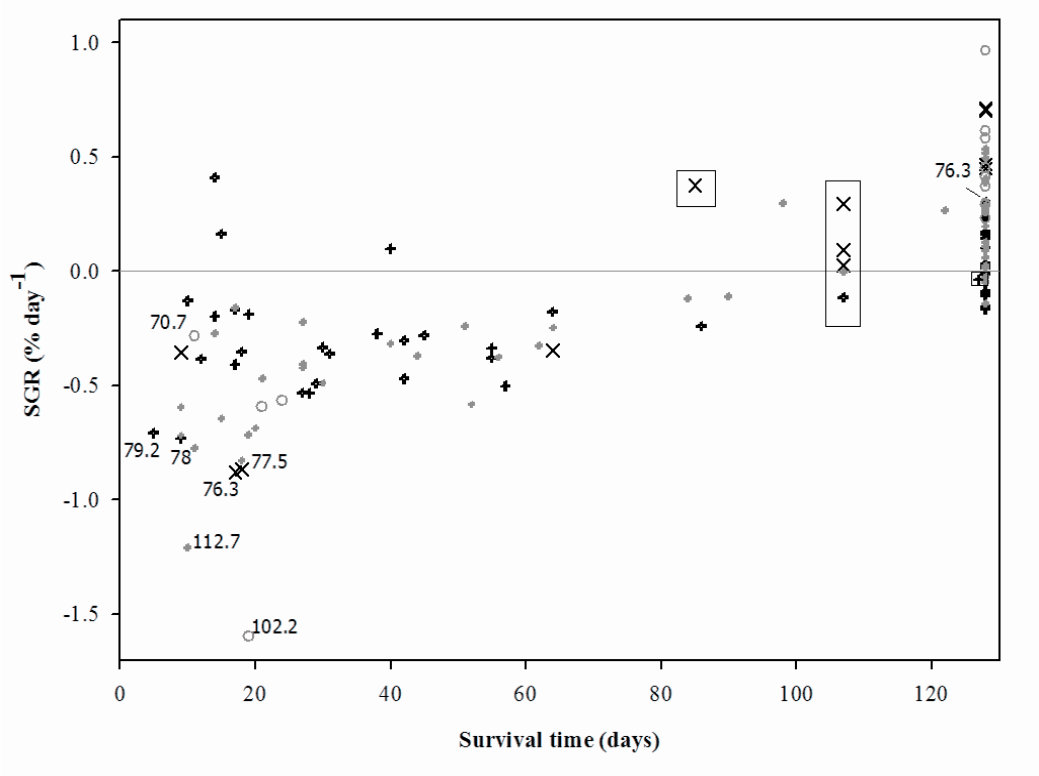

Figure 4: Specific Growth Rate (% day^{-1}) estimated at fish death according to survival time, shown with respect to fish size (LF and SF) and temperature treatments (9 and 13 °C): LF 9 °C (+), LF 13 °C (●), SF 9 °C (×) and SF 13 °C (○). Condition indices KT_1 are given for fish that had very low SGR or for fish that had a very poor initial condition. SGR corresponding to 'suicide' fish are shown in frames.

In the LF group, growth rates (GR and SGR) was significantly higher at 13 than at 9 °C ($P < 0.05$), whereas in the SF group growth rates did not appear to depend on temperature ($P > 0.05$). The maximum observed growth rate during the experimental period was 0.07 cm day^{-1}, corresponding to a SGR of 0.40 % day^{-1}, for a fish from LF2 (reared at 13 °C). This fish measured 39.5 cm for 500 g at T_1 and 48.5 cm for 838 g at T_2, 128 days later.

For the SF group, there was no effect of sex on growth rate within either temperature treatment ($P > 0.05$). In the LF group, females showed higher growth rates at 13 °C than 9 °C (Table 4, $P < 0.05$); no such difference was observed for males (Table 4, $P > 0.05$).

At the end of the experiment, differences were observed in the stage of maturity (Table 4). In the LF group the majority of females showed developing gonads, regardless of temperature, in contrast to the males (Table 4). The fish with developing gonads tended to be those with higher growth rates in both sexes, regardless of temperature (Table 4). In the SF group, fish were mainly immature and only three females showed gonadal development, one at 9 °C and two at 13 °C. Growth rates (GR and SGR) were significantly different and higher for females with developing gonads, in particular at 13 °C ($P < 0.05$, Table 4).

			Males			Females		
Size group	Temp (°C)		Total	Stage I	Stage II	Total	Stage I	Stage II
Large fish	9°C	N	6	0%	100%	13	0%	100%
		GR	0.02 ± 0.01		0.02 ± 0.01	0.02 ± 0,01		0.02 ± 0,01
		SGR	0.11 ± 0.16		0.11 ± 0.16	0.026 ± 0,13		0.026 ± 0,13
	13°C	N	5	60%	40%	15	7%	93%
		GR	0.01 ± 0.01	0.01 ± 0.01	0.02 ± 0.02	0.03 ± 0,02	0,014	0.036 ± 0.02
		SGR	0.04 ± 0.11	0 ± 0.13	0.1 ± 0.01	0.26 ± 0,20	0,023	0.28 ± 0.2
	Total	N	11	27%	73%	28	4%	96%
		GR	0.02 ± 0.01	0.01 ± 0.01	0.02 ± 0.01	0.03 ± 0.02	0,014	0.03 ± 0.02
		SGR	0.08 ± 0.14	0 ± 0.13	0.11 ± 0.14	0.15 ± 0.21	0,023	0.16 ± 0.21
Small fish	9°C	N	0			4	75%	25%
		GR				0.05 ± 0.01	0.04 ± 0.01	0,063
		SGR				0.58 ± 0.14	0.54 ± 0.15	0,702
	13°C	N	2	100%		7	71%	29%
		GR	0.04 ± 0.01	0.04 ± 0.01		0.03 ± 0.02	0.02 ± 0.01	0.06 ± 0.01
		SGR	0.37 ± 0.11	0.37 ± 0.11		0.49 ± 0.25	0.38 ± 0.1	0.79 ± 0.25
	Total	N	2	100%		11	73%	27%
		GR	0.04 ± 0.005	0.04 ± 0.005		0.04 ± 0.02	0.03 ± 0.01	0.06 ± 0.01
		SGR	0.37 ± 0.11	0.37 ± 0.11		0.53 ± 0.21	0.4 ± 0.15	0.76 ± 0.2

Table 4: Characteristics of males and females at the end of the temperature experiment (T_2) with respect to size group (SF and LF group) and rearing temperature (9 or 13°C): number of individuals (N), growth rate (GR: cm day^{-1}), specific growth rate (SGR: % day^{-1}), proportion displaying different maturity stage (%), where stage I corresponds to immature fish and stage II to individuals with developing gonads.

Discussion

Survival

Throughout the period of this study, considering both acclimatisation and the temperature experiment, survival rates reflected that rearing conditions (feeding in particular) were inappropriate for the adaptation of the fish to captive rearing. In this study, each fish was tagged twice: the first time between October and December, with the insertion of a pit tag and an injection of oxytetracycline, and the second time at the beginning of the temperature experiment (T_1, February) with just an oxytetracycline injection. These two tagging events were stressful, but had different effects on the two size groups. A greater effect was observed for the SF group during the acclimatisation period, with a mortality phase extending until about 50 days post T_0 handling and tagging. Survival rates of the large fish were comparable (about 40 %) after each tagging procedures. These survival rates were better than those obtained in a previous pilot experiment (Jolivet *et al.* in press). The impact of tagging has been already demonstrated on salmon (Hansen and Johnson 1988; Crozier and Kennedy 2002). Pit tagging in captivity seems to be less harmful for hake than the type of tagging process used in the wild. Although a pit tag might damage nerves or organs, particularly on small fish, when it is placed in the dorsal musculature, pit tags are easily inserted and have high retention rates (Dussault and Rodrìguez 1997; Hale and Gray 1998; Thomassen *et al.* 2000; Simon and Dorner 2005). The delay between pit tagging and the temperature experiment was designed to favour recovery from the tagging process as well as acclimatisation to new rearing conditions (particularly the smaller tank size).

Effects of condition index KT on survival can be compared to similar experiments on cod, such as the one reported by Dutil et al. (2006). In this past study, it was shown that fish with very low condition indices had difficulty recovering from stresses like starvation. Low

condition indices might have increased the mortality and reduced both the capacity to recover from tagging events and the capacity to feed on forage preys. This hypothesis is supported by the fact that the hake with a condition index below 80 % died quickly in the present study. in contrast, fish with a condition index between 80 and 100 % recovered properly and grew fast.

Growth during the acclimatization period

Two size ranges, small fish and large fish, were distinguished and reared separately in this study. Acclimatisation proved to be quite problematic, particularly for the small fish reared in large tanks. All indices indicated that the chosen rearing conditions were inappropriate for this species: low survival rate (15 %), hardly any growth (0.005 cm day^{-1}) and low food intake (0.474 g per day per fish ± 1.356). This led to a decrease in average condition of about 10.5 %. Although such poor results might indicate a low ability to recover from stress induced by handling and tagging at T_0, they might well also reflect unsuitable rearing conditions such as the ratio of prey density to predator biomass or tank volume (15 m^3). The biomass density of tank A (SF) was low, less than 0.5 kg m^{-3}. Although increasing rearing density has usually been reported to have a negative effect on feeding and growth (Holm *et al.* 1990; Christiansen *et al.* 1992; Björnsson 1994; Lambert and Dutil 2001), low biomass in a high volume might have been a disadvantage in the present study as the hake were fed with forage preys rather than inert food. In a previous experiment (Jolivet *et al.* in press), using similar conditions and size range, survival rate was 76 % at 76 days post tagging with an initial biomass of 1 kg m^{-3} and a growth rate of 0.022 cm day^{-1}. Only the feeding mode was different, as fish in the pilot study were fed daily with inert food that was easier for them to catch at low densities. Indirect support for this hypothesis lies in the result of one

group of small fish that was maintained at a density below 1 kg m^{-3} but in a small tank ($2m^3$). This group had a greater survival rate and a daily food intake of 2.4 g per day per fish.

In contrast to the small fish, those of the larger groups adapted quickly to rearing conditions during acclimatisation and showed a growth rate similar to that later observed at 13 °C in the temperature experiment. Density in tank B (LF) was higher than in tank A (SF) and remained at 2.5 kg m^{-3}. Similar density levels have been reported as favourable for growth in Atlantic cod (Jobling 1988; Lambert and Dutil 2001). Moreover, parameters such as specific growth rate, feed conversion ratio and evolution of condition index indicated that these rearing conditions were suitable. It should be noted that 12 °C was chosen as the temperature for acclimatisation because it corresponds to the average sea bottom temperature (SBT) observed in the Bay of Biscay.

Relation between growth and temperature

During the temperature experiment itself, the small fish were distributed between two 2 m^3 tanks. The observed growth rates of these small fish were much higher than during acclimatisation and did not depend on temperature. This result might well reflect a compensatory mechanism following the restricted feeding during the acclimatisation period. Compensatory growth has already been observed in juvenile turbot, which had faster growth after severe food restriction (Saether and Jobling 1999) and in rainbow trout (Grima *et al.* 2008). This compensatory growth is generally associated with increasing efficiency of food utilization (Ali *et al.* 2003), which was also observed in the SF groups of the present experiment. This compensatory mechanism was also supported by the fact that few fish from the SF group showed KT below 80 % despite starvation. As previously demonstrated in cod by Dutil et al. (2006), the compensatory mechanism could be inhibited by extremely low

condition having a detrimental effect on growth capacity. Our study clearly shows the high capacity that hake have to recover from a low growth period resulting from inappropriate rearing (feeding) conditions. These high growth rates can also be explained by the higher growth potential of younger fish. Results obtained on the SF groups provide evidence for high growth potential in this species and indicate that it may be somewhat eurythermal, as they were no growth differences between the two temperatures (9 and 13 °C) tested. These temperatures had been chosen to simulate seasonal variations of SBT in the Bay of Biscay

In larger fish, growth rate and daily food intake were significantly influenced by temperature and were higher at 13 °C than at 9 °C, as already shown for Atlantic cod (Imsland *et al.* 2005). Moreover, feeding efficiency and energy utilization were greater at 13 °C than 9 °C in the LF groups, indicating that optimal rearing temperature could be around 13 °C. During the temperature experiment, the specific growth rate appeared to be negatively correlated with the initial condition. The same relationship was previously shown in cod by Dutil et al. (2006) after a starvation period. Fish in poor condition grew more rapidly than fish in good condition, suggesting that catch-up growth took place even in fish with the low condition index. Nevertheless, fish showing extremely low condition index (KT_1 below 80 %) had negative growth rates and quickly died, suggesting a detrimental effect on growth capacity.

At the end of the experiment, 73 % of the males and 96 % of the females showed gonadal development. These hake thus seemed to have begun their maturation during the temperature experiment. European hake is a multiple egg batch spawner that spawns in the Bay of Biscay from January to May, with a defined spawning peak between February and March (Murua and Motos 2006). In our study, the development of gonads was observed after the main natural spawning period. Murua et al. (2006) has already demonstrated that females can spawn all year and natural spawnings have been seen in two broodstocks reared under

controlled conditions between June and September 2007 and 2008 in Norway (Geffen et al., unpublished data) and between April and July 2007 in France (de Pontual et al., unpublished data). This maturation shift between rearing and natural conditions might be due to the acclimatisation and the use of suitable rearing conditions for reproductive maturation (temperature and photoperiod). As the number of fish with gonadal development was slightly higher at 9 °C than at 13 °C, 9 °C may be considered as a more appropriate temperature for maturation.

Photoperiod is known to be another important parameter acting on somatic growth. Hake is a demersal fish that undertakes vertical migrations during the night (de Pontual et al. in prepartion). In the present study, the natural photoperiod was used, but the daytime light exposition was much higher than in the wild. This may have influenced growth and maturation, as photoperiod manipulations have been shown to enhance growth for several species such as Atlantic salmon (*Salmo salar*) (Stefansson *et al.* 1989; Solbakken *et al.* 1994) and early Atlantic cod juveniles (Folkvord and Otterå 1993). In particular, juvenile Atlantic cod exposed to continuous light had greater growth rate and better food conversion compared with cod reared under natural photoperiod (Imsland *et al.* 2007). Photoperiod manipulations have also been reported to affect the sexual maturation and growth of adult cod (Hansen *et al.* 2001; Karlsen *et al.* 2006; Taranger *et al.* 2006). Increasing daytime light exposition (up to the use of constant 24h light photoperiods) can affect maturation up to the point of causing its inhibition, which can improve growth performance in farmed fish stocks (Van der Meeren and Ivannikov 2006; Davie *et al.* 2007). In our study, the greater daytime light exposition compared with natural conditions may explain the late development of gonads observed in the LF group relative to the main spawning period in wild.

Contribution to aquaculture and fisheries research

During the temperature experiment, the maximum growth rate observed at 9 °C was 0.063 cm day $^{-1}$ for a growth rate of 0.702 % day^{-1} corresponding to a weight gain of 290 g for an initial weight of 200 g. At 13 °C, the maximum growth was 0.070 cm day $^{-1}$ for a growth rate of 0.403 % day^{-1} with corresponding initial and final weights of 500 g and 838 g, respectively. These particular fish had therefore doubled their weight in less than 4 months. This result clearly shows that the growth potential of hake is similar to that of cod, which is able to double its body weight in 4-6 months with similar growth rates if fed *ad libitum* (Murphy 2002; Björnsson *et al.* 2007). Hake thus appears to be an interesting candidate species for the diversification of gadiform aquaculture. There is obviously still much work to be done on the development of appropriate rearing conditions for this species. One improvement could be achieved trough the formation of a hake broodstock from larval rearing. However, the biological cycle of the species is not yet under full technical control. Apart from the single successful result by Bjelland and Skiftesvik (2006), no attempt to rear larvae has gone beyond 30 days post hatching (de Pontual et al unpublished data).

Regarding fisheries management, our results provide additional evidence that hake is a fast growing species. This has been demonstrated only recently in parts of its natural distribution such as the Bay of Biscay (de Pontual *et al.* 2006), Iberian Peninsula (Piñeiro *et al.* 2007) and the Golf of Lions (Mellon *et al.* submitted). Such a change in the estimation of major life history traits (growth and age at first maturity) can have a real impact on the assessment of wild stocks (Bertignac and de Pontual 2007). A better knowledge of the biology of this heavily exploited species is clearly required for its sustainable management. Such progress could be achieved with a combination of experiments in the wild and under controlled conditions. Besides the confirmation of the growth potential of the species, our results showed

that hake can withstand restricted feeding conditions for quite a long time and are able to recover if suitable feeding conditions are re-established. Additionally, this species appears to be somewhat eurythermal, as is Atlantic cod (Imsland *et al.* 2005), since high growth rates were observed over a relatively wide temperature range (9-13 °C). The analysis of electronic tags has recently shown that hake can experience high thermal variations associated with their nocturnal vertical movements, which they are probably related to foraging behaviour (de Pontual et al in prep). Further work on material of this experiment will provide additional results from the analysis of otolith material from the same fish, with the aim of improving our understanding of otolith biomineralization (Allemand *et al.* 2007) and the particularly complex otolith patterns of this species (de Pontual *et al.* 2006).

Acknowledgments

The authors wish to thank François Garren, André Ogor and Nicolas Le Bayon for their technical assistance and help during the rearing experiments. We are also grateful to Marc Suquet for fruitful discussions on fish rearing. This work was supported by national ANR grant "OTOCAL". This study was conducted under the approval of the Animal Care Committee of France under the official licence of H. de Pontual.

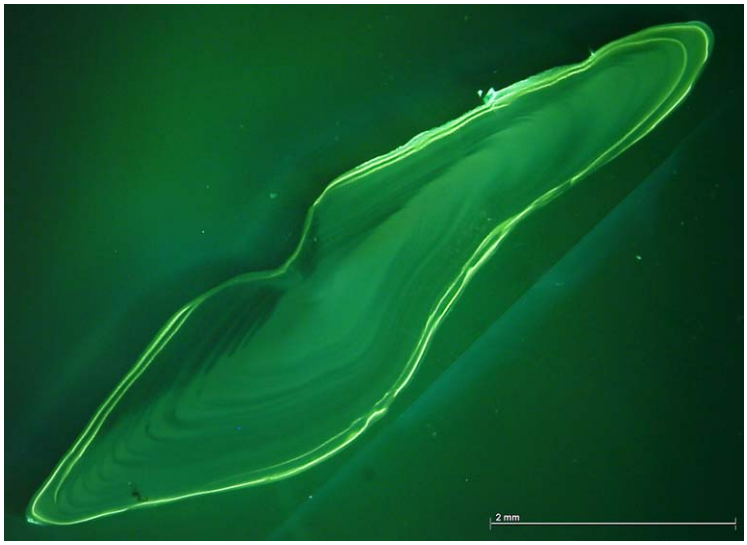

Chapitre 3 :

Opacité de l’otolithe en relation avec la croissance, le métabolisme et la température

Chapitre 3 :

Opacité de l'otolithe en relation avec la croissance, le métabolisme et la température

De nombreux otolithes sont reconnus pour être difficiles à interpréter de par l'existence de structures secondaires pouvant s'apparenter à des structures saisonnières. Pour améliorer cette interprétation, l'étude des conditions induisant la formation de ces structures est indispensable. L'expérimentation effectuée sur la croissance du merlu et les effets de la température en milieu contrôlé a permis d'obtenir des otolithes calibrés avec un nombre limités de facteurs pouvant intervenir sur l'opacité.

Comme décrit précédemment, cette expérimentation a consisté en deux périodes : une période d'acclimatation pendant laquelle les poissons étaient maintenus à 12 °C dans des bassins de 15 m^3 et une seconde période pendant laquelle les poissons étaient à 9 ou 13 °C dans des bassins de 2 m^3. Deux classes de tailles ont été considérées et les individus ont été marqués par deux fois à l'aide d'oxytétracycline (en début de chaque période) permettant de marquer l'otolithe et d'y délimiter les deux périodes expérimentales.

Une première partie de l'analyse a consisté à étudier la relation entre croissance somatique et croissance de l'otolithe. Une corrélation positive, fortement significative, a été observée entre ces deux taux de croissance pour le groupe des plus grands individus (LF) tout au long de l'expérimentation et pour le groupe des plus petits individus (SF) au cours de la seconde période. Comme précédemment démontré au niveau somatique, le groupe des SF a subit une période de sous-alimentation au cours de la première période due à un manque de connaissances sur les conditions appropriées pour l'élevage du merlu. Ces conditions

résultèrent en un découplage entre la croissance somatique et la croissance de l'otolithe. De manière générale, une relation significative a pu être établie définissant la croissance de l'otolithe comme une fonction de la croissance somatique et généralisable à l'ensemble des cas.

Dans une seconde partie, l'analyse s'est portée sur les effets influençant l'opacité observée sur l'otolithe. Trois effets ont été détectés : 1) un effet lié à la croissance somatique induisant la formation d'une zone translucide dans le cas de faibles taux de croissance pendant la période de sous-alimentation ; 2) un effet lié au métabolisme induisant la formation d'une zone translucide dans le cas de changement physiologique tel que le développement des gonades ; 3) un effet température, mineur par rapport aux deux autres effets précédemment cités tendant à induire la formation d'une zone translucide dans le cas d'une augmentation de température.

A partir des résultats obtenus sur l'opacité, un modèle fut proposé prenant en compte de façon explicite les deux principaux facteurs : la fraction de la croissance de l'otolithe directement corrélée à la croissance somatique et la fraction de la croissance de l'otolithe qui ne peut pas être expliquée par la croissance somatique et par conséquent directement liée à des mécanismes de type maintenance. Une paramétrisation globale du modèle sur l'ensemble de l'expérimentation et pour les deux classes de tailles a été démontrée comme significative mettant en évidence l'action complémentaire de ces deux contributions sur l'opacité et la généricité du modèle.

Otolith opacity in relation to growth rate, metabolism and temperature

Aurélie Jolivet, Ronan Fablet, André Ogor, Yves-Marie Paulet, Hélène de Pontual

En préparation

Abstract

The purpose of this work was to examine the effect of metabolism, somatic growth and temperature on fish otolith opacity. Two size groups of European hake (*Merluccius merluccius*) were considered: smaller fish (SF) and larger fish (LF) and maintained under controlled conditions during two successive periods of 4 months: period P_1 where fish were kept at 12°C in 15 m^3 tanks; and P_2 where groups were kept at 9 or 13°C in 2m^3 tanks. Significant positive correlations were observed between otolith and somatic growth rates during the overall experiment for the LF group and only during the second period for the SF group. Due to non optimal rearing conditions (hake is not yet a farmed species) and lack of knowledge regarding appropriate rearing conditions, the SF group actually experimented reduced feeding conditions at constant temperature during the acclimatisation period resulting in a decoupling between otolith and somatic growth. For opacity, three factor's effects were detected: 1) a growth effect with the formation of a translucent area in case of low somatic growth rates during the reduced feeding period, 2) a metabolism effect with the formation of a translucent area in case of reduced feeding condition or maturation, 3) a temperature effect, which was minor relative to the two previous ones and tended to induce the formation of translucent area when temperature increased. From the experimental results, an opacity model was proposed that explicitly take into account two main factors: the fraction of otolith growth directly correlated with somatic growth and the fraction of otolith growth that cannot be explained by the somatic growth. A general

parametrization of the model common to the two size group and periods was proven significant evidencing the two complementary contributions and the genericity of the model.

Introduction

Otoliths are calcareous concretions in fish inner ears. Their accretional growth follows a circadian rhythm that is physiologically controlled but influenced by environmental conditions (Pannella 1971; Panfili *et al.* 2002a). It results in the formation of microstructures namely L- and D- zones as well as macrostructures referred to as opaque and translucent zones. This fish "black box" can be viewed as a stable record of metabolic and environmental conditions encountered by the fish and is operationally used for fish age estimation. Routine analysis of fish otoliths (nearly one million per year) is for instance at the core of age-based assessment of fish stocks (Campana and Thorrold 2001). This routine analysis relies on the interpretation by experts of translucent and opaque zones on fish otolith sections according to agreed interpretation protocols (Campana 2001). This interpretation can be made difficult by the presence of translucent and opaque zones, called structures of secondary growth, that do not correspond to seasonal zone formation. Such secondary structures have been reported to be formed due to shift in feeding conditions (e.g. starvation), temperature changes as well as ontogenic events (e.g. reproduction) (Wright *et al.* 2002b). They are among the main sources of the variability observed in the formation of otolith macrostructures (both in terms of opacity and width) at the individual, population and species level (Beckman and Wilson 1995). The lack in the understanding of the biochemical processes and conditions driving the formation of fish otoliths in relation to fish physiology and environmental conditions is then a great cause of error in the interpretation of fish otoliths by experts (de Pontual *et al.* 2006).

Optically, translucent zones absorb less light than opaque zones; therefore the translucent zones appear brighter under transmitted light and darker under reflected light. Conversely, opaque zones appear darker under transmitted light and brighter under reflected light (Panfili *et al.* 2002a). Opacity changes have been linked to variations in the relative amount of the organic matrix of the otolith (Mugiya 1984; Tomás *et al.* 2004), in amino acid composition (Hüssy *et al.* 2004), in elemental ratios (Kalish 1991) as well as to structural properties of primary increments: width, thickness, size of aragonite crystals (Morales-Nin 1987). Opacity was also shown to be dependent on fish development: growth rate (Hüssy and Mosegaard 2004), age and metabolism (Hoff and Fuiman 1993; Høie and Folkvord 2006), sexual maturity (Beckman and Wilson 1995). Regarding environmental conditions, feeding conditions, such as starvation (Neilson and Geen 1985), temperature and photoperiod (Beckman and Wilson 1995) have also been reported as affecting otolith opacity.

The understanding of the relative effects, opposite or not, of these different factors on otolith opacity remains however unclear. These issues can be addressed through controlled experiments. For instance, Høie et al. (2008) analyzed the effects of reduced feeding at constant temperature on cod (*Gadus morhua*) otolith opacity and observed the deposition of a translucent zone in response to reduced feeding. In our study, we examined the effects of growth, metabolism and temperature on otolith opacity of European hake (*Merluccius merluccius*). We followed two size groups of fish during acclimatisation and at two temperature conditions while keeping *ad libitum* feeding. From this context, our contributions are two-fold:

1) analysing the interaction between growth, metabolism and temperature on opacity of otolith with:

2) providing an opacity model from these experimental data explicitly taking into account growth and metabolism factors.

Results are discussed and compared to previous studies (Hüssy *et al.* 2004; Høie and Folkvord 2006; Høie *et al.* 2008) and to the model predictions of Hüssy and Modegaard (2004). Although the interpretation criteria of hake otoliths were internationally validated (Piñeiro and Sainza 2003) previous results from mark-recapture campaign underlined the overestimation of age due to the presence of secondary structure on otoliths (de Pontual *et al.* 2006a). In this study, hake otoliths were chosen to give new insights on the formation of the translucent zones on their otoliths.

Material and Methods

The samples used in this study came from an experiment in controlled conditions on the growth of hake where the rearing protocols were detailed in Jolivet et al. (in submission).

Acclimatisation to captivity

Fish were caught in the Bay of Biscay in mid-July 2006 using a method developed by de Pontual et al. (2003a) for mark-recapture experiments. To acclimatize fish, individuals were sorted by size range and kept in 15 m^3 circular tanks at controlled temperature (12°C ± 0.5). Fish were fed *ad libitum* on forage fish.

Between mid-October and mid-December 2006, all fish were individually tagged. The procedure consisted in: 1) measurements of total length (TL_0 in mm) and weight (W_0 in g); 2) insertion, at the base and in front of the second dorsal fin, of pit tag and 3) injection with a veterinary solution of oxytetracycline at a dose of 60 mg kg^{-1} of fish. This antibiotic is commonly used to mark otoliths with fluorescent marks visible under UV epi-illumination light for ageing methodology validation (Panfili *et al.* 2002a). Fish sorted by size range were

transferred in 15 m^3 tanks: tank A for smaller fish, referred to as SF_A, and tank B for larger ones, referred to as LF_B. Temperature in tanks A and B was 12°C ± 0.5. Thereafter, we denote the first tagging date by T_0.

Temperature experiment

The temperature experiment started on February 27th, 2007 (subsequently called T_1) until July 5th, 2007 (T_2). At day T_1, total length (TL_1 in mm) and weight (W_1 in g) were recorded and fish were tagged again with oxytetracycline. Fish were moved to new experimental tanks with respect to the two size groups SF and LF. Their characteristics at day T_1 were the following: small fish from tank A (SF: average ± standard deviation SD TL_1= 29 cm ± 1.5 and W_1 = 151.2 g ± 29.8, N = 25) and larger fish from tank B (LF: TL_1= 36.4 cm ± 3.4 and W_1 = 368.3 g ± 138.8, N = 96). Within each size group, fish were randomly assigned to two temperature conditions (9 and 13°C). Two replicates per temperature were considered for the LF group but only one for the SF group. The experiment was conducted in six 2 m^3 tanks under natural photoperiod. Until April 1st, 2007, water temperature was maintained at 11°C to acclimatize fish to their new rearing conditions (2 m^3 tanks). After this date, the temperature was gradually changed to the designed setting. Temperature did not significantly vary with time or between tanks during the experiment. It averaged 9.4°C ± 0.4 and 13°C ± 0.4. Fish were fed *ad libitum* on forage fish and the consumption was daily estimated, based on the number and the weight of the preys provided and the number of preys unconsumed. At the end of experiment fish were killed with an overdose of anaesthetic. They were then measured (TL_2 and W_2) and sexed. Fish were deep frozen as were dead fish during the course of the experiment.

Otoliths

Preparation protocol

The otoliths of the 52 survivors were extracted, cleaned, rinsed with milliQ water, dried and weighed. The left and right sagittae were stored in clean polypropylene vials and stored in a dessicator before further treatment. For standardization purpose, we systematically used the left sagittae. Otolith preparation consisted in: 1) embedding in epoxy resin, 2) sectioning in transverse plane, 3) grinding, and 4) polishing to 200-500 µm sections through the core. Thickness of sections could not be standardized due to the difficulty to locate the core required for the reading of hake otoliths. All sections were observed under a stereo microscope equipped with three light sources (transmitted, reflected, and UV) using the same light orientation and intensity netting. We used TNPC software to acquire calibrated numerical images and make measurements of otolith growth and opacity (Ogor and Fablet, 2004).

Opacity treatments

From reflected and UV images, the positions of the two oxytetracycline marks, at times T_0 and T_1, denoted by OTC_0 and OTC_1, were located (Fig. 1). The dorsal side has been preferred for opacity analysis, as it depicted a greater growth which made easier the analysis of the opacity signal. Measures were performed along the main growth axis. Transect information obtained with TNPC included distances from the nucleus to tagging marks and

the edge and reflected light intensities as grey values distributed between 0 (black) to 255 (white). In this study reflected light was used, so brighter areas with greater intensity correspond to the opaque zones and darker areas with lower intensity values to the translucent zones. Each period of the experiment, from T_0 to T_1 and from T_1 to T_2, was assigned a mean opacity value. To account for potential effects of tagging stress on opacity, the mean opacity value was estimated restricting within the stable area of each period.

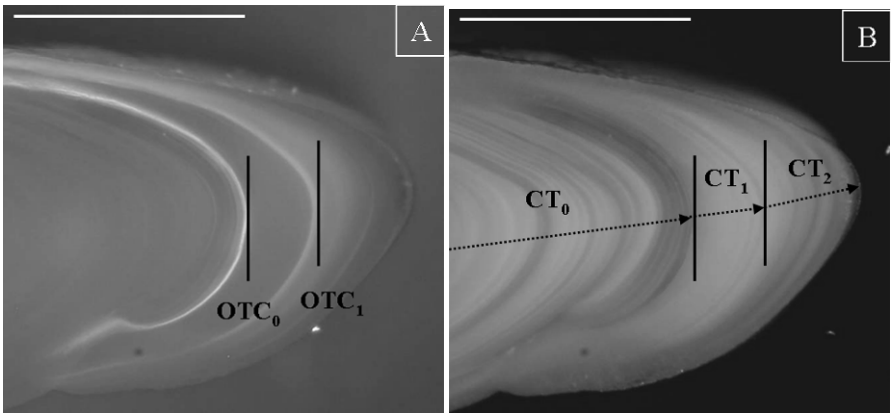

Figure 1: Dorsal side of otolith section from the LF group reared at 9°C focused on experimental zone photographed with a) UV epi-illumination light and b) reflected light. Vertical black lines locate oxytetracycline marks OTC_0 and OTC_1 corresponding to tagging T_0 and T_1, at a distance CT_0 and CT_1 from the core. The distance called CT_2 corresponds to the distance between the core and the otolith edge. (Scale bars = 500 µm)

In order to be independent from thickness and preparation effects, the logarithm of the opacity values was considered as suggested by Hüssy et al. (2004) and opacity was standardized allowing the comparison between size groups and treatments. Variability in sections thickness were tested and found to be homogeneous between size groups and temperature conditions ($P > 0.05$). A statistical analysis has been carried out for the three sets

of opacity measurements corresponding to the different temperature conditions (9, 12 and 13°C).

Data analysis and statistical methods

A Specific otolith growth rate (% day^{-1}) for period T was calculated as:

$$OGR_T = (e^g - 1) \times 100 \qquad \text{with } g = [\ln(CT_{tf})-\ln(CT_{ti})]/(D_T)] \qquad \text{(Eq1)}$$

where T holds for period P_1 or P_2, CT_{tf} and CT_{ti} are the distance between the core and the tagging marks OTC_0 and OTC_1 for the period P_1 and between OTC_1 and the edge for the period P_2. D_T corresponds to the duration of period T. The Specific somatic growth rate (% day^{-1}) for period T was calculated from total length as:

$$SGR_T = (e^g - 1) \times 100 \qquad \text{with } g = [\ln(TL_{tf})-\ln(TL_{ti})]/(D_T)] \qquad \text{(Eq2)}$$

where TL_{tf} and TL_{ti} denote the total length respectively at the end of period T, denoted by t_f, and the beginning of period T, denoted by t_i.

The correlation of otolith and somatic growth was tested according to a linear model:

$$OGR_T = \alpha \times SGR_T + \beta \qquad \text{(Eq 3)}$$

We defined the residual otolith growth $resOGR_T$ as the residual of this linear regression. This residual can be interpreted as the fraction of the otolith growth that cannot be explained by the somatic growth.

A model of otolith opacity was also investigated. In previous work, otolith growth and opacity has been shown to be correlated to the metabolic activity (Hüssy and Mosegaard 2004). The interpretation of the formation of the otolith might then be carried out from energy growth fluxes. The following opacity linear model was then proposed:

$$Op_T = \alpha' \times SGR_T / OGR_T + \beta' \times resOGR_T / OGR_T + \varepsilon \qquad \text{(Eq 4)}$$

where Op_t is the opacity computed for period T. SGR_T / OGR_T accounts for the relative effect of somatic energy flux on otolith opacity and $resOGR_T / OGR_T$ can be interpreted as a contribution of other energy fluxes, especially maintenance. The above regressions were initially applied to each group and each period. We also tested whether a generalized model could be valid among groups and periods. For each regression, the contribution of each variable was defined as the decrease of the determination coefficient R^2 (in %) if the variable was not included in the equation.

Otolith growth and opacity measures are expressed as average ± Standard Deviation SD. The statistical analysis is carried out using ANOVA and T-test if homogeneity of variances was demonstrated with Levene-test else they were analyzed with Kruskal-Wallis test. Correlation between variables was tested with Spearman test and noted C^2 (significant level at 5%).

Results

Otolith and somatic growth

We first analyzed otolith growth with respect to temperature. For the LF group, the otolith growth was correlated to temperature (C^2= 0.258, P = 0.023), with a minimum at 9°C significantly different from 12 and 13°C (P < 0.05). No such correlation was observed for SF group (C^2=0.083, P = 0.687). The minimum otolith growth was observed during the acclimatisation period (12°C) and was significantly different from 9°C (P < 0.05) contrary to 13°C (P > 0.05).

Size-group	N	Period	OGR	SGR	α	β	R²	P
SF	4	P2 9°C	0.085 ± 0.05	0.14 ± 0.03	0,507	0,014	0,089	P > 0.05
SF	9	P2 13°C	0.062 ± 0.02	0.11 ± 0.05	0,338	0,025	0,876	P < 0.05
SF	13	P2	0.07 ± 0.03	0.12 ± 0.05	0,397	0,022	0,355	P < 0.05
SF	13	P1	0.047 ± 0.03	0.02 ± 0.02	0,259	0,042	0,027	P > 0.05
SF	**26**	**P1+P2**	**0.058 ± 0.03**	**0.07 ± 0.06**	**0,27**	**0,04**	**0,298**	**P < 0.05**
LF	19	P2 9°C	0.039 ± 0.02	0.04 ± 0.03	0,492	0,018	0,698	P < 0.05
LF	20	P2 13°C	0.057 ± 0.02	0.08 ± 0.05	0,353	0,03	0,505	P < 0.05
LF	39	P2	0.048 ± 0.02	0.06 ± 0.04	0,411	0,023	0,612	P < 0.05
LF	39	P1	0.058 ± 0.04	0.07 ± 0.05	0,514	0,02	0,493	P < 0.05
LF	**78**	**P1+P2**	**0.053 ± 0.03**	**0.07 ± 0.05**	**0,475**	**0,021**	**0,532**	**P < 0.05**
LF + SF	52	P1	0.056 ± 0.03	0.06 ± 0.05	0,432	0,029	0,397	P < 0.05
LF + SF	52	P2	0.053 ± 0.03	0.07 ± 0.05	0,394	0,024	0,58	P < 0.05
LF + SF	**104**	**P1+P2**	**0.054 ± 0.03**	**0.07 ± 0.05**	**0,403**	**0,027**	**0,448**	**P < 0.05**

Table 1: Overview of growth data for the different size groups, periods and temperature conditions: Number of samples (N), specific somatic growth rate (SGR, % day^{-1}) and specific otolith growth rates (OGR, % day^{-1}) (average ± SD) with respect to size group (SF and LF) and period (acclimatisation P_1, temperature conditions P_2 at 9 and 13°C) and results of regressions on OGR as a function of SGR with: α and β parameters (Eq 3), determination coefficient R² and significance P.

The results of the regression analysis between otolith and somatic growth (Eq. 3) are reported in Table 1. For the SF group, the regression was significant except for period P_1 (R^2 = 0.027, P > 0.05) and for the 9°C setting during period P_2 (R^2 = 0.089, P > 0.05). Besides, a significant generalized relation was exhibited for the overall experiment (R^2=0.298, P < 0.05, Fig 2A). Regarding the LF group, a significant correlation was observed over the two periods and a generalized linear was relevant (R^2=0.532, P < 0.05, Fig 2B). Comparisons between the two size groups showed that a common model could be considered for all periods and groups (Table 1, R^2 = 0.448, P < 0.05) as:

$$OGR_T = 0.403 \times SGR_T + 0.027 \quad \text{(Eq 5)}$$

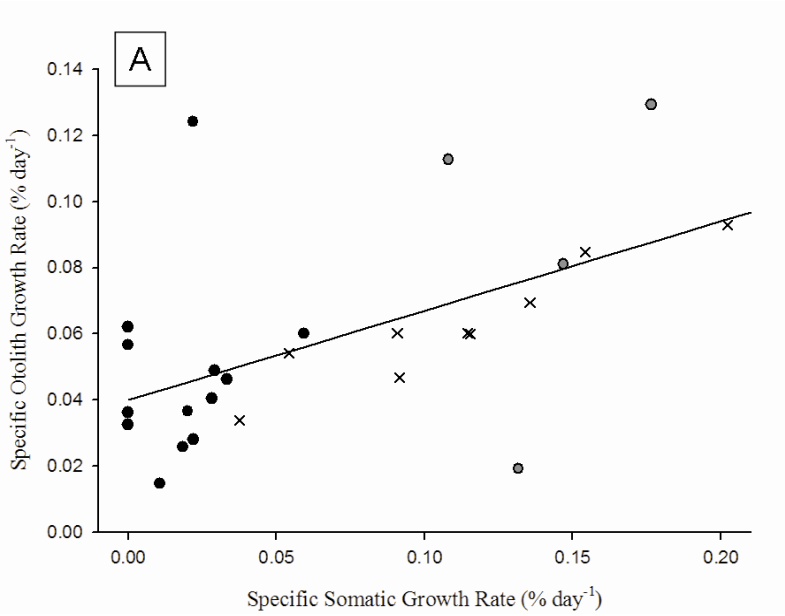

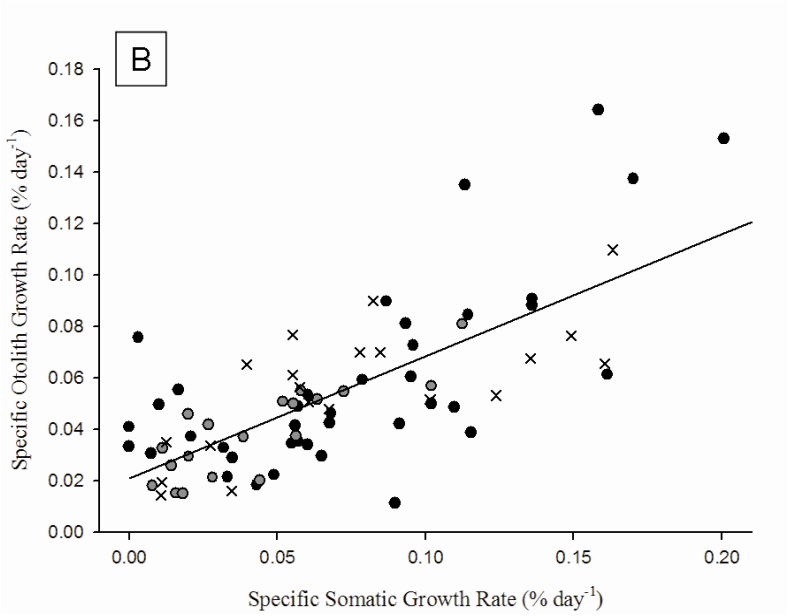

Figure 2: Relationship between the specific otolith and somatic growth rates for each size group: SF (A) and LF (B) with respect to temperature conditions: dark circle, grey circle and dark cross for 12, 9 and 13°C respectively.

Opacity

Otolith opacity was analyzed with respect to temperature conditions. For the SF group, otolith opacity during period P_1 was slightly more translucent, but was not significantly different from the opacity during period P_2 at 9 and 13°C (Table 2, $P > 0.05$). Regarding the LF group, no significant difference was detected between opacities at 9 and 13°C during the period P_2 (Table 2, $P > 0.05$) but these two opacities appeared significantly more translucent than opacity during the period P_1 ($P < 0.05$).

Size-group	N	Period	Op	α'	β'	ε	R^2	P	SGR	resOGR
SF	4	P2 9°C	-1.36 ± 2.29	7,523	13,597	-13,115	0,985	P > 0.05	6,86	8,41
SF	9	P2 13°C	-1.7 ± 0.41	1,219	2,249	-3,43	0,612	P > 0.05	60,22	22,56
SF	13	P2	-1.6 ± 1.24	1,664	3,913	-3,755	0,83	P < 0.05	17,31	32,95
SF	13	P1	-1.98 ± 0.7	0,97	1,407	-2,534	0,538	P < 0.05	15,13	53,58
SF	**26**	**P1+P2**	**-1.79 ± 1.02**	**0,647**	**1,977**	**-2,363**	**0,635**	**P < 0.05**	18,66	50,69
LF	19	P2 9°C	-2.45 ± 1.3	0,835	2,076	-2,505	0,534	P < 0.05	8,24	53,29
LF	20	P2 13°C	-1.6 ± 1.6	1,667	2,93	-3,27	0,809	P < 0.05	37,45	70,90
LF	39	P2	-1.91 ± 1.48	1,353	2,527	-2,926	0,691	P < 0.05	24,21	63,20

LF	39	P1	-0.74 ± 1.04	1,244	2,093	-2,083	0,388	P < 0.05	30,58	38,32
LF	**78**	**P1+P2**	**-1.33 ± 1.40**	**1,552**	**2,537**	**-2,796**	**0,586**	**P < 0.05**	44,76	57,46
LF + SF	52	P1	-1.05 ± 1.11	1,373	2,158	-2,389	0,482	P < 0.05	44,76	46,51
LF + SF	52	P2	-1.84 ± 1.42	0,991	2,604	-2,559	0,683	P < 0.05	24,30	67,57
LF + SF	**104**	**P1+P2**	**-1.44 ± 1.33**	**1,192**	**2,281**	**-2,532**	**0,493**	**P < 0.05**	32,60	49,28

Table 2: Overview of opacity results with respect to size group (SF and LF), period and temperature conditions (acclimatisation P_1, temperature conditions P_2 at 9 and 13°C): number of samples (N), standardized opacity statistics (Op), parameters of the opacity regression α', β' and ε, determination coefficient R^2, significance P and the contributions of each variable (SGR and resOGR) to R^2 (in %). Lower opacity values define darker zones corresponding to translucent zones. .

The opacity model (Eq 4) was calculated using the residuals issues from the generela otolith growth model (Eq 5). The regression results are proposed in the Table 2. For the SF group, the opacity model was significant overall (R^2= 0.635, P < 0.05, Fig. 3A). But, fitting the model for each period and temperature conditions did not lead to significant regressions for period P_2 at 13°C and 9°C, in particular due to the low number of samples at 9°C. For the LF group, significant regression statistics were computed for each period (P_1: R^2 = 0.388, P_2: R^2 = 0.691, P < 0.05) and the regression model common to both periods was significant (R^2=0.586, P < 0.05, Fig 3B). Moreover the two size-groups could be described with a single regression model (R^2= 0.493, p < 0.05), as:

$$Op_T = 1.192 \times SGR_T / OGR_T + 2.281 \times resOGR_T / OGR_T - 2.532 \quad \text{(Eq 6)}$$

The contributions of the two variables varied following the case. Concerning the SF group, the $resOGR_T / OGR_T$ mainly contributed to the model during the period P_1 unlike the period P_2 at 13°C. For the LF group, the contribution of the two variables was closer for the period P_1 unlike the period P2 where $resOGR_T / OGR_T$ corresponded to the main contribution

(Table 2). It's worth noting that in the majority of case the sum of the two contributions was higher than the observed R^2 that was explained by the inverse effects of these two variables on opacity.

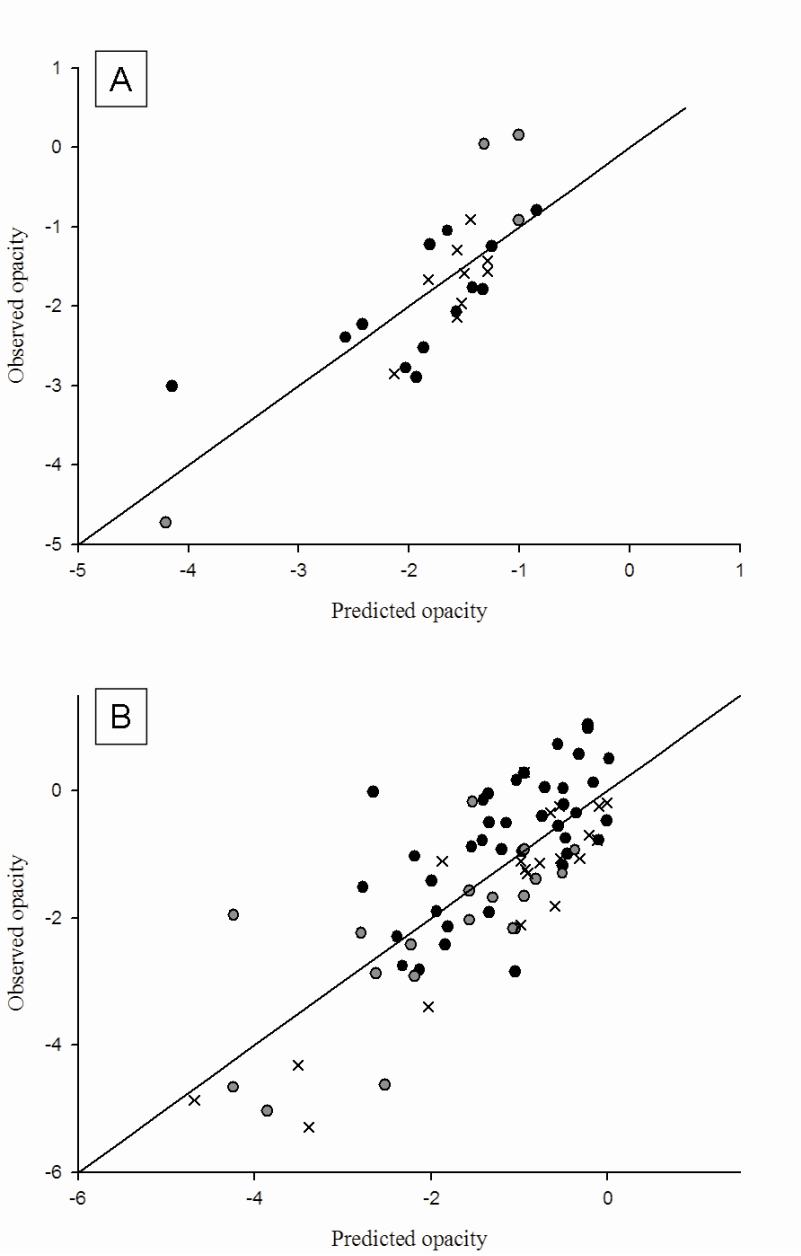

Figure 3: Relationship between opacity and predicted values from the general model of the SF group (A) and the LF group (B) with respect to temperature conditions:

dark circle, grey circle, and dark cross for 12, 9 and 13°C respectively. Dark line corresponds to y = x.

To analyze a temperature-specific effect on otolith opacity, opacity residuals from Eq. 6 were used and the difference between residuals of the period P_2 (at 9 or 13°C) and those of the period P_1 (12°C) was calculated. They correspond to the temperature changes of -3°C and +1°C. This difference was not significantly significant for the two size groups. However a same trend was observed with opacity residuals more opaque when the temperature decreased and inversely, opacity residuals tended to be more translucent when the temperature increased.

Discussion

Somatic and otolith growth

Significant positive correlations were observed between otolith and somatic growth rates during the overall experiment for the LF group and only during the second period for the SF group. Such relation was already known (Campana and Neilson 1985; Neilson and Geen 1985) and widely used in back-calculation models (Francis 1990; Morita and Matsuishi 2001). The temperature effect was however not comparable between the two size-groups. The growth rates of the LF group were positively correlated to temperature under *ad libitum* feeding conditions. This type of growth pattern has already been reported for cod otoliths, as the growth rate is greater at high temperature and high prey abundance (Campana 1996; Otterlei *et al.* 2002). This relation between the temperature and the otolith growth can be

linked to an increase of the aragonite deposition known to be temperature-specific dependent (Romanek and Gauldie 1996; Hüssy and Mosegaard 2004; Hüssy 2008).

On the contrary, the SF group showed growth rates independent on temperature during period P_2. That was interpreted as a result of a compensation mechanism following a low feeding period as already observed on juvenile turbot which presented a faster growth after severe food restriction (Saether and Jobling 1999) or to the high growth potential of young fish under suitable rearing conditions (Jolivet *et al.* submitted). During period P_1, fish of the SF group were maintained in non-optimal rearing conditions, in particular due to the combination of large tanks inducing low prey density and low fish density. These rearing conditions, described as low food uptake, resulted in a low somatic growth and uncoupled otolith growth. Such uncoupling has already been observed (Wright *et al.* 1990; Barber and Jenkins 2001; Baumann *et al.* 2005) and could be caused by several factors such as ontogenic development (Otterlei *et al.* 2000), temperature higher than thermal optimum (Mosegaard *et al.* 1988) and more frequently by effects of starvation or low somatic growth (Campana 1983b; Secor and Dean 1989). Results obtained on the SF group showed that the feeding level predominated on temperature.

In this study a generalized otolith growth model was proven significant for the two size groups and on the overall experiment. This generalized model was then applied both when otolith growth was correlated to somatic growth and when a uncoupling was observed during reduced feeding conditions. These results led to the hypothesis that otolith accretion depends and is regulated by different compounds of fish somatic metabolism and only correlated to somatic growth during favourable feeding conditions (Mosegaard *et al.* 1988) The otolith growth model exhibited two contributions: a main contribution of the somatic growth and a second contribution which can be interpreted as a contribution of other metabolic fluxes such as maintenance fluxes. Several studies have shown a close relation between otolith growth

rate and standard metabolic rate, but the two processes are not directly proportional (Wright 1991b; Wright *et al.* 2001). Moreover, the otolith is a metabolically inert structure of calcium carbonate and protein which is bathed in a solution which contains the ionic and organic precursors (Borelli *et al.* 2001; Payan *et al.* 2002). Ionic precursors are known to be both passively and actively transported into the endolymph and organics precursors to be secreted by the epithelium (Allemand *et al.* 2007). These processes are energy-demanding and therefore linked to fish metabolism. Hüssy (2008) suggested thus that processes coupled to the secretory capacity and thus the metabolic rate of the endolymphatic epithelium are the driving forces behind otolith growth.

Otolith opacity

Effect of the somatic growth on otolith opacity: The variations of otolith opacity in relation to otolith and somatic growth differed depending on size groups and experimental periods. During period P_1, the formation of a more translucent otolith zone was observed for the SF group. These results were similar to those obtained by Høie et al (2008) on reared cod showing that under restricted feeding conditions otoliths were more translucent. Here, these opacity changes were however not significant. That might be explained by the considerable individual variability or by the fact that the observed restricted feeding conditions was not comparable to starvation conditions previously described in experimental conditions (Neilson and Geen 1985; Hüssy and Mosegaard 2004; Høie and Folkvord 2006) and in the wild (Admassu and Casselman 2000; Colloca *et al.* 2003; Johnson and Belk 2004). During period P_2, the formation of a more opaque otolith area was observed.. Here, otolith opacity during period P_2, after the restricted feeding period, was thus mostly controlled by the growth rates and hence feeding conditions and not by temperature. In the LF group, the observed otolith

opacity was significantly different between the two temperature settings with the formation of a more translucent area at 9°C than at 13°C but firstly strongly correlated to otolith growth in the both cases. This is in accordance to previous studies which showed that periods of low somatic growth correspond to translucent areas unlike the opaque areas (Hüssy *et al.* 2004; Høie *et al.* 2008).

Temperature effect on otolith opacity: The effect of the temperature shift from 12°C to 9°C and 13°C on otolith opacity was not directly evident and significant. As previously demonstrated on juvenile cod by Hüssy et al. (2004), a predominance of somatic growth effects, compared to temperature effects, was observed on opacity changes. A temperature effects on otolith opacity were exhibited when considering residuals of opacity prediction from somatic and otolith growth. For the two size groups, a decrease of 3°C tended to induce the formation of more opaque otolith zones than an increase of 1°C. These trends confirm temperature effects reported using stable isotope analysis (Weidman and Millner 2000; Høie and Folkvord 2006). That is also explained by the temperature depend effect of the aragonite precipitation inducing greater concentrations of aragonite during period with higher temperature (Romanek and Gauldie 1996). In this study, the fact that this effect was not significant can be explained by the chosen range of temperature which was not sufficient to detect real differences in opacity. Moreover, for the SF group, the residuals of the period P_2 characterized by a compensation mechanism were compared to those of the period P_1 characterized by restricted feeding conditions.

Effect of physiologic change on otolith opacity: Comparisons between opacities of periods P_1 and P_2 showed the formation of a more translucent area during the period P_1 for the SF group and during the period P_2 for the LF group. For the SF group, this translucent area

was explained by the inappropriate feeding conditions. For the LF group, the opacity decrease can be explained for fish reared at 9°C by lowers somatic and otolith growth rates during period P_2 compared to period P_1. For the fish reared at 13°C, the formation of this more translucent area is in opposition with the growth effect and ad libitum feeding conditions. An increase of temperature was shown to induce the formation of translucent area but was defined as minor than growth effect. Thus this increase of only 1°C would unlikely explain this opacity decrease. It could be interpreted as a consequence of a physiological control which was not observed for smaller fish. At the end of the experiment, hakes were killed, measured and sexed. 80% and 100% of fish from the LF group reared at 13°C and 9°C respectively showed gonads in development that was clearly more important than for the 23% fish from the SF group (Jolivet *et al.* submitted). Older fishes generally allocated relative more energy into the development of their gonads than younger fishes. Høie and Folkvord (2006) suggested in their study on cod that this allocation of energy into gonads might explain variations in otolith opacity and explain the formation of translucent area. This sexual maturity effect could be an explanation of the observed opacity decrease between the two experimental periods in particular for fish reared at 13°C. The metabolism effect on opacity was reflected through the somatic and otolith growth contributions in opacity model. In the two size groups the contribution of the otolith growth residuals was greater on the period P_1 for the SF group and on the period P_2 for the LF group.

Hake otolith interpretation: As summarised in Table 3, this study brings cues for the interpretation of hake otolith macrostructures. Among the important contribution is the strong metabolic effect exhibited on opacity. Both restricted feeding conditions and gonad development have been shown to greatly impact otolith opacity compared to somatic growth

and temperature. Therefore, the formation of the translucent areas may be caused in similar ranges by warmer sea temperatures, by metabolic changes as well as by starvation.

These properties may explain why hake otolith opacity cannot be simply related to seasonal variations of environmental factors. This makes age estimation so complex for this species, as stressed by mark-recapture experiments which have shown that growth was highly underestimated because of age overestimation (de Pontual *et al.* 2006). The records of electronic tags have also shown that hake may undergo nocturnal vertical movements associated with significant temperature gradients in addition to horizontal migratory periods (de Pontual, et al., unpublished). As proven by the results reported in this study, behavioural variability may impact otolith opacity and complicate even more the interpretation of otolith macrostructures for age and growth estimation at an individual level, although some behavioural characteristics might be synchronous at population or stock level as it suggested by Courbin et al (2007).

Size group	Period	T	Feeding	growth	opacity	metabolism effect	growth effect	temperature effect
SF	1	12°C	reduced	low SGR uncorrelated with OGR	translucent	significant due to feeding conditions	no significant	
SF	2	9 or 13°C	ad libitum	positive SGR correlated to OGR	opaque	significant due to feeding and growth conditions	significant	minor : decrease of temperature tends to opaque area
LF	1	12°C	ad libitum	SGR and OGR correlated	opaque		significant	
LF	2	9 or 13°C	ad libitum	SGR correlated with OGR and temperature	translucent	significant, due to gonads development : led to translucent area	significant : low growth led to translucent area	minor : decrease of temperature tends to opaque area

Table 3: Summary of the main results obtained during this experiment.

Growth and opacity modelling

This study of otolith opacity from the two size-groups highlighted the interaction of numerous factors: metabolism, growth and temperature. The proposed otolith opacity model (Eq.4) explicitly takes into account two main factors: the fraction of the otolith growth that can be explained by the somatic growth and the fraction of the otolith growth that cannot be predicted from somatic growth. A model relating otolith growth and otolith opacity was previously investigated by Hüssy and Mosegaard (2004) who linked otolith opacity to protein synthesis. A drawback of this model was that protein synthesis was parameterized from fish feeding and was difficult to link to somatic growth. In the proposed otolith opacity model, a link to metabolic energy fluxes can also be established: the first factor is clearly associated with the contribution of the somatic growth energy flux, and the second one can be regarded as the contribution of the others metabolic fluxes, especially maintenance, to otolith growth. This formulation is coherent with Hüssy and Mosegaard, (2004), as both somatic growth and maintenance fluxes are associated with protein synthesis. The interest is that it makes explicit two complementary contributions.

This model provides a suitable basis for interpreting the observed opacity changes. The parameter setting of the general model (Eq.6) resulted in the following expected behaviour: for low somatic growth rates, more translucent opacity were predicted and conversely for high somatic growth rates. Interestingly, a general parameterization of the model common to both size-groups and periods was proven significant, stressing the interest and the potential genericity of the model. This model was also valid for interpreting opacity changes between periods P_1 and P_2 due to metabolic changes. For the SF group, the restricted

feeding conditions during period P_1 led to a low somatic growth and consequently to more translucent opacities due to the lower contribution of the somatic growth in the otolith growth. The proposed opacity model did not explicitly take into account a temperature effect. From the analysis reported in this study as well as previous work (Høie and Folkvord 2006; Høie *et al.* 2008), a temperature effect (f(T)) could be formally introduced in the model through a modulation of opacity by temperature as follows:

$$Op = f(T) [\alpha' \times SGR/ OGR + \beta' \times resOGR / OGR + \varepsilon] \quad \text{(Eq 8)}$$

Temperature modulation would be such that function would be a decreasing function of T, predicting more translucent opacities at greater temperature for similar metabolic variables as observed in the present study for the LF group and for cod in previous studies (Høie and Folkvord 2006; Høie *et al.* 2008). The experimental data presented in this work does not permit investigating further such a model and this issue will be considered in future work experimenting larger range of temperature. This work also provides the experimental basis for developing numerical otolith models, based on bio-energetic models which could jointly predict otolith growth and opacity in relation to metabolic and temperature conditions (Fablet et al, unpublished). As these bio-energetic models took into account the growth in volume, the growth and opacity models established in this work were again estimated with the volume data giving comparable results.

Acknowledgments

The authors are thankful to François Garren and Magali Hervy for their technical assistance and for their help during rearing experiments and otoliths preparations. This work has been supported by national ANR grant “OTOCAL”.

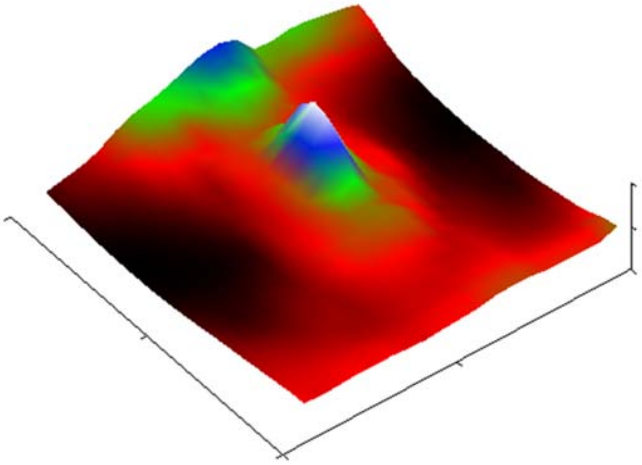

Chapitre 4 :

Compréhension du processus de biominéralisation de l'otolithe: analyse micro-échelle par micro-spectrométrie Raman de la distribution spatiale des fractions organique et minérale

Chapitre 4 :

Compréhension du processus de biominéralisation de l'otolithe: analyse micro-échelle par micro-spectrométrie Raman de la distribution spatiale des fractions organique et minérale

L'étude des relations entre les caractéristiques physico-chimiques des structures de l'otolithe et les facteurs environnements est d'importance pour la compréhension du processus de biominéralisation et donc l'intégration de ces informations sur l'otolithe. L'analyse des fractions minérale et organique est particulièrement difficile du fait de la taille des otolithes et des quantités en matière organique présentes (quelques pourcents de la masse). Néanmoins il est généralement admis que ces fractions varient sur un rythme journalier définissant des zones L, supposées comme majoritairement composées de fraction minérale et des zones D majoritairement composées de fraction organique. Ces résultats proviennent d'observations faites après attaque acide et analyse au microscope électronique à balayage (MEB) ou après coloration. Ces techniques ont cependant un inconvénient : elles modifient l'échantillon et en particulier la composition des structures analysées par l'intervention de l'attaque acide.

La micro-spectrométrie Raman correspond à l'analyse des réponses de la matière sous forme de spectres vibrationnels à un rayonnement lumineux monochromatique. Non destructive, elle permet d'analyser conjointement les composés des fractions minérale et organique à l'échelle du micron. Cette étude constitue une première approche de la micro-spectrométrie Raman et contribue donc à la mise au point des conditions analytiques optimales pour l'étude des otolithes et à la caractérisation des signatures d'intérêts sur les

spectres vibrationnels. Nous avons appliqué cette technique sur des coupes transversales fines de merlu en vue de : 1) caractériser de façon simultanée les variations des fractions minérale et organique à la fois au niveau du nucleus de l'otolithe ainsi que sur une succession de microstructures ; 2) mettre en évidence les différences significatives entre ces fractions ; 3) quantifier les effets des techniques d'attaque acide et de coloration au niveau des structures étudiées. Ces résultats ont été confrontés aux précédentes informations sur la composition du nucleus et des microstructures ainsi qu'à une récente étude parue en 2008 utilisant la micro-spectrométrie Raman pour caractériser le nucleus.

Concernant le nucleus, le primordium, structure initiale de l'otolithe, apparaît comme un point très localisé montrant une forte luminescence et des concentrations élevées en composés organiques contenant des groupes CH. La zone du sulcus, sillon médial de l'otolithe en contact avec la macula, est caractérisée par une composition similaire à celle du primordium suggérant que l'orientation de l'otolithe et son lien avec la macula se produisent tôt dans la vie du poisson (dans les 10 premiers jours).

La caractérisation des zones L et D en zone opaque indique que les deux structures contiennent les fractions organique et minérale affichant des variations cycliques et synchrones. Contrairement aux résultats obtenus après une attaque acide à l'EDTA, les zones L sont plus des concentrées en composés organiques contenant des groupes CH, à l'inverse des zones D plus riches en aragonite. Cette fraction organique semblait être révélée par la coloration de Mutvei's et affectée par l'attaque acide à l'EDTA ce qui suggèrent qu'elle correspond à la fraction soluble (à l'EDTA) de la matière organique contenue dans l'otolithe. De tels résultats indiquent que les zones L et D diffèrent dans leurs constituant organiques. La micro-spectrométrie Raman apparaît donc comme une puissante technique d'analyse quantitative des caractéristiques physico-chimiques de l'otolithe pour une meilleure compréhension du processus de biominéralisation.

Understanding otolith biomineralization process: new insights on microscale spatial distribution of organic and mineral fractions from Raman micro-spectrometry

Aurélie Jolivet[1], Jean-François Bardeau[2], Ronan Fablet[1,3], Yves-Marie Paulet[4], Hélène de Pontual[1]

Analytical and Bioanalytical Chemistry (2008) 392: 551-560

Abstract

It is generally accepted that the formation of otolith microstructures (L- and D- zones) and in particular the organic and mineral fractions vary on a daily basis. Raman micro-spectrometry provides a non destructive technique that can be used to prove structural information on organic and mineral compounds. We applied it on thin otolith sections of hake and addressed the following issues: 1) the simultaneous characterization of variations in the organic and mineral fractions both in the core area and along successive otolith microstructures; 2) elucidating significant differences between these fractions; 3) quantifying the effects of etching and staining protocols on otolith structures. The primordium appeared as a punctual area depicting higher luminescence and greater concentrations in organic compounds containing CH-groups. Sulcus side showed similar composition suggesting that the contact of the otolith with the macula and its orientation in otosac occur rapidly (about ten days). The characterization of L- and D-zones in the opaque zones indicated that both structures contained organic and aragonitic fractions with cyclic and synchronous variations. Contrary to the results obtained after EDTA etching, L-zones depicted greater concentrations in organic compounds containing CH-groups, conversely to D-zones richer in aragonite. This organic fraction seemed to be revealed by Mutvei's staining and affected by EDTA etching which suggests that it corresponds to the

soluble fraction of organic matrix. Such results indicate that L- and D- zones differ in their respective organic constituents. Raman micro-spectrometry thus appears as a powerful technique to acquire quantitative information that is required for a better understanding of otolith biomineralization.

Introduction

Otoliths are calcareous concretions in fish inner ears. Their accretional growth follows a circadian rhythm that is physiologically controlled and influenced by environmental conditions (Pannela 1971; Panfili *et al.* 2002a). The formation of daily L- and D-zones result, also referred to as microstructures as well as of opaque and translucent macrostructures (Figure 1). The otoliths act as biological archives providing the basis for the reconstruction of individual life traits and environmental parameters. They thus deliver invaluable information in fisheries sciences and marine ecology (Campana 2005). However in many cases the interpretation schemes of both structural and chemical information remain incomplete and debatable. New advances in the analysis and the understanding of otolith biomineralization, especially regarding the relationships between the physico-chemical characteristics of the accretion and the associated environmental and physiological conditions, are of key importance to fully exploit the potential of these biological archives (Campana 2005; Allemand *et al.* 2007).

Overall the calcium carbonate fraction, mainly in aragonite form, represents 90-99 % of the total mass of fish otoliths. The remaining 1-10% includes the organic matrix, composed of collagens, proteoglycans and proteins (Murayama *et al.* 2000; Murayama *et al.* 2002; Borelli *et al.* 2003b). The role of organic matrix in the formation of the deposited layer is not fully understood, although different studies have demonstrated that it controls the biomineralization of the otolith (Murayama *et al.* 2002; Söllner *et al.* 2003). L- and D-zones

have been described as depicting different compositions in term of organic and mineral fractions (Campana 1999; Payan *et al.* 2004b; McCreadie *et al.* 2006) by global quantitative and fine scale qualitative experiments. To our knowledge, these compositions have never been quantified at a micro-scale. Given the spatial resolution and the capacity of simultaneously characterizing organic and mineral compounds, Raman micro-spectrometry is particularly well-suited to address these issues.

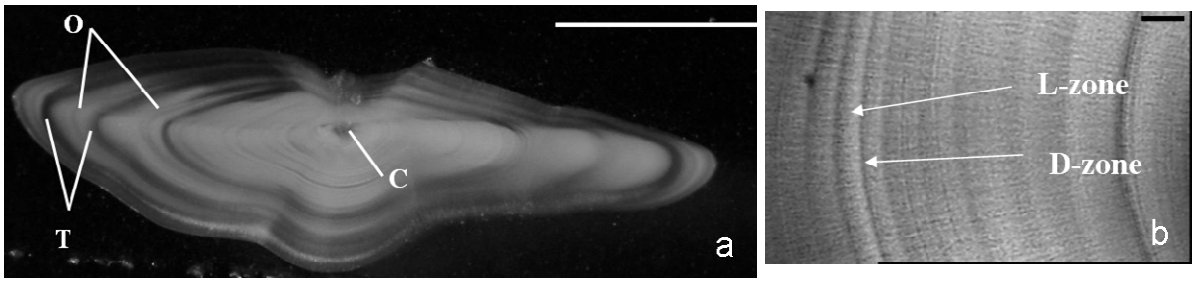

Figure 1: Otolith structures at macro and microsocopic scales. a) Transverse section of a hake otolith observed under reflected light showing opaque (O) and translucent (T) zones. Opaque zones appear dark in transmitted light and bright in reflected light, and vice versa for translucent zones. The core (C) corresponds to the area surrounding the primordium which is the initial structure of otolith. Scale bar: 1 mm. b) Thin transverse section of a hake otolith under transmitted light microscopy. Primary increments composed of L- and D-zones are clearly visible. Scale bar: 10 µm

Raman micro-spectrometry is a non destructive technique which provides a quantitative characterization of vibrational physico-chemico features of both organic and mineral compounds. Regarding calcified structures, Raman micro-spectrometry permits discriminating vaterite, aragonite and calcite in otoliths of different species (Gauldie *et al.* 1997; Tomás and Geffen 2003; Melancon *et al.* 2005; Tzeng *et al.* 2007), and is also particularly well-suited to study the organic matrix of corals (Kaczorowska *et al.* 2003), the

degradation of skeletal organic matrix (Perrin and Smith 2007) and mollusc shell pigments (Hedegaard *et al.* 2006). More recently Raman micro-spectrometry was used to identify and analyze variations of the characteristics of the organic matrix in fish otoliths (Zhang *et al.* 2008).

Here, we use Raman micro-spectrometry to investigate physico-chemical variations in the organic and mineral constituents of fish otoliths in relation to observed micro-structures. Experiments are reported for thin sections of European hake (*Merluccius merluccius*) otoliths. Our main contributions are three-fold: 1) characterizing mineral and organic fractions within otoliths microstructures (namely, primordium and L- and D-zones); 2) elucidating significant differences between L- and D- zones; 3) highlighting the differential effects of etching and staining on the organic and mineral fractions of these zones.

Material and Methods

Otolith samples

We considered a series of otoliths extracted from hake caught in the Bay of Biscay in June 2005 and 2007 or reared in controlled facilities (Table 1). Larval, juvenile and adult fish were available and fish size (total length) ranged from 4.3 mm (larva size) to 50 cm. To obtain thin sections, the standard otolith preparation method consisted of: 1) embedding in epoxy resin, 2) sectioning in transverse or sagittal plane, 3) grinding, and 4) polishing to the core. Larval otolith was extracted under polarized light, mounted on an epoxy resin drop and directly analysed on sagittal plan without any further preparation.

Name	Origin	Size (cm)	Thickness (µm)	Section	Preparation method	Area	Analysis	
S1	Rearing	25	150	Transversal	Standard	Core	T: 20µm	S: 6µm
S2	Wild	33	394	Transversal			T: 40µm	S: 2.5µm
S3	Wild	20	325	Transversal			T: 40µm	S: 2.5µm
				Transversal			2D-M: 30µm x 40µm	S X: 2.5µm
								S Y: 3µm
S4	Rearing	4.3 mm		Sagittal			T: 15µm	7, 12, 14 µm
S5	Wild	21	100	Sagittal		L- and D-zones	T: 44µm	S: 0.7µm
S6	Wild	34	299	Sagittal			T: 36µm	S: 0.8µm
S7	Wild	20	375	Transversal	Acid etching		T: 12µm	S: 0.7µm
S8	Wild	30	132	Transversal	Mutvei's staining		T: 5µm	S: 0.2µm

Table 1: Details on otoliths samples investigated by Raman micro-spectrometry: fish origin and size (cm), thickness (µm) and type of otolith section (transversal or sagittal), preparation method, analyzed area and characteristics of the analysis (T: transect, M: Mapping, D: Distance between two analysed points).

Etching and staining protocols

Etching was performed using a 5% EDTA (ethylene diamine tetra-acetate) solution at pH 7. EDTA is as calcium chelator frequently used for otolith decalcification. Section S7 was exposed to the EDTA solution for a period of 90 seconds after which the sample was rinsed with milliQ water.

To enhance the optical contrast of otolith structures, otolith sections were stained. For this purpose, we used Mutvei's solution (Schöne *et al.* 2005) composed in the following manner: 500 ml 1% acetic acid for 500 ml 25% glutaraldehyde and ca. 5 to 10 g alcian blue. The latter stains mucopolyssacharides and glycosaminoglycans. This dye also performs a

slight etching of the surface as it contains diluted acetic acid. Section S8 was immersed in the Mutvei's solution for 10 min at 45°C and subsequently rinsed with milliQ water.

Analyses of fine-scale otolith structures

Three different types of analysis were carried out at core area, micro-increments in L- and D-zones on 1) standard preparations, 2) EDTA etched preparations, and 3) preparations stained with Mutvei's solution. Details about the analysis are summarized in Table 1.

For the core area, three transversal sections (S1-S3) were analysed. In addition, the sagittal section of an 18 days larva otolith (S4) was considered. Dorso-ventral Raman transects spectra centred on the primordium were acquired with steps varying from 2.5 to 6 µm. For S4, the transect was 14 µm long with points at 7, 12 and 14 µm. In addition, a 2D mapping centred on the primordium was acquired on S3.

Regarding the characterization of L- and D-zones, Raman spectra on transects covering several successive increments were acquired in opaque zones of two sagittal otolith sections (S5 and S6). The sagittal plane was preferred to the transverse one as wider D- and L-zones, typically 2 and 4 µm respectively, were observed.

Regarding EDTA etching, Raman spectra were acquired before and after etching on the opaque zone of S7 along a transect covering two D-zones and two L-zones. Raman measurements were carried out after staining within an opaque zone of S8 along a transect covering three D-zones and two L-zones.

Raman spectrometry

A micro-Raman spectrometer (Jobin-Yvon T64000) equipped with a confocal system and a motorized microscope stage (for Raman mapping purpose) was used and specific experimental conditions were defined. A coherent spectrum argon/krypton ion laser was used to produce radiation with a wavelength of 514.5 nm and a good signal-noise ratio. The laser was focused onto the sample by using a microscope equipped with a x100 objective. The resulting spatial resolution is about 1-2 µm. The scattered light was analysed by a spectrometer with a single monochromator (600 gratings mm^{-1}), coupled to a nitrogen cooled CCD detector. To check that the experimental setting is non-destructive for fish otoliths, several Raman spectra were recorded at the same points between 20 to 200 mW. No heating alteration was observed on spectra when controlling relative intensities and profiles. For the analysis of the otolith core and microstructures, a 50 mW laser power was selected. Stained otoliths were analysed with a 10 mW laser. Spectra were accumulated two to four times with exposure times varying from 30 to 300 s depending on the sample. The depth of analysis was systematically set to 2 µm below the surface to avoid possible contamination linked to surface preparations.

Analysis of Raman spectra

Raman spectra were corrected for background luminescence using baseline subtraction. In the subsequent analysis, reported Raman spectra are baseline corrected and normalized with respect to a reference acquisition time of 50 s and a reference of 50 mW laser. The positions and integrated intensities of identifiable vibrational bands on spectra were determined using the LABSPEC software. Optical images under transmitted light were

acquired before each analysis to record the locations of Raman analysis for subsequent treatment.

Quantitative analysis for characterization of aragonitic and organic fractions

With respect to Raman spectra of fish otoliths, 14 vibrational bands can be directly attributed to aragonite (Urmos *et al.* 1991): symmetric stretching mode (1085 cm^{-1}), anti-symmetric stretching modes (1462, 1574 cm^{-1}), in plane bending modes of CO_3^{2-} (701 and 705 cm^{-1}) and the lattice modes (9 peaks between 113 and 284 cm^{-1}) (Figure 2A). The broad bands observed at 2950-3070 and 3390 cm^{-1} are respectively associated to CH and OH stretching modes (Figure 2B).

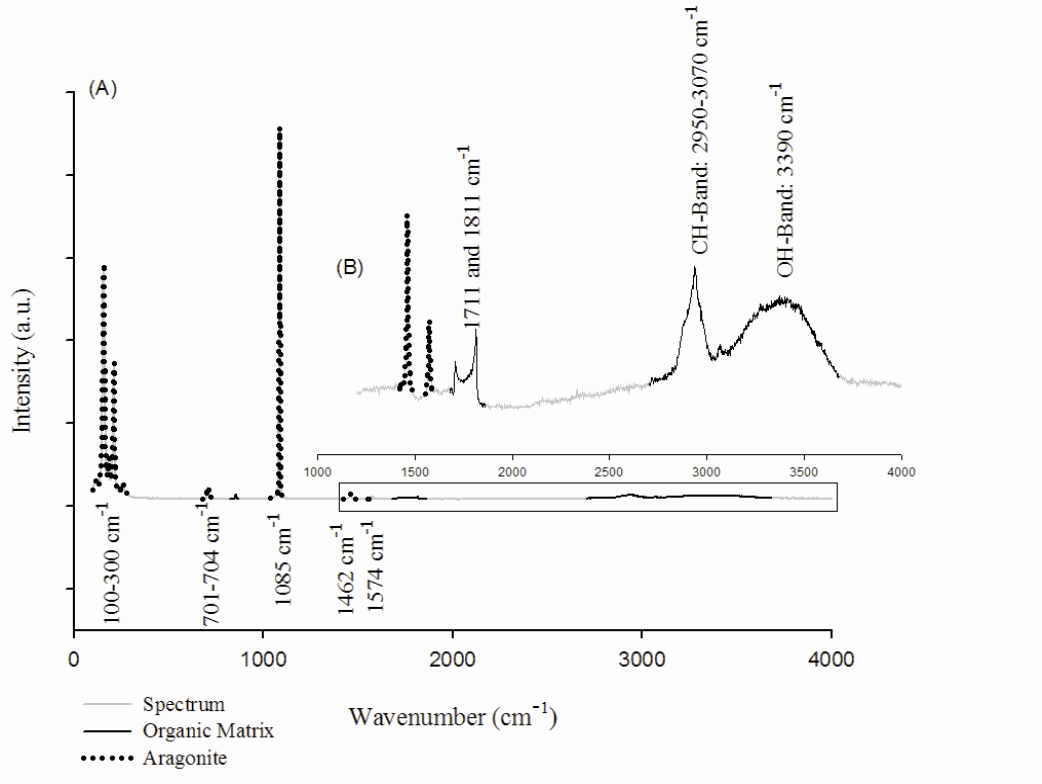

Figure 2: Raman spectrum acquired on sample S5: the spectrum is dominated by the response of Aragonite (in dotted line) in the frequency range 100-4000 cm^{-1} but also

reveals (B) the presence of organic matrix (in black solid line) with main response on CH-peak in the frequency range 1000-4000 cm^{-1}.

The aragonite peak at 1085 cm^{-1} was chosen as the reference peak for the spectra normalization. In this study, we considered the ratio between the response of the CH-group and the peak of aragonite at 1085 cm^{-1} as a proxy of the ratio between the organic and mineral fraction of the otolith structures.

Figure 3 shows the Raman spectra of Mutvei's solution and of the stained otolith. The Mutvei's solution is known to result in a specific response between 1200 and 1700 cm^{-1}. From the Raman analysis of the stained otolith section, we determined the relative fraction of the stained organic matrix *vs* the aragonitic fraction. As the aragonitic peak at 1085 cm^{-1} is occluded by the Raman response of the dye, we used the peaks between 100 and 300 cm^{-1} as the aragonitic references. The ratio between this aragonitic reference and the dye-specific Raman response between 1200 and 1700 cm^{-1} was then calculated.

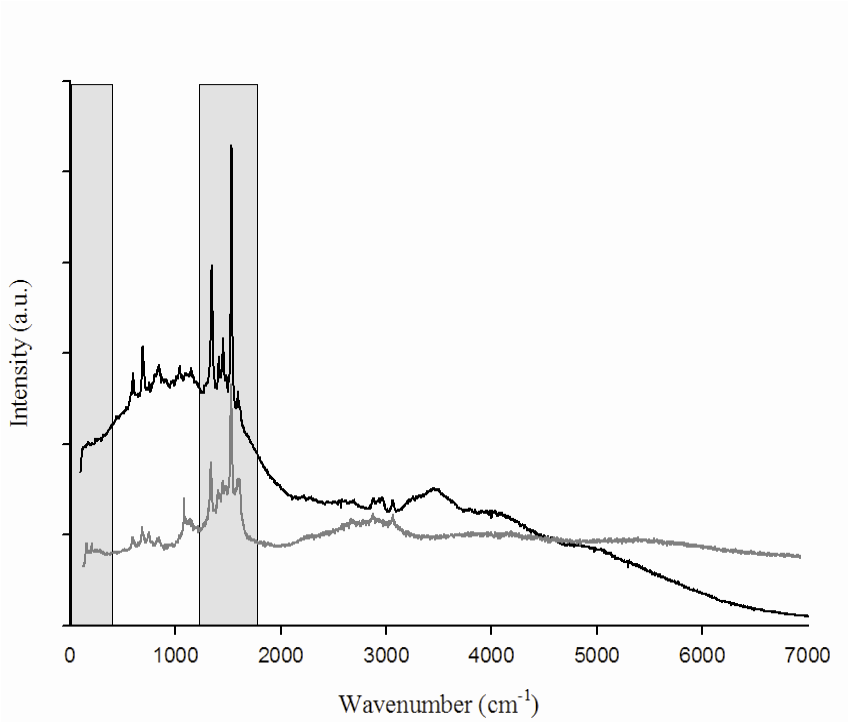

Figure 3: Raman spectra of Mutvei's solution (in dark) and on S8 stained with Mutvei's solution (in grey): the main signature of the staining agent between 500 and 2000 cm^{-1}

(514.5 nm wavelength radiation, laser power of 20 mW and acquisition time of 20 s, 20 times). The two grey areas underline aragonite signatures (100-300 cm^{-1}) and Mutvei's solution signatures (1200-1700 cm^{-1}) considered for the analyses.

Glossary

For the sake of clarity, we abbreviated organic matrix (OM), Aragonite (AR) represented by the band at 1085 cm^{-1}, CH-group (CH) the whole bands observed in the region 2950-3070 cm^{-1}, OH-group (OH) bands in the region 3390-4000 cm^{-1}, and OM/AR, CH/AR and OH/AR, the respective ratios between the integrated intensity of the bands described previously.

Results

Core area

For samples S1-S4, the main peaks of the Raman spectra acquired in the core area are reported in Table 2. Their wavelength and possible assignments to known vibrational modes are given and compared to previous results (Careche *et al.* 1999; Piot *et al.* 2000; Ikoma *et al.* 2003; Zhang *et al.* 2008).

Wavenumbers (cm^{-1}) Zhang (2008)	Wavenumbers (cm^{-1}) Samples S1-S4	Band attribution (Careche *et al.* 1999; Piot *et al.* 2000; Ikoma *et al.* 2003; Briget Mary and Ramakrishnan 2005; Zhang *et al.* 2008)
	641	$(SO_4)^{2-}$ asym bend
765	755	Trp, Amide IV, V
830	824	ν- ring, Tyr, Ac Asp
853	853	δ(CCH) ring, ν(C-C), Tyr, Ac asp
880	878	δ(CCH) ring, Trp, Val, Hyp
940	937	Nonaromatic ν(C-C), Lys, Val, Leu
1003	NS	Phe
1031	NS	Phe
	1085	Aragonite
	1110	ν CN
	1185	Tyr
	1200-1272	amide III
1272	NS	amide III
1297	1297	δ(C=H), phospholipids
1443	1444	CH_2, CH, CH_3 bending
1461	1460	Aragonite
1555	NS	Trp
1574	1574	Aragonite
	1610	Trp, Phe, Tyr ν-ring
1660		Amide I
2852	2851	$\nu(CH_2)_{sym}$ lipids
2882	2876	$\nu(CH_2)_{asym}$ lipids, $\nu(CH_2)_{sym}$ proteins
2942	2941	$\nu(CH_3)_{sym}$ proteins and lipids, $\nu(CH_2)_{asym}$ proteins
	3067	CH stretch

Table 2: Wavenumbers and assignments of the Raman bands observed in the core area: comparisons between results reported by Zhang *et al.* (2008) on small yellow croaker and sample S1 from our study. In the table, NS is indicated a non significant intensity on Raman spectra.

Figure 4 shows Raman spectra of the S1 primordium zone. A greater luminance was observed in conjunction with the primordium than the surrounding points. The intensities of amides and amino acids peaks reached maxima in the primordium (Figure 4B) as well as CH and OH groups (Figure 5A).

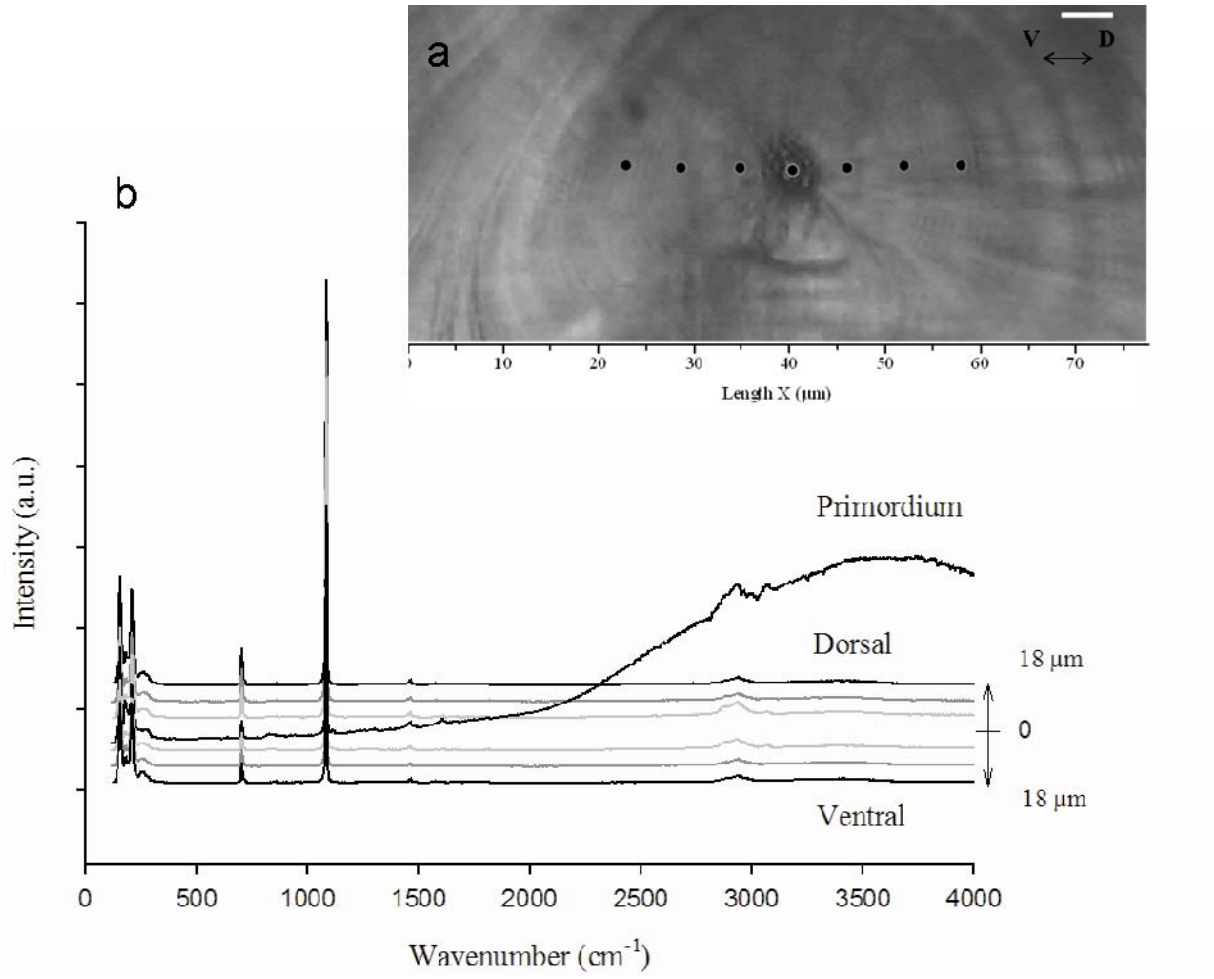

Figure 4: (A) Typical view of S1 thin section obtained by light microscopy. The ventral (V) and dorsal (D) area are shown as well as the source point positions (adjacent points are separated by 6 µm) where spectra were collected (scale bar = 5 µm); (B) Raman spectra acquired along the considered dorso-ventral transect in the 100-4000 cm^{-1} region. For clarity, the spectra are only shifted (and not background corrected).

Similar results were observed for S2-S4 samples as shown in Figure 5B with the evolution of CH/AR as a function of the distance from the primordium. The primordium was also shown to be 10 times more concentrated in CH than points located at 18 µm in the dorsal and ventral directions.

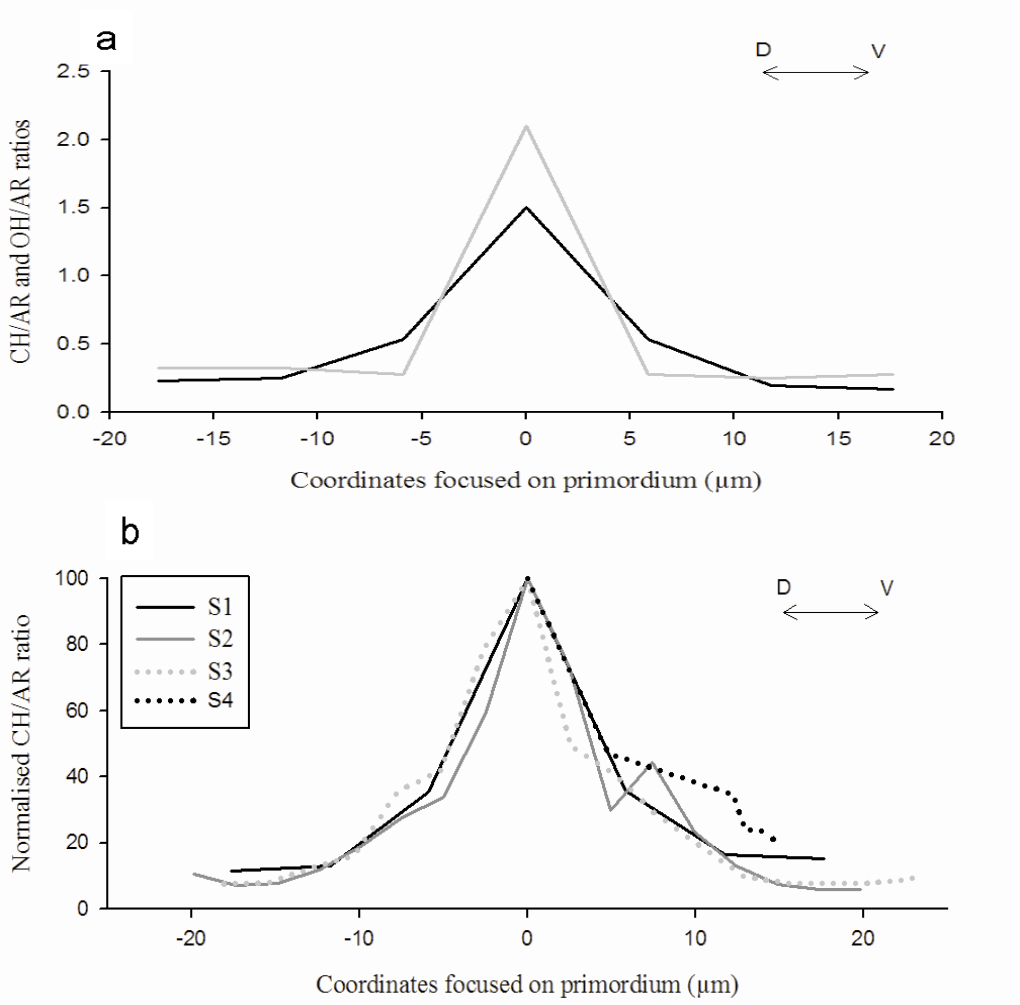

Figure 5: Normalized integrated intensity of OM/AR calculated for S1 to S4 in the primordium area. (A) CH/AR (in dark) and OH/AR (in grey) as a function of the distance from the primordium for the sample S1. (B) Evolution of CH/AR signature (CH/AR was normalised by CH/AR from the primordium) as a function of the distance from the primordium for samples S1 to S4.

Besides, the spatial distribution of the CH/AR ratio in the core area (30 µm x 40 µm mapping around the primordium) of S3 is reported (Figure 6). Whereas the decrease of the CH/AR ratio along the anti-sulcus, dorsal and ventral directions is isotropic and similar to the profile depicted in Figure 5, the sulcus area is characterized by a greater CH/AR ratio.

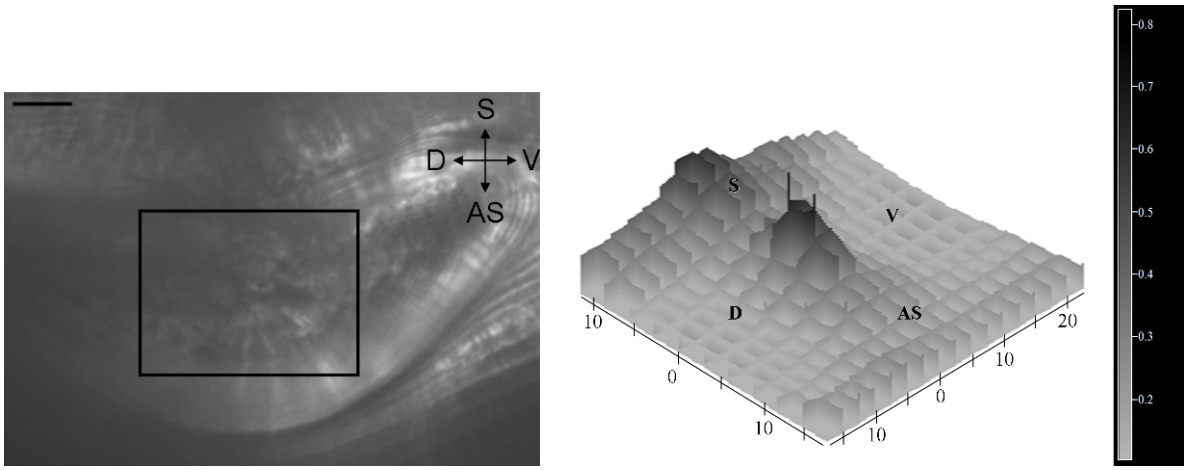

Figure 6: (A) View of S3 thin section under light microscopy. The rectangle (30 µm x 40 µm) centred on primordium, represents the 2D Raman mapping area: step increments were fixed to 3 µm and 2.5 µm in the X and Y directions respectively (scale bar = 10 µm); (B) XY micro Raman mapping of the normalized integrated intensity of CH/AR (D: dorsal, V: ventral, S: sulcus AS: antisulcus). Coordinates were focused on primordium (µm).

L- and D-zones

Analyses of L- and D-zones were carried out on S5 and S6. The Raman spectra of one L-zone and one D-zone are shown in Figure 7 along with the evolution of the AR, CH (Figure 8B) and CH/AR ratio (Figure 8C) along the transects considered. OH-response was relatively stable compared to the CH-signature, which varies according to alternating L- and D-zones (Figure 7).

(A)

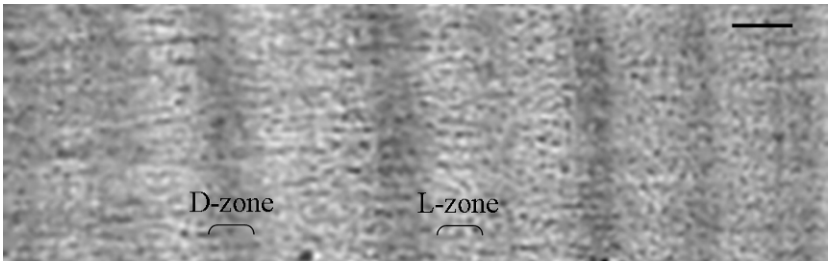

(B)

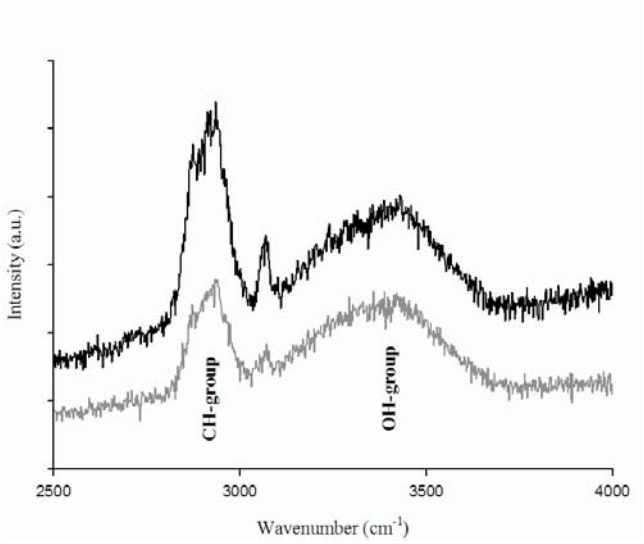

Figure 7: (A) Typical view of S5 thin section obtained by light microscopy; (B) Raman spectra in the 2500-4000 cm^{-1} region of one L-zone (dark spectrum) and one D-zone (grey spectrum) on S5 (scale bar = 5 μm).

Both CH and AR responses showed cyclic variations but different ranges of variations (Figure 8B). Cycles with maxima located on L-zones and minima on D-zones were also observed for CH/AR (Figure 8C). L-zones displayed a greater relative concentration in CH and D-zones a greater relative concentration of AR (Figure 8B). Similar results were obtained from the analysis of the second S6 sample.

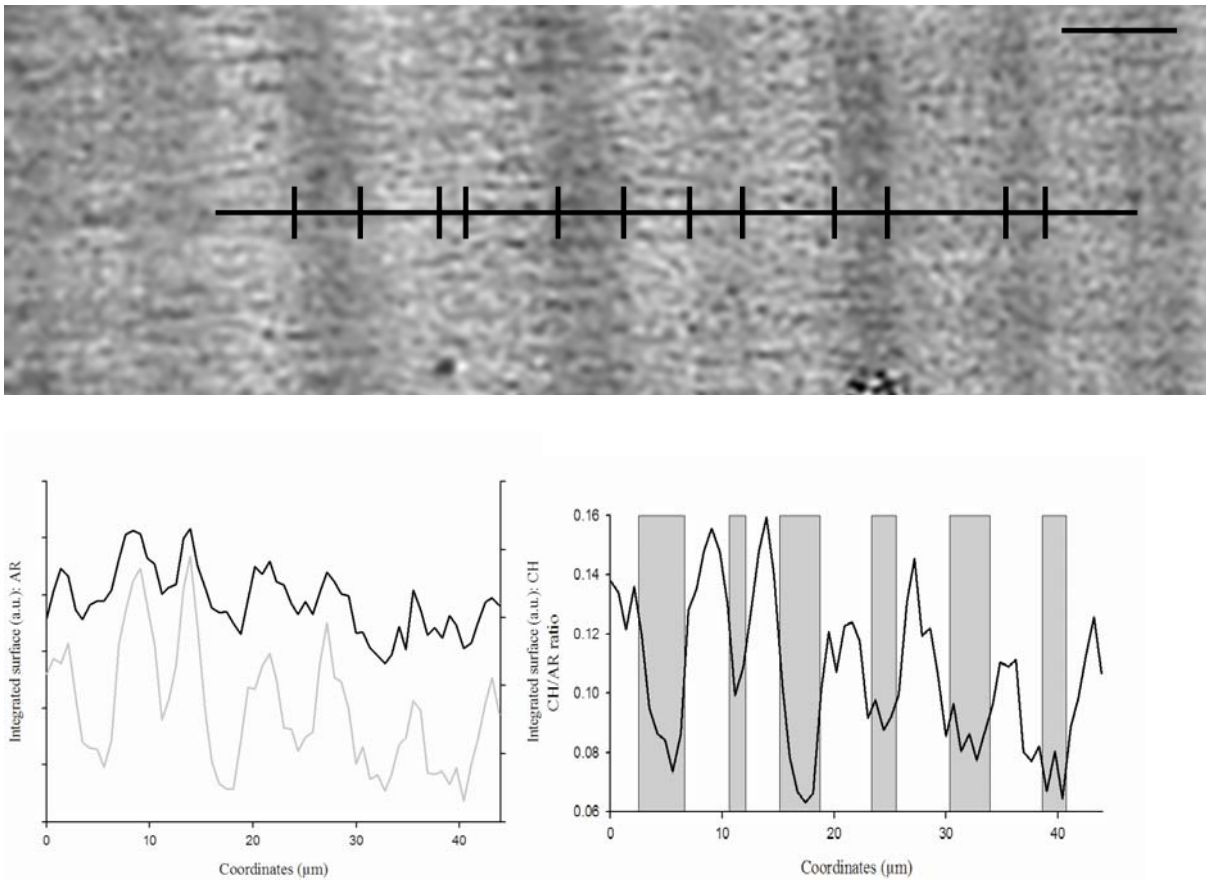

Figure 8: (A) Typical view of S5 thin section under light microscopy. Markers delimit the successive L- and D-zones (scale bar = 5 µm); (B) Integrated Raman intensities of AR (dark line) and CH (grey line) along the line direction. (C) Evolution of CH/AR with D-zones depicted as grey areas.

Effects of EDTA etching

The variation of CH/AR along the considered transects before and after etching is shown in Figure 9. Whereas CH/AR depicted a maximum response in L-zones before etching, the maxima were located in D-zones after etching. AR responses after etching were lowered by a factor of 0.8. On the contrary, CH variations were greater by a factor of 1.3 after etching. This resulted in a greater CH/AR after etching (Figure 9).

(A)

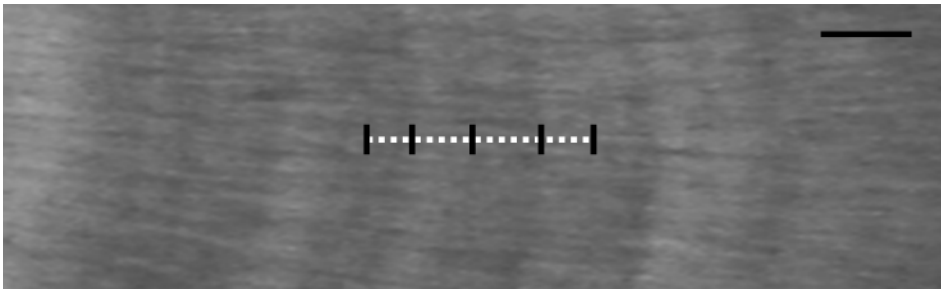

(B)

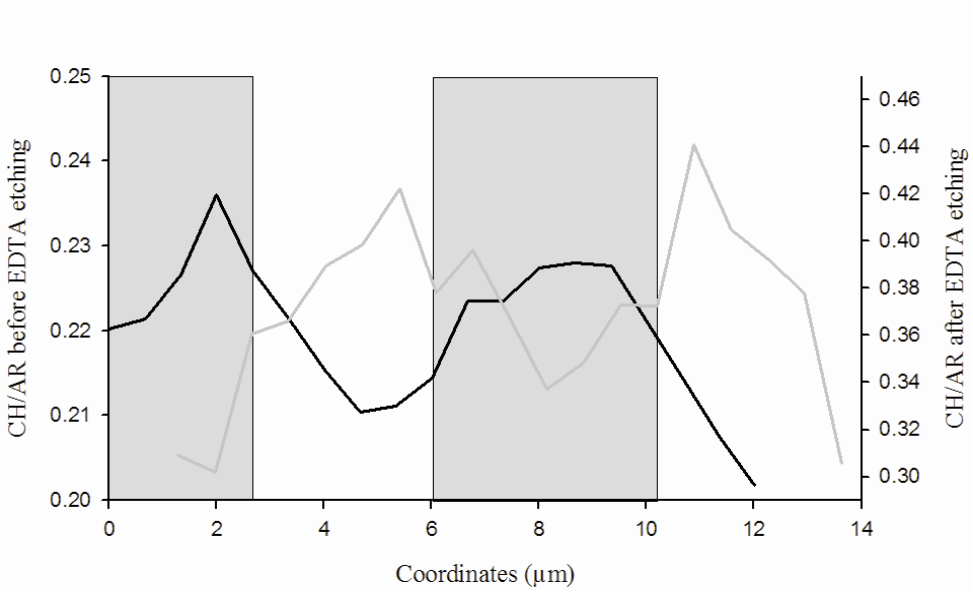

Figure 9: (A) Typical view of S7 thin section of otolith obtained under light microscopy before acid etching. Markers delimit the successive L- and D-zones (scale bar = 5µm); (B) Evolution of CH/AR before (grey line) and after (dark line) acid etching with D-zones marked by grey areas.

Effects of staining

The analyses of the Raman responses of the AR fraction and of the dye after otolith staining with Mutvei's solution are reported in Figure 10 for a transverse otolith section. Optically L-zones displayed greater degree of staining. The Raman response of the Mutvei's dye on otolith showed cyclic variations in phase with the variations in AR. Maxima are

located in L-zones (Figure 10A), and the ratio between these two signatures varied according to cyclic behaviour with maxima in L-zones (Figure 10B).

(A)

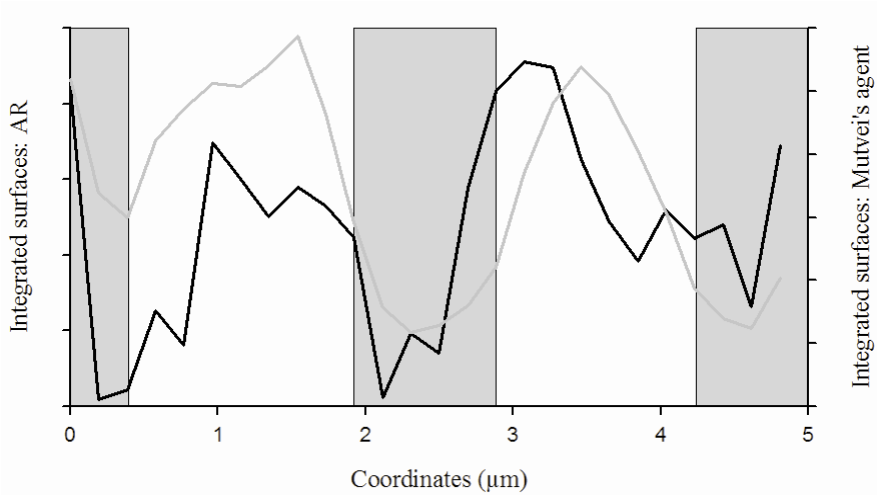

(B)

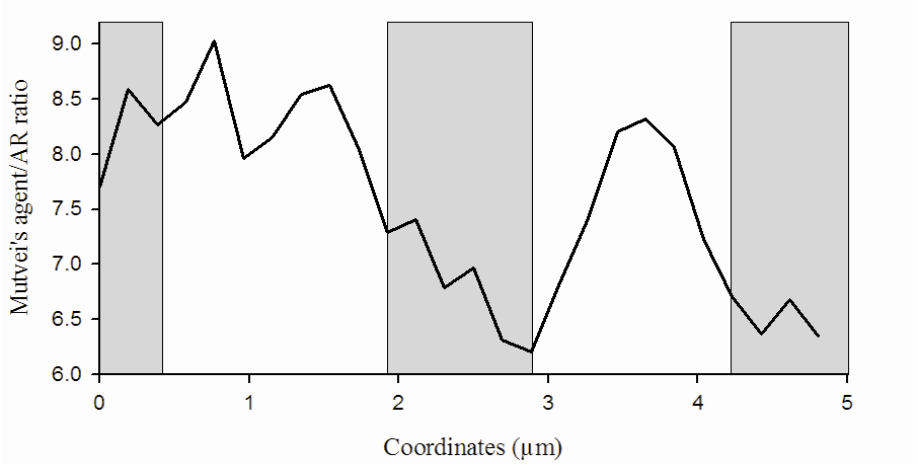

Figure 10: Integrated surfaces of Mutvei's and AR signatures and Mutvei's/AR from Raman spectra after Mutvei's staining on sample S8. Analyses were made on transect covering 3 L-zones and 2 D-zones. (A) Evolution of the AR (dark line) and Mutvei's solution (grey line) responses on otolith. (B) Evolution of the ratio between Mutvei's and AR signatures as a function of the position along the transect.

Discussion

Core

The analysis of the Raman spectra confirmed that primordium is a very specific point of the otolith with a greater concentration of CH and other organic compounds, such as collagen and amino acids, compared to other areas of the otolith. SEM observations lead to similar conclusions with the primordium being detected as a point of greater density (Morales-Nin 1987). According to Pisam *et al.* (2002) this structure is highly concentrated in glycogen and collagens. The analysis of the Raman spectra also showed that this feature was very punctual, corresponding to the primordium (about 2µm width). Zhang *et al.* (2008) recently reported a qualitative Raman characterization of small yellow croaker and discussed the identification of main organic compounds namely collagen with signatures of amides I, III, IV and V and aromatic amino acid such as phenylalanine, tyrosine and tryptophan. It is worth noting that Zhang *et al.* (2008) did not show and discuss the 1050-1200 cm^{-1}spectral region. For this reason, no comparison can be made in this frequency range. Otherwise, most of the peaks found in our study have been observed by Zhang *et al.* (2008) except Phe-signatures at 1003 and 1031 cm^{-1} and Trp-peak at 1555 cm^{-1} that might be masked by the strong aragonite signatures at 1085 and 1574 cm^{-1} respectively. The peak observed at 1272 cm^{-1} in our spectra was integrated in a larger band (1206 and 1280 cm^{-1}) with maximum at 1234 cm^{-1}. In contrast, some peaks observed for samples S1-S3 were mentioned by Zhang *et al.* (2008). These peaks correspond to Tyr-signatures at 1185 and 1610 cm^{-1}, CN group at 1110 cm^{-1} and CH-stretch at 3067 cm^{-1}.

The 2D mapping of the region surrounding the primordium exhibited interesting features. The concentration of the CH-related compounds was found to decrease from the primordium zone along the dorsal, ventral and anti-sulcus directions. Regarding the sulcus

area, a similar initial decrease was observed up to 9µm from the primordium. Subsequently, the concentration of the CH-related compounds increased again, up to values comparable to those of the primordium zone. It is known that the sulcus zone is in contact with the macula (Dunkelberger *et al.* 1980; Platt and Popper 1981; Fay 1984). Moreover, the cells of the macula and of the adjacent zone are the sources of both organic precursors and calcium ions in the endolymph (Pisam *et al.* 1998). Given the distance from the primordium to the valley is about 9 µm, this observation suggests that the otolith was in close proximity to the macula at a recent stage and thus oriented in the otosac. Such link would be established at about 10 days post hatching (Alvarez and Cotano 2005).

L and D-zones

Previous studies on the characterization of L- and D-zones concluded that D-zones were richer in OM than L-zones (Morales-Nin 1987; Secor *et al.* 1992). Such characterizations of L- and D-zones were carried out after EDTA etching. Under this condition, the reported Raman characterizations provided similar results. Variations of AR responses depicted maxima located on L-zones, and conversely for CH, such that the relative proportion of CH *vs* AR was greater in the D-zones than in L-zones after etching.

The analysis of the Raman spectra on L- and D-zones before EDTA etching led to different conclusions. The responses of the organic compounds and aragonitic fraction as well as the CH/AR were greater on L-zones than on D-zones. As a consequence, these results contradict the widely accepted model stating that organic material concentration is greater in D-zones (Panfili *et al.* 2002a). Whereas differences in crystal organization (e.g., crystal orientation and density) might affect the absolute values of the responses of the aragonite and organic compounds, such physical properties should not affect the CH/AR. L-zones are richer

in CH-related organic fraction (relatively to the AR fraction) which suggests that L- and D-zones are associated with different biomineralization processes. Both of these processes involve the biomineralization of organic and mineral factions but some organic compounds being more specific to L-zones.

The comparison of the results before and after etching pointed out that the action of EDTA etching reversed the analysis of the CH/AR in L- and D-zones. It is shown that EDTA etching acted differently on L- and D-zones. Hence, L- and D-zones did not only differ in the relative proportions of organic and mineral compounds but also in their structural organization, such that D-zones are less sensitive to EDTA etching. D-zones appeared to be richer in CH after etching. That could be explained by highlighted CH signature after AR etching. As suggested by SEM observations of thin otolith sections (Morales-Nin 1987; Secor *et al.* 1992) D-zones may be associated with a denser organic mesh, in which CH organic compounds would be weakly involved, such that the overall deposited structure would be more stable in D-zones. This inversion presupposed that L- and D-zones contained different OM compositions with L-zones richer in compounds that are soluble in EDTA.

Mutvei's staining reveals etch-resistant lines called growth lines and etched depressions called growth increments (Schöne *et al.* 2005). Alcian blue in Mutvei's solution is used as an indicator of acid mucopolyssacharides (Marxen *et al.* 1998) and underlined carbon and nitrogen content of carbohydrates (Alldredge *et al.* 1993). These compounds have been detected in the soluble organic matrix extracted from several fish species (*Salmo salar* (Wright 1991a); *Oncorhynchus mykiss* and *Psetta maxima* (Borelli *et al.* 2001) and *Gadus morhua* (Dauphin and Dufour 2003). L-zones were optically blue-stained by the dye and the agent signature followed that of AR. These results corroborated the above conclusion stating that L-zones are richer in organic compounds revealed by the dye, such as polysaccharides (carbohydrates such as glycogen). Mutvei's staining was also shown to react more strongly

with organic compounds soluble in EDTA (Schöne *et al.* 2005). Therefore, the agreement between Raman characterization of CH responses and Mutvei's staining in L-zones may suggest that CH-responses are partly associated with the EDTA-soluble fraction of the OM. In Murayama *et al.* (2000), the OMP-1, a collagen-like protein assumed to be involved in structuring the otolith biomineralization, was shown to be weakly present in the EDTA-soluble organic fractions. Such a structuring organic fraction would be relatively more present in the D-zones such that these zones would be less affected by EDTA etching, providing an explanation to the inversion observed before and after acid etching in terms of relative proportion of the organic and mineral compounds.

The agreement between the Raman characterization of the responses of CH and Mutvei's staining in L- and D-zones may also be interpreted as an evidence that CH signatures are associated with otolith organic compounds such as polysaccharides, glycosaminoglycans and proteoglycans. An additional evidence supports this assumption. Mutvei's solution was shown to underline water-soluble macromolecules (polysaccharides) previously reported to play a key role in biomineralization and in particular in the nucleation of otolith (Pisam *et al.* 2002). This is in accordance with the strong CH-response observed on Raman spectra on the primordium.

Conclusion

A lot of effort have been devoted to the analysis of the chemical composition of the otolith (de Pontual and Geffen 2002) at scales from one up to hundreds of micrometers depending on the chemical signatures of interest (e.g., elemental composition, isotopic ratios) and on the considered analytical method (e.g., WDS, LA-ICPMS, IRMS) (de Pontual and Geffen 2002; de Pontual *et al.* 2003c; Tomás *et al.* 2006). Such chemical analysis provide data that are required for specific fisheries issues (e.g. reconstructing individual life traits,

analysing population structure etc.). However they do not supply information on the relative organic and mineral fractions of the otolith which has a key role in the understanding of the underlying biomineralization processes.

Because Raman micro-spectrometry (unlike Fourier transformed infrared spectroscopy) has potential for non destructive and micro-scale diagnostics, this study was designed to quantify and characterize organic and mineral fractions in otoliths structures. The main contributions, exemplified here by the determination of the relative spatial variations of the AR and CH fractions are three-fold: 1) the simultaneous analysis of the organic and mineral fractions of the otolith; 2) a subscale analysis (1µm) corresponding to daily if not subdaily timescales on otolith sections; 3) a quantitative characterization through the magnitude of specific peaks observed in the Raman spectra. The Raman-based analysis shows that fine scale otolith structures depict variations both in absolute and relative concentrations of mineral and organic compounds. This finding challenges the current perception of L- and D- zones in terms of mineral and organic compounds. In relation to the daily eurhythmics observed in L- and D-zone deposition, concentrations in endolymph organic precursors and total CO_2 depict circadian cycles (Mugiya 1987; Edeyer *et al.* 2000; Borelli *et al.* 2003a), in antiphasic ryhtm (Payan *et al.* 2004a; Allemand *et al.* 2007). Raman spectra reflected cyclic variations according to alternation of L- and D-zones but with synchronous variations between CH and AR. This could be explained by the fact that the CH-signature does not involve all the organic compounds present in the endolymph (proteins, collagens, proteoglycans, inhibitor factor). *In situ* Raman analysis of the endolymph along a daily cycle might validate this assumption.

Future work will be aimed at refining our analysis of the Raman spectra. In the present study, we mainly focused on two specific Raman signatures, the responses of the aragonitic fractions observed at 1085 cm^{-1} and the responses of organic compounds involving CH-

groups observed at 2950 cm^{-1}. Raman spectra convey much more information and future works will aim to better relate Raman signatures to known specific organic compounds (e.g., isolated proteins, sugars, proteoglycans) using complementary tools (electrophoresis or immuno-histochemical analysis).

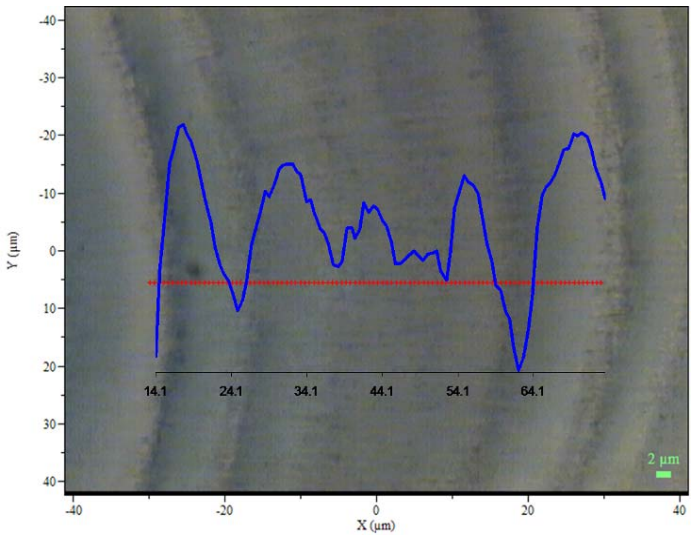

Chapitre 5 :

Comment l'opacité des otolithes de poissons est-elle contrôlée par ses fractions minérale et organique ?

Approche utilisant la micro-spectrométrie Raman

Chapitre 5 :

Comment l'opacité des otolithes de poissons est-elle contrôlée par ses fractions minérale et organique ? Approche utilisant la micro-spectrométrie Raman

Bien que les macrostructures de l'otolithe, zones translucides et opaques, soient largement utilisées pour l'exploitation des otolithes comme archive des traits de vie individuels (e.g. la construction des clés taille-âge), le processus contrôlant ces différences d'opacité n'est pas connu. Il est généralement admis que les zones opaques sont plus concentrées en matière organique que les zones translucides. Cette hypothèse se rapporte essentiellement à des observations optiques qualitatives et des dosages de l'azote comme marqueur de la matrice organique (Mugiya, 1965). A notre connaissance, aucune étude ne s'est intéressée à la caractérisation conjointe des fractions aragonitique et organique dans ces macrostructures. Dans notre précédente étude, nous avons mis en évidence le potentiel de la micro-spectrométrie Raman pour aborder cette problématique.

Dans cette étude, la micro-spectrométrie Raman a donc été appliquée sur des coupes d'otolithes de deux espèces différentes : le merlu européen (*Merluccius merluccius*) et le lieu noir (*Pollachius virens*) pour lequel la saisonnalité des macrostructures a été établie. Différentes zones translucides et opaques sont analysées pour répondre aux objectifs suivants : 1) mise en évidence de différences dans les caractéristiques physico-chimiques des zones opaques et translucides incluant des checks, discontinuité structurale caractérisant un stress ; 2) estimation d'un modèle d'opacité à partir des signatures Raman de ces deux fractions.

Pour les deux espèces analysées, les signatures Raman des fractions aragonitique et organique montrent des variations cycliques et synchrones avec des maxima localisés en zones translucides. Lors de l'analyse de ces zones, et en particulier des zones translucides de coupes de merlus, des structures nommées checks ont été identifiées. Elles apparaissent plus opaques que les régions adjacentes et présentent des signatures plus faibles en aragonite contrairement aux signatures organiques plus élevées que dans les régions adjacentes.

Un modèle de prédiction d'opacité a été établi sur le modèle d'une régression linéaire à partir des signatures Raman des fractions aragonitique et organique. Les prédictions obtenues à partir de ce modèle sont fortement corrélées à l'opacité observée pour les deux espèces. Il met en évidence : 1) une décorrélation partielle entre les différentes signatures de l'aragonite suggérant des différences dans la taille et l'orientation des cristaux entre les macrostructures ; 2) des contributions distinctes de deux catégories de signatures de la fraction organique, qui peuvent être interprétées comme associées à des quantités et/ou des propriétés différentes des composés organiques contenues dans les deux zones étudiées. La généricité du modèle aux deux espèces étudiées démontre l'existence d'un processus commun de formation des zones translucides et opaques. Ce modèle permet de détecter les checks comme des zones de très fort écart à la prédiction du modèle. Ce résultat suggère une différence des processus de biominéralisation en terme de nature et/ou quantité des composés organiques et minéraux, associées à la formation des zones opaques et translucides et des checks, souvent relatifs à des événements de stress. Ce résultat démontre également le potentiel de la micro-spectrométrie Raman pour discriminer des processus de biominéralisation non discriminés en termes d'opacité.

How is the opacity of fish otoliths driven by their organic and mineral fractions? Insights using Raman micro-spectrometry

Aurélie Jolivet[1], Jean-François Bardeau[2], Ronan Fablet[1,3,5], Yves-Marie Paulet[4,5], Hélène de Pontual[1]

En préparation

Abstract

The purpose of this study was to analyse the relations between the observed opacity on fish otoliths and the spatial variations in the physico-chemical characteristics of the otolith, more precisely descriptors of its aragonitic and organic fractions. To our knowledge, the simultaneous analysis of these two fractions on the otoliths macrostructures was uninvestigated. Raman micro-spectrometry was applied on translucent and opaque zones of otoliths for two different species: pollock (*Pollachius virens*) and European hake (*Merluccius merluccius*) to address the following issues: 1) demonstrating differences in the physico-chemical compositions, both for the mineral and organic fractions, between translucent and opaque zones including checks; 2) providing a numerical model of opacity from these Raman based signatures. For the two species, both the aragonitic and organic fractions were analysed in the translucent and opaque zones, and the magnitude of the associated Raman signatures was strongly correlated to otolith opacity with maxima in translucent zones. Not following this general trend, checks, appearing as thin opaque structures, depicting lower aragonite signatures than the adjacent regions and greater organic signatures. An opacity model stated as a multiple linear regression from the Raman signatures was proven meaningful to predict the observed opacity for both

species. This model highlighted: 1) a partial decorrelation between aragonite signatures which might be associated with changes in the orientation and size of aragonite crystals between translucent and opaque zones; 2) two different categories of organic signatures with opposite effects on the opacity. The latter might be hypothesized to be a consequence of differences in the quantities and proprieties of the organic compounds involved in the two zones. The genericity of this model for two different species underlined a common process for the formation of translucent and opaque zones. This model could also be used for detecting checks as large deviations from model predictions. This result first shows that the formation of checks involved changes in the nature and/or the quantities of mineral and organic compounds in relation to stressful events. Second, it also stresses that Raman signatures could provide the mean for discriminating structures optically similar based on their physico-chemical characteristics.

Introduction

Otoliths are calcareous concretions in fish inner ears. Their accretional growth follows circadian rhythm that is physiologically controlled and influenced by environmental conditions. It results in the formation of structures which deposition rhythms vary from daily or sub-daily, referred to as microstructures with L- and D-zones, to annual or seasonal, referred to as macrostructures with translucent and opaque zones. Due to the fact that otoliths are stable, they can be considered as a fish "black box" recording metabolic and environmental conditions encountered by fish. Otoliths are operationally used for fish age estimation (nearly one million by year) and are thus at the core of age-based assessment of fish stocks (Campana and Thorrold 2001). For some species such as hake (*Merluccius merluccius*), although the interpretation schemes was internationally agreed, it was not validated (Piñeiro and Sainza 2003). Recent mark-recapture experiments revealed the under-estimation of the hake growth due to an age overestimation (de Pontual *et al.* 2006; Piñeiro *et*

al. 2007; Mellon *et al.* submitted) This age overestimation was mainly due to the presence of translucent zones, called structures of secondary growth, that do not correspond to seasonal zone formation. Such secondary structures have been reported as a response to different factors such as shifts in feeding conditions (e.g. starvation), temperature changes as well as ontogenic events (e.g. metamorphosis, reproduction) (Wright *et al.* 2002b).

The understanding of the biological process leading to the formation of otolith macrostructures and of the temporal significance of translucent and opaque zones is incomplete and an important variability is acknowledged at the individual, population and species level (Beckman and Wilson 1995). Opacity changes were shown to be dependent on: growth rate (Hüssy and Mosegaard 2004), age and metabolism (Hoff and Fuiman 1993; Høie and Folkvord 2006), and sexual maturity (Beckman and Wilson 1995; Høie and Folkvord 2006). Regarding environmental factors, feeding conditions, such as low feeding conditions (Neilson and Geen 1985), temperature and photoperiod (Beckman and Wilson 1995) were also reported as affecting otolith opacity. Opacity properties have also been linked to variations in the relative amount of the organic matrix versus mineral fraction of the otolith, in amino acid composition (Hüssy *et al.* 2004), and in elemental ratios (Kalish 1991; Tomás *et al.* 2006) as well as to structural properties of primary increments such as width, thickness and size of aragonite crystals (Morales-Nin 1987). However some of the latter analyses were applied on a pool of otoliths, typically a few tens, in order to obtain the sufficient quantities of organic matrix necessary for the analysis. Thus, the study of such characteristics in translucent and opaque zones could not be achieved.

Raman micro-spectrometry is a non destructive technique which provides a quantitative characterization of vibrational physico-chemical features of both organic and mineral compounds. Regarding calcified structures, Raman micro-spectrometry already allows discriminating vaterite, aragonite and calcite in otoliths of different species (Gauldie *et*

al. 1997; Tomás and Geffen 2003; Melancon *et al.* 2005; Tzeng *et al.* 2007). More recently Raman micro-spectrometry was used to characterize otolith microstructures (Jolivet *et al.* 2008; Zhang *et al.* 2008). In particular, in our previous work, we have shown that the fraction of the organic matrix comprising CH signatures was more concentrated on L-zones than in D-zones (Jolivet *et al.* 2008).

In this study, we investigate the physico-chemical characteristics of otolith macrostructures in relation to opacity changes using the Raman micro-spectrometry. We developed a quantitative framework to relate the Raman otolith signatures to otolith opacity. Experiments were made on sections of European hake otoliths for which interpretation of the structures was unknown, and pollock otoliths for which the seasonal rhythm of translucent and opaque zones was previously validated (Andrade and Smith 1988). Our main contributions are two-fold:

1) demonstrating that translucent and opaque macrostructures, including structural discontinuities referred to as checks, differ in their physico-chemical characteristics, both for their mineral and organic fractions;

2) identifying a consistent numerical model of opacity from these Raman based signatures.

As emphasized in the discussion, these original contributions provided new insights for discriminating and interpreting otolith macrostructures.

Material and Methods

Otolith samples

We considered two series of otoliths extracted from: 1) hakes caught in the North of the Bay of Biscay in June 2006 and November 2007 or reared in controlled facilities, and 2) pollocks caught in ICES area VIa (West of Scotland) during the first quarter of 2008 (Table 1). Only adult fish were considered and fish size (Total Length, TL) ranged from 28 to 63 cm for hakes and 56 to 58 cm for pollocks.

Name	Species	Origin	Catch date	Size (cm)	Thickness (µm)	Magnitude	TR	OP	Size of Transects
P1	Pollock	West of Scotland	08/01/2008	58	491	x50	2	2	D=66µm, S=5µm
P2	Pollock	West of Scotland	05/03/2008	56	359	x50	2	2	D=70µm, S=5µm
P2	Pollock	West of Scotland	05/03/2008	56	359	x100	2	2	D=55µm, S=0.5µm
P3	Pollock	West of Scotland	05/03/2008	57	338	x50	2	2	D=57µm, S=4µm
H1	Hake	North of Bay of Biscay	01/09/2005	50	270	x50	2	2	D=42µm, S=3µm
H2	Hake	Rearing	11/12/2007	57	248	x50	2	2	D=44µm, S=3µm
H3	Hake	Rearing	11/12/2007	49	255	x50	2	2	D=46µm, S=3.3µm
H4	Hake	North of Bay of Biscay	02/11/2007	28	255	x100	1	1	D=55µm, S=0.5µm
H5	Hake	North of Bay of Biscay	10/11/2007	36	120	x100	1	1	D=55µm, S=0.5µm
H6	Hake	North of Bay of Biscay	05/11/2007	35	91	x100	1	1	D=55µm, S=0.5µm

Table 1: Details on otolith samples investigated by Raman micro-spectrometry: fish origin, date of capture, size (cm), thickness of otolith sections (µm), magnification of analysis, number of translucent (TR) and opaque (OP) areas analyzed and characteristics of analyses (D : length of transect, S: step between two analysed points).

The otoliths were extracted, rinsed with milliQ water, dried and weighted. For standardization purpose, the left sagittae was systematically used. To obtain thin sections, otolith preparation consisted in: 1) embedding in epoxy resin, 2) sectioning in transverse plane, 3) grinding, and 4) polishing to the core. All sections were observed under an optical microscope equipped with two light sources (transmitted and reflected) without changing light orientation or intensity settings. TNPC software was used to acquire calibrated numerical

images and measure otolith opacity (Ogor and Fablet 2004). Data were acquired on transects and consisted in transmitted light intensity as grey values distributed between 0 (black) to 255 (white) and distance to the core. In this study, transmitted light was used, so areas with relatively low intensities corresponded to the opaque zones.

To reduce the effect of preparation thickness for the overall of samples, the logarithm of the opacity values was considered (Hüssy *et al.* 2004) and data were standardized with respect to the mean and standard deviation of the whole grey level values along the transect from the core to the edge.

Raman micro-spectrometry

A micro-Raman spectrometer (Jobin-Yvon T64000) equipped with a confocal system and a motorized microscope stage was used. The experimental setting was the same as in Jolivet et al. (2008). A coherent spectrum argon/krypton ion laser was used to produce radiation with a wavelength of 514.5 nm and a good signal-noise ratio. The laser was focused onto the sample by using a microscope equipped with a x100 objective, resulting in a spatial resolution of 1µm, namely very high resolution and a x50 objective, resulting in a spatial resolution of 4µm, namely high resolution. The scattered light was analysed by a spectrometer with a single monochromator (600 gratings mm^{-1}), coupled to a nitrogen cooled CCD detector. A 50 mW laser power was selected. Spectra were accumulated two times with exposure times varying from 30 to 300 s depending on the sample. The depth of analysis was systematically set to 2 µm below the surface to avoid possible contamination due to preparations techniques.

Analyses of structures

Two different scales of analysis were carried out on pollock and hake samples. Details on the analyses are summarized in Table 1.

For high resolution analyses, a x 50 magnitude was chosen resulting in a spatial resolution of 4 µm. Three transversal sections (P1-P3 and H1-H3) were analysed for each species. Raman transects spectra were acquired on two opaque and two translucent zones of each otolith with steps varying from 3 to 5 µm depending on the width of macrostructures (Table 1).

For very high resolution analyses, a x 100 magnitude was chosen resulting in a spatial resolution of 1µm. Raman spectra on transects covering several successive micro-increments were acquired with a step of 0.5 µm on one translucent and one opaque zones of three hake otolith sections (H4-H6) and on two translucent and two opaque zones of one pollock otolith section (P2).

For each resolution, optical images were acquired before each analysis in order to record the locations of the Raman analysis and measure otolith opacity as defined previously to obtain: a high resolution opacity measured on images made with a x 50 magnitude and a very high resolution opacity measured on images made with a x100 magnitude.

Analysis of Raman spectra

Raman spectra were corrected for background luminescence using baseline subtraction. The baseline was also included as a potential descriptor in further treatments. The positions and integrated intensities of detected vibrational bands in Raman spectra were determined using the LABSPEC software.

The analysis of the Raman spectra was carried out as follows. Five bands or groups of peaks were considered for the description of the aragonitic fraction and nine bands or group of peaks for the organic fraction (Table 2). For each considered band, the integrated surfaces was calculated and normalized by the overall energy of the Raman spectra in view to be independent from analysis conditions. The resulting Raman signatures were then standardized with respect to their mean and standard deviation. The normalization by the overall energy was preferred to the normalization with respect to the main aragonite signature (i.e. the peak at 1085 cm^{-1}) as done in our previous study (Jolivet et al. 2008). This allowed to keep this signature as a feature for the analysis as the different aragonite signatures were shown to be partially uncorrelated. The correlation between the different normalized Raman signatures was analysed through a principal component analysis issued from the very high resolution data of the two species and applied to high resolution data.

Wavenumbers (cm^{-1})	Characterization	Assignments
Group 150: 9 peaks between 113 and 284	lattice modes	AR
Group 700: 2 peaks at 701 and 705	in plane bending of O-C-O	AR
855	δ(CCH) ring, ν(C-C), Tyr, Ac asp	OM
1085	symmetric stretching of C-O	AR
1462	anti-symmetric stretching of C-O	AR
	anti-symetric bending of CH_3	OM
1574	anti-symmetric stretching of C-O	AR
	bending of CH_2	OM
1611	Trp, Phe, Tyr ν-ring	OM
Group 1700 : 2 peaks at 1711 and 1811	C=O stretching mode	OM
2950	ν(CH_3) sym proteins and lipids, ν(CH_2) asym proteins	OM
3050	CH stretch	OM
3399	OH deformation	OM
Baseline		OM

Table 2: Wavenumbers, characterization and assignments of the Raman bands associated with the aragonitic (AR) and organic fractions (OM) of fish otoliths (Urmos *et al.* 1991; Careche *et al.* 1999; Piot *et al.* 2000; Ikoma *et al.* 2003; Briget Mary and Ramakrishnan 2005; Zhang *et al.* 2008)

Models of otolith opacity were investigated from Raman signatures. Following, previous work, we first tested a linear model of otolith opacity parameterized by the ratio between the aragonitic and organic fractions given by the ratio between the normalized integrated peaks intensities of the main aragonite peak at 1085 cm^{-1} (IS1085) and of the CH-group band centred at 2950 cm^{-1} (IS2950). We used the following formulation:

$$\text{Opacity} = \alpha \times IS1085 / IS2950 + \beta \qquad \text{(Eq 1)}$$

where α and β are the coefficient of the linear regression.

A more general model was also considered using a multiple linear regression from the whole vector of Raman signatures. The estimation of this regression was achieved by a stepwise approach. Three different types of data were considered to train these models: 1) a general model fitted to the high resolution data of the two species; 2) two species-specific models fitted to the high resolution data of each species; and 3) a general model fitted to the very high resolution data of the two species. The regressions validity was given through the determination coefficient (R^2) and the significant test (level at 5%).

Results

Comparison of Raman signatures in otolith macrostructures

At high resolution, two translucent and two opaque areas were analyzed on each sample as shown on Figure 1A. The evolution of the aragonite response (peak at 1085 cm^{-1}) and of the CH-related organic fraction (peak at 2950 cm^{-1}) are shown on Figure 1B. Cyclic

variations were observed with maxima located in translucent areas and minima in opaque areas and significantly different between both zones ($P < 0.05$). The others aragonite and organic peaks showed similar cycles with maxima in translucent areas significantly different from minima in opaque areas ($P < 0.05$).

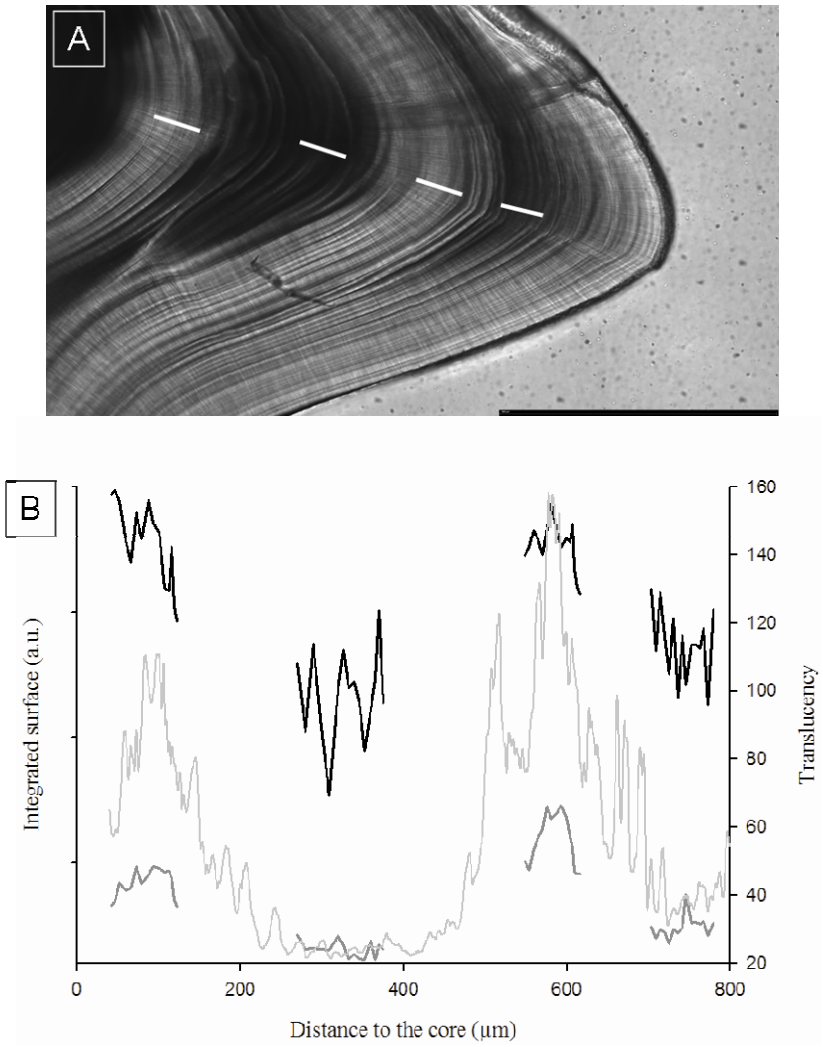

Figure 1: (A) Typical view of a pollock section (P2) under light microscopy. Analyses were made on transects covering two translucent zones and two opaque zones (dark scale bar = 500µm). (B) Integrated Raman intensities of the peak at 1085 cm^{-1} (aragonite response in dark line) and of the peak at 2950 cm^{-1} (CH group in dark grey line) along the line direction. On the background the opacity profile (grey line) was represented.

Similar results were obtained from the analysis at very high resolution. Significant differences were observed between the responses of the aragonite and organic peaks in the translucent and opaque areas with maxima located in translucent areas ($P < 0.05$).

The analysis of the Raman signatures of checks, structural discontinuities (Panfili *et al.* 2002a), mostly located in translucent zones of hake samples, was also considered. These checks depicted aragonite signatures lower than adjacent translucent regions in the translucent areas but greater than in opaque areas. Conversely organic compounds exhibited opposite variations, except for the peak at 3999 cm^{-1} and the group of peaks at 1700 cm^{-1} which remained constant (Figure 2).

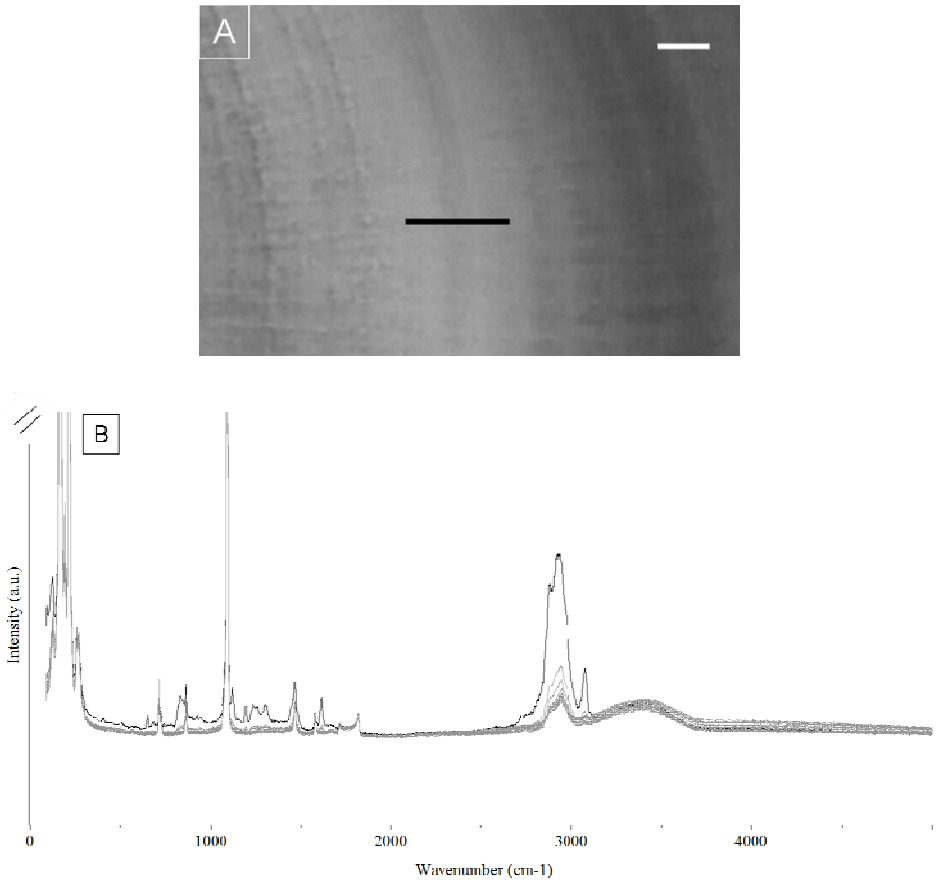

Figure 2: (A) Typical view of a translucent area on hake section H5 obtained under transmitted light. The transect (dark line) delimits the analysed area which comprised a check that appeared optically more opaque. Along each transect, Raman spectra were acquired every 1.2 µm (white scale bare = 5µm). (B) The superposition of the Raman spectra in the 100-4000 cm^{-1} region acquired along the transect with check in dark and the adjacent region in grey. For clarity, focus was made on lower intensities.

Correlation analysis of Raman signatures

With a view to analyzing the correlation between the different Raman signatures, a principal component analysis was performed on very high resolution data. The first two

components (PC1 and PC2) explained 71% of the total variation. The relative contribution of the different Raman signatures to the two first principal components is given in Table 3 and the graphic representation in Figure 3.

	Raman signature	Principal Component PC1	PC2
Aragonite peaks	GP150	-0.904	-0.172
	GP700	-0.517	0.804
	1085	-0.721	0.145
	1462	0.686	0.656
	1571	-0.439	0.366
Organic matrix peaks	855	0.87	-0.243
	1611	0.814	0.423
	GP1700	0.361	-0.874
	2950	0.907	0.106
	3050	0.899	0.379
	3399	0.733	-0.206
	Baseline	0.207	-0.142

Table 3: Contributions of the considered Raman signatures to the first two components of the principal component analysis.

The principal component analysis clearly discriminated the aragonitic and organic signatures, except for the peak at 1462 cm^{-1} usually considered as an aragonite response (Urmos *et al.* 1991; Gauldie *et al.* 1997; Lin and Liu 1997). The projection of the high and very high resolutions centroids for both opaque and translucent zones onto the first two principal components plane was also analyzed (Figure 3). Translucent and opaque areas, at macro- and micro-scales of analysis, were located as intermediate points between the two groupings of aragonite and organic compounds. Interestingly, the projections obtained with the two analysed resolutions are not overlapping. Regarding checks, associated signatures are clearly separated from those observed in translucent and opaque areas (Figure 3).

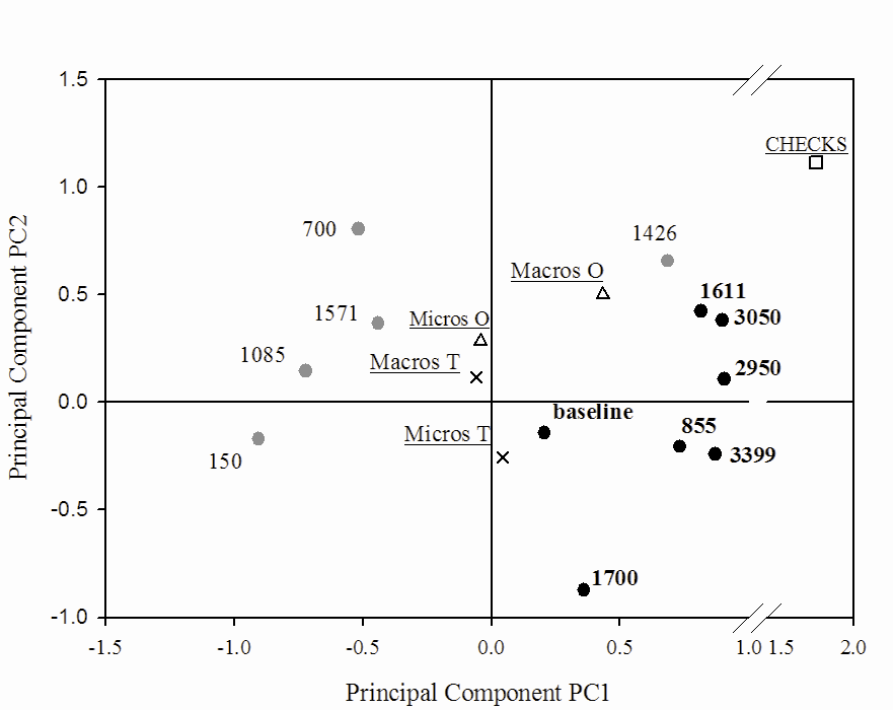

Figure 3: Principal components analysis of the normalized Raman signatures of pollock and hake otoliths. Contributions variables are representative of the organic matrix peaks (dark circle), aragonite peaks (grey circle). Centroids of translucent area T (×), opaque area O (Δ) and checks (□) are also projected onto the first PCA plane.

The comparison of the Raman signatures acquired at high and very high resolutions in the same areas of the sample P2 showed that opaque areas exhibited lower values than translucent areas at a given resolution but distributions were not fully overlapping with values at very high resolution lower than at high resolution (Figure 4).

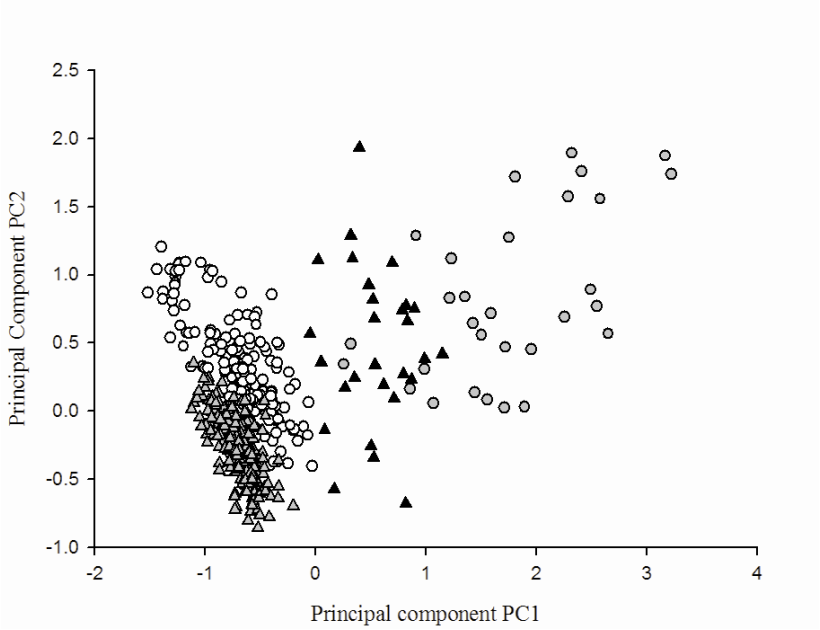

Figure 4: Scores of the principal components analysis of normalized Raman signatures of the pollock sample P2 analysed at micro and macro-scales in the same areas. Data are representative of analysed points in translucent area (grey circle), and opaque areas (dark triangle) analyzed at macro-scale and in translucent area (circle), and opaque area (grey triangle) analysed at micro-scale.

Opacity model parameterized from RAMAN data

The relation between the opacity and the ratio between the CH-related response and the aragonite reference (Eq. 1) was not significant ($R^2 < 0.05$, $P > 0.05$), neither at very high resolution nor at high resolution for the two species and opacity predictions were significantly different from measured opacity ($P < 0.001$).

The application of the opacity models stated as a multiple linear regression from the Raman signatures selected by a stepwise approach is summarized in Table 4.

	macro model	Hake model	Pollock model	micro model
all data	**0.119**	0.067	0.052	**0.548**
hake data	0.001	**0.151**	**-0.103**	**0.469**
pollock data	**0.557**	**0.266**	**0.721**	**0.637**
macro data	**0.738**	**0.665**	**0.548**	**0.302**
hake	**0.704**	**0.759**	**0.341**	0.056
pollock	**0.768**	**0.539**	**0.820**	**0.557**
micro data	**-0.104**	**-0.135**	**-0.119**	**0.652**
hake	**-0.200**	-0.021	**-0.194**	**0.592**
pollock	**0.587**	**0.244**	**0.706**	**0.744**

Table 4: Correlation statistics of the fitted opacity models: significant correlations are reported in bold.

The model established from high resolution data was suitable for the two species with predictions highly correlated to measured opacity values (R^2 hake = 0.704, $P < 0.05$; R^2 pollock = 0.768, $P < 0.05$ Figure 5A). This model could also predict very high resolution opacity for pollock samples ($R^2 = 0.244$, $P < 0.05$, Figure 5B) but not for hake samples ($R^2 = -0.2$, $P > 0.05$). Predictions were improved at high resolution analyses with the species-specific models but in both cases very high resolution opacity for hake samples was not satisfactorily predicted by high resolution models (Hake model $R^2 = -0.021$, $P > 0.05$, Pollock model $R^2 = -0.194$, $P > 0.05$).

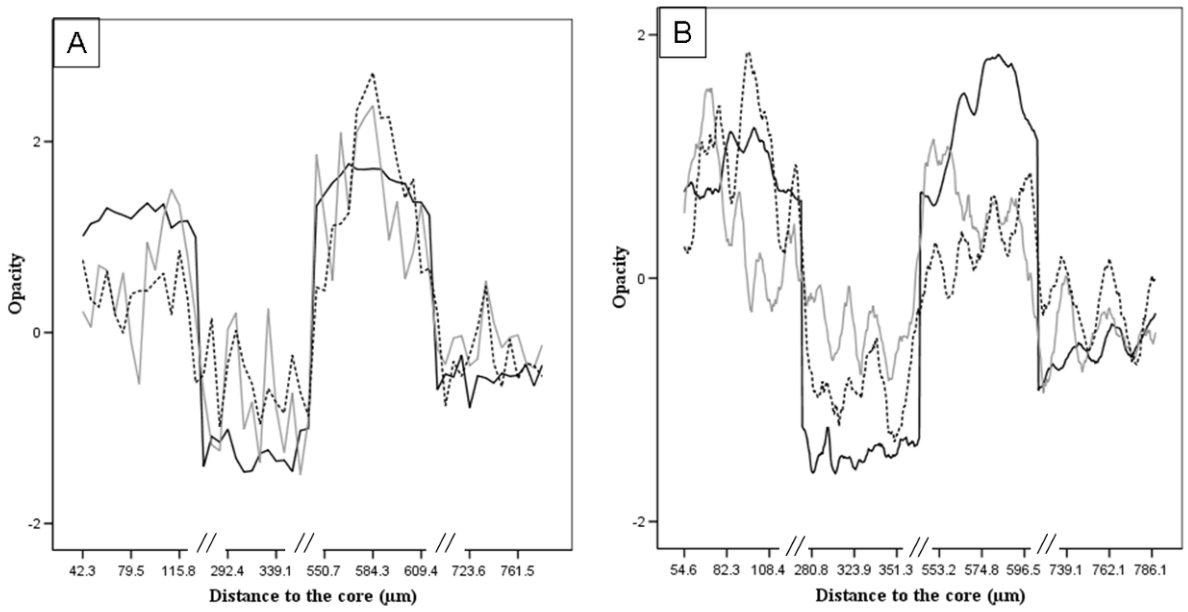

Figure 5: Confrontation between measured opacity (dark lines) on a transverse section of pollock sample P2 and predictions of models based on high resolution data (grey lines) and very high resolution data (dotted lines): (A) Comparison of measured high resolution opacity and the two models prediction. B) Comparison of measured very high resolution opacity and the two models prediction. For clarity a ten points average was applied on models predictions.

The model established from very high resolution data achieved good predictions for the two species (Hake $R^2 = 0.592$, $P < 0.05$; Pollock $R^2 = 0.744$, $P < 0.05$, Figure 5B). It could also predict high resolution opacity of pollock samples ($R^2 = 0.557$, $P < 0.05$, Figure 4A) but not of hake samples ($R^2 = 0.056$, $P > 0.05$). The opacities of the checks were large deviations to model predictions (Figure 6).

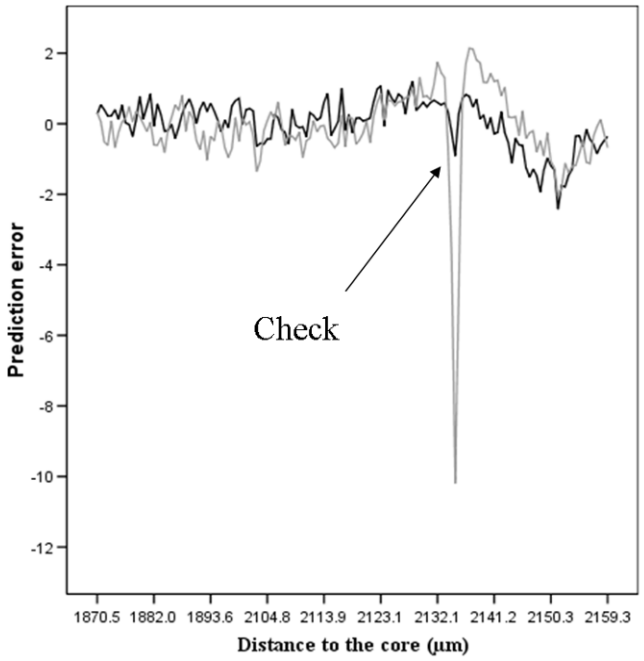

Figure 6: Prediction error between the actual opacity and predictions issued from the opacity models learned fitted to high resolution data (dark line) and very high resolution data (grey line).

Raman signatures used in each model are provided in Table 5. The signatures showing a positive contribution tended to increase grey level values and then to participate to the formation of translucent area, and conversely for negative contributions. Concerning aragonite-related signatures, most of the models took into account the group of peaks at 700 cm^{-1} with a negative effect on opacity. This signature was generally accompanied by two or three others aragonite peaks which conversely had a positive effect on opacity (Table 5). Pollock model was an exception with a second negative contribution of aragonite fraction through group of peaks at 150 cm^{-1}. Concerning the organic fraction, the contributions might be categorized in two groups: a positive effect on opacity with peak at 3050 cm^{-1} and the baseline and a negative effect on opacity with the group of peaks at 1700 cm^{-1} and the signatures at 855, 2950 and 3399 cm^{-1}.

	Normalized peak	HR model	Hake model	Pollock model	VHR model
CONSTANT		0.23	0.418	-0.257	0.513
Aragonite peaks	GP150	1.104	0.554	-1.105	
	GP700	-1.567	-1.648	-1.340	-0.822
	1085	0.449			1.164
	1462	0.284	0.304		
	1571			0.323	0.217
Organic matrix peaks	855			-0.210	-0.451
	1611				
	GP1700	-0.728	-0.604	-0.597	
	2950		-1.401	-0.994	
	3050	0.329	0.901		1.620
	3399			-1.507	-0.998
	Baseline	0.454		0.783	0.870
Determination coefficient R^2		0.523	0.582	0.719	0.4

Table 5: Contribution of the different Raman signatures to the opacity models fitted on four different training databases: 1) high resolution data of the two species (HR model), 2) high resolution data of each species (hake and pollock model), 3) very high resolution data of the two species (VHR model). Determination coefficients (R^2) were also given.

Discussion

Spatial resolution: In this study, we considered two different resolutions for the analysis: a first one using a x 50 magnitude resulting in a spatial resolution of 4 µm and a second one with the x 100 magnitude resulting in a spatial resolution of 1µm. In both cases, the Raman signatures were highly correlated to the opacity. However, the projection of the two resolutions data onto the two first factors of the principal component analysis showed that their distributions were not overlapping although the trends were the same between the translucent and opaque zones. The physico-chemical signatures of otolith microstructures, as revealed by Raman micro-spectrometry, may differ within a given macrostructure as well as

between two macrostructures. On transverse sections, in particular in translucent zones, L- and D-zones are thin and a 1µm resolution often led to averaging the information from D-zones with adjacent L-zones. The different averaging effects corresponding to 1µm and 4µm-wide Raman spots might explain the differences in the results reported for the very high resolution and high resolution analysis. The latter however achieved a good trade off between acquisition time and sensitivity for the analysis of otolith macrostructures.

Spatial distribution of aragonite and organic matrix fractions: The total mass of fish otolith is constituted of 90-99 % of calcium carbonate, mainly in aragonite form and the remaining 1-10% correspond to the organic matrix composed of collagens, proteoglycans and proteins (Murayama *et al.* 2000; Murayama *et al.* 2002; Borelli *et al.* 2003b). The spatial distribution of these two fractions on the otolith structures remained mainly uninvestigated. From the effects of burning on otoliths, Dannevig (1956) hypothesized that opaque zones contained more organic compounds. Later, Mugiya (1965) used the nitrogen content of the otoliths by Kjedahl method as an organic proxy to obtained comparable results. To our knowledge, simultaneous analysis of the aragonitic and organic fractions of otolith macrostructures has not been performed yet. In this study the use of the Raman spectra allowed to observe the evolution of these two fractions along transects on pollock and hake otoliths. Both the aragonitic and organic fractions were observed in the translucent and opaque zones. The magnitude of the associated Raman signatures is strongly correlated to otolith opacity with maxima in translucent zones. In our previous work focused on micro-increments analysis, the ratio between the CH-related response (peak at 2950 cm^{-1}) and the aragonite reference (peak at 1085 cm^{-1}) has shown the alternation of L- and D-zones to be correlated to opacity. In this study, this ratio appeared not to be appropriate to explain the opacity variations between translucent and opaque macrostructures.

Specific characterization of checks: Otoliths checks correspond to discontinuities in the sequence of micro-increments and have shown to record periods of perturbation or stress of fish (Campana 1983a). The intensity of the check may be proportional to the degree of stress that the fish has undergone (Pannela 1980). Campana (1983a) analyzed the composition of the otolith checks and measured a significant decrease in calcium carbonate deposition. This result was later confirmed by Payan et al (2004b) who analysed check induced by gaseous Cl_2 exposure. This also corresponds with the reported experiments which showed a decrease in the Raman aragonite signatures. Checks were also characterized by an increase in the responses of organic compounds (Mugiya and Takahashi 1985; Payan *et al.* 2004b). Payan et al. (2004b) showed that the check deposition was associated to an increase in the concentrations of proteins in the endolymph, especially in the proximal area. Here we report for the first time, an increase in some Raman signatures associated with organic compounds (e.g. peaks between 600 and 1650 cm^{-1}). Noticeably, other organic signatures, such as the group of peaks at 1700 cm^{-1}, peak at 3399 cm^{-1} and the baseline remain constant. Besides, checks presented very large deviations to the predicted Raman-driven opacities. Whereas the analyzed checks appeared as opaque zones, they were predicted as very translucent areas. These results suggested that changes occur either in the nature and/ or the relative quantities of the organic compounds involved in otolith accretion in relation to stressful events. They also stress the potential of Raman micro-spectrometer for detecting and characterizing otolith structures which cannot be optically discriminated.

Opacity model: The prediction of the otolith opacity from Raman signatures highlighted the interaction of several aragonitic and organic signatures. Concerning the aragonite-related peaks, the analysis showed that they were only partially uncorrelated. In

particular, the group of peaks located at 700 cm^{-1} seemed to have an opposite effect on opacity opposite to the effect of other aragonite-signatures. A first hypothesis would be a superimposition of organic responses to some aragonitic peaks. Zhang et al (2008) showed from the analysis of the core of small yellow croaker (*Pseudociaena polyactis*) that some organic signatures were close to the main aragonitic peak at 1085 cm^{-1} and could be occluded in opaque and translucent zones due to the magnitude of the aragonite response. This hypothesis could also be consolidated by the fact that the band at 1462 cm^{-1} was correlated to the organic signatures in the principal component analysis, whereas it was previously associated with the Raman signatures of several amino acids (Piot *et al.* 2000; Ikoma *et al.* 2003; Briget Mary and Ramakrishnan 2005). In this study, Raman signatures were analysed through their integrated peak intensities. Others descriptors might be relevant, such as the magnitudes and the widths of the Raman modes. Widths variations was already hypothesized to depend on variations in crystallite size or crystal structure disorder (Urmos *et al.* 1991). That might also result from the crystallite environment and in particular from the type and the proportion of the ions or the organic compounds trapped in crystal units. Additional experiments coupling Raman micro-spectrometry and atomic force microscopy (Dauphin and Dufour 2008) could be explored to analyze Raman otolith signatures in relation to the orientations of crystals.

Concerning the organic fraction, two categories of peaks were distinguished in the opacity models. A first one comprising the baseline and the peak at 3050 cm^{-1} was negatively correlated to opacity. The second category included the group of peaks at 1700 cm^{-1} and peaks at 855, 2950 and 3399 cm^{-1} and was positively correlated to opacity. The signature at 3399 cm^{-1} was associated with the vibrations of OH groups and could reflect hydration forces between molecules. In a previous work (Jolivet *et al.* 2008), this signature was shown to be greater at the core but almost constant between L-and D-zones on opaque zones. The baseline

which was also proven greater at the core (Jolivet *et al.* 2008) had here an opposite effect on opacity. The baseline was regarded as resulting from the excitation of an organic compound at green wavelength. Interestingly these two signatures were not discriminatory for the identification of the checks. Overall, these results suggested that opacity changes are related both to the relative variations of the organic and mineral fractions, as well as the modifications in the nature and the relative quantities of the different organic compounds.

A key issue to address is the determination of the actual compounds of the otoliths revealed by the extracted Raman signatures. Regarding the composition in amino-acids, previous works have shown that fish otoliths are mainly comprised of glutamic and aspartic acids, leucine, serine and proline (Morales-Nin 1986a; b; Baba *et al.* 1991; Asano and Mugiya 1993; Sasagawa and Mugiya 1996; Hüssy *et al.* 2004). Some of the Raman signatures of these different amino acids are very close (Piot *et al.* 2000; Ikoma *et al.* 2003; Briget Mary and Ramakrishnan 2005) and correspond to the signatures considered in our study, for instance peaks at 855, 1462 and 1576 cm^{-1}. All these features were associated with negative weights in the opacity models. The discrimination of these different amino acids is difficult. Glutamic and aspartic acids could however be distinguished due to their acid functions that could be associated with the group of peaks at 1700 cm^{-1} corresponding to the vibrational responses of C=O groups. In the estimated opacity models the Raman signatures at 1700 cm^{-1} positively affected opacity. These particular Raman signatures supposed to be attributed to glutamic and aspartic acids would be new tracers of their compounds demonstrated to be associated with polysaccharides, lipoproteins and glycoproteins corresponding to water soluble compounds (Baba *et al.* 1991; Asano and Mugiya 1993; Murayama *et al.* 2000). Regarding otolith proteins, only four instances have been identified: otolin-1, OMP-1 (Murayama *et al.* 2005), starmaker (Söllner *et al.* 2003) and recently OMM-64 (Tohse *et al.* 2008). To our knowledge these proteins have not been analysed with Raman micro-spectrometry yet. As a number of

Raman signatures could be associated with the signatures of amino-acids, further investigations on the characterization of the organic matrix should be carried out to identify the compounds revealed by the Raman characterization. In particular, organic compounds such as sugars and polysaccharides, should be of great interest. Complementary analysis using immunohistochemical techniques might also be meaningful to address these issues.

Macrostructures on the two analysed species: A general parameterization of the opacity model for the two species was proven significant, stressing the interest and the potential genericity of the model. The formation of the translucent and opaque zones of the two species obeyed to the same model whereas different metabolic and environmental conditions were experimented by individuals. The lower correlations between predicted and actual opacities for the hake samples underlined the complexity of hake otolith pattern. The interpretation of pollock otoliths is validated and well defined. An opaque zone is typically deposited in relation to summer growth whereas slow winter growth leads to the formation of a translucent zone (Andrade and Smith 1988). Concerning hake otoliths, the interpretation was challenged and its complexity highlighted by the recent mark-recapture campaign (de Pontual *et al.* 2003c; de Pontual *et al.* 2006). Hake otoliths patterns cannot be simply related to seasonal variations of environmental factors with formation of more than one translucent zone per year (Morales-Nin *et al.* 1998; de Pontual *et al.* 2006; Courbin *et al.* 2007). The greater variability of the Raman signatures may be explained by the greater variability of the metabolic and environmental conditions experienced by fish. In a future work, the relations between the Raman signatures of the otoliths and the endogenous and exogenous parameters, such as temperature, growth, feeding or metabolism changes, could be investigated from the analysis of samples issued from experiments in controlled conditions (Hüssy *et al.* 2004; Høie *et al.* 2008; Jolivet *et al.* submitted).

Acknowledgments

The authors are thankful to the Kelig Mahe who has provided pollock otoliths. This work has been supported by national ANR grant "OTOCAL".

Discussion générale et perspectives

Discussion générale et perspectives

Malgré un grand nombre d'études relatives à l'utilisation des otolithes tant à l'échelle populationnelle qu'individuelle, les connaissances sur les mécanismes de formation de l'otolithe et leurs relations avec les facteurs environnementaux ou physiologiques restent parcellaires (Payan *et al.* 2004a). En particulier, la caractérisation des fractions minérales et organiques des structures de l'otolithe et l'influence de leurs propriétés qualitatives et quantitatives sur l'opacité restent peu documentées. Pourtant ces informations sont d'importance en vue d'une calibration de l'archive « otolithe » permettant une analyse robuste de l'information. Cette problématique nous a conduit à développer la micro-spectrométrie Raman ainsi que des expérimentations en milieu contrôlé afin d'analyser les caractéristiques physico-chimiques et les facteurs pouvant influer sur l'opacité. Les conclusions et les perspectives de cette étude s'articulent autour de trois questions :

- Comment la caractérisation des fractions minérale et organique des structures de l'otolithe contribue à la compréhension de la formation de l'otolithe ?
- La modélisation de l'otolithe, un outil pour la compréhension du processus de biominéralisation ?
- Comment la caractérisation des structures en fonction des facteurs métaboliques et environnementaux permet-elle de calibrer l'otolithe?

Comment la caractérisation des fractions minérale et organique des structures de l'otolithe contribue à la compréhension de la formation de l'otolithe ?

Le processus de biominéralisation a jusqu'à présent principalement été analysé à travers l'étude de l'endolymphe et la caractérisation de la matière organique (cf. Introduction). Ces études ont permis de mettre en évidence des variations à la fois spatiales et temporelles des principaux éléments intervenant dans la calcification. Peu d'études ont cependant porté sur la comparaison entre observations faites dans l'endolymphe et les caractéristiques des structures observées sur l'otolithe.

L'analyse de la composition des otolithes à l'échelle des macro- et microstructures est en effet contrainte par les quantités à analyser (la matière organique ne correspond qu'à quelques pourcents de la masse de l'otolithe) nécessitant des techniques à haute résolution spatiale et à forte sensibilité. Avec le développement des techniques de biogéochimie, les analyses ponctuelles se sont développées notamment dans les domaines de la quantification et de la spatialisation de la composition chimique des otolithes. Cependant, l'étude de la fraction organique contenue dans l'otolithe se rapportait essentiellement à des analyses globales par dilution intégrant alors l'ensemble de la vie du poisson, voire même le plus souvent d'un ensemble d'échantillons. Dans cette étude, la micro-spectrométrie Raman s'est révélée comme un outil performant pour répondre à cette problématique. Appliquée seulement depuis la fin des années 90 à l'analyse des otolithes, elle a jusqu'à présent été essentiellement utilisée pour discriminer les polymorphes de carbonates de calcium bien que l'information organique soit présente sur les spectres d'analyses.

Dans cette étude, nous avons démontré que la micro-spectrométrie Raman présente un potentiel beaucoup plus important pour la caractérisation physico-chimique de l'otolithe à petite échelle. Ainsi son application a tout d'abord été envisagée au niveau du noyau et des microstructures en zones opaques pour l'évaluation et la calibration de la méthode (Chapitre 4). Cette méthode a en premier lieu été « validée » par l'obtention de résultats concordants avec de précédentes études tant pour le nucleus qui présente des signatures organiques élevées

(Pisam *et al.* 2002) que par l'analyse des zones L et D après l'attaque à l'EDTA avec des signatures organiques plus élevées en zones D (Dunkelberger *et al.* 1980; Morales-Nin 1987; Mugiya 1987). Les apports spécifiques de cette technique ont été d'une part l'obtention de signatures caractéristiques de la matière organique du sulcus comparable à celles du nucleus et d'autre part l'analyse des zones L et D *in situ* sans préparation particulière. Ces derniers résultats mettent en évidence la présence des fractions minérale et organique à la fois dans les zones L et D dont l'évolution suit des cycles synchrones avec des maxima localisés en zones L. L'analyse effectuée sur les macrostructures a confirmé cette variation cyclique des fractions minérale et organique, fonction de l'opacité avec des maxima en zones translucides. Le potentiel du Raman à des fins de définition de marqueurs a été démontré par la mise en évidence de checks qui bien qu'optiquement relativement peu différenciés des structures adjacentes, présentent des spectres particuliers avec des signatures organiques nettement plus élevées (Chapitre 5). Ces différents résultats remettent alors en cause les résultats de précédentes études définissant les zones opaques comme majoritairement constituées de matière organique (Dannevig 1956; Mugiya 1965). Nous avons également démontré que l'opacité ne résulte pas uniquement d'un ratio entre fraction minérale et organique mais est une fonction de plusieurs fractions organiques ainsi que de possibles changements de configurations de l'aragonite probablement liées à la taille ou à l'orientation des cristaux.

L'analyse des variations nycthémérales des concentrations des principaux composés intervenant dans la calcification avait conduit à l'hypothèse que la formation de la matrice organique avait principalement lieu la nuit et le dépôt en carbonate de calcium le jour conduisant à la formation respective des zones D et L (Payan *et al.* 2004a). Les premiers résultats présentés ci-dessus suggèrent un processus plus complexe avec un dépôt simultané des deux fractions dans les deux zones d'une microstructure sans cependant aboutir à une réelle chronologie de formation des structures de l'otolithe. Les perspectives envisagées dans

ce domaine sont de deux ordres : la caractérisation des signatures extraites des spectres Raman et l'analyse conjointe de la spatialisation des composés organiques et minéraux dans l'endolymphe et sur l'otolithe.

Caractérisation des signatures :

Les signatures considérées des spectres Raman ont été catégorisées en premier lieu en deux classes, minérale ou organique. Cependant l'analyse de ces signatures lors de l'étude des macrostructures suggère la nécessité de considérer l'intervention de plusieurs fractions de la matière organique. Ces différentes fractions, révélatrices de différences de caractéristiques physico-chimiques des composés organiques, pourraient être liées aux fractions dites solubles et insolubles de la littérature (cf. Introduction). Ces observations mettent en évidence la nécessité de mieux identifier les composés intervenant dans les différents groupes de signatures Raman. L'acquisition de spectres Raman de référence pour des composés organiques identifiés, e.g. des extraits de protéines actuellement isolées de l'otolithe, constitue une première étape pour identifier et catégoriser, dans les spectres vibrationnels de zones spécifiques de l'otolithe, les différents composés de références. Il sera particulièrement intéressant d'étudier les différences observées entre les zones présentant de forte concentration de la fraction organique (e.g. nucleus, check) et les autres zones de l'otolithe.

Une étude de même type doit être conduite pour la fraction aragonitique qui semble présenter des variations des propriétés de cristallisation. La microscopie de champ proche (AFM, Atomic Force Microscopy) correspond à une technique d'imagerie et d'analyse de la topographie des surfaces à très haute résolution. Elle permet à l'échelle de quelques dizaines de nanomètres l'analyse des arrangements structuraux entre fractions minérale et organique ainsi que la caractérisation *in situ* des cristaux par leur taille et leur orientation (Gauldie and

Xhie 1995; Gauldie 1999; Dauphin and Dufour 2008). Quelques exemples sont présentés en Annexe 1 sur des microstructures L et D. Ainsi cette analyse par AFM pourrait être associée à une analyse plus approfondie des spectres RAMAN et portant en particulier sur la largeur et le déplacement des pics (Urmos *et al.* 1991) pour une caractérisation de la fraction minérale et de ses configurations en relation avec la fraction organique.

Spatialisation endolymphe/otolithe :

La composition des microstructures a été abordée dans cette étude à travers l'analyse en coupe sagittale de zones L et D en zones opaques permettant l'analyses de microstructures nettement distinctes. Cette approche doit tout d'abord être complétée par l'analyse des zones L et D en zones translucides et par une cartographie (mapping) de l'ensemble de la section d'otolithe. Cette cartographie permettra à la fois l'observation de différences intra- et inter-macrostructures mais aussi une distinction distal / proximal sur l'otolithe. Ainsi la variabilité spatiale de l'otolithe pourra être confrontée avec celle existant dans l'endolymphe : des concentrations distinctes en précurseurs de la calcification, qu'on pense être à l'origine des axes de croissance de l'otolithe, ayant été mis en évidence entre les zones proximale et distale de l'endolymphe. Des premiers résultats ont déjà été obtenus avec la caractérisation de la zone du sulcus présentant des réponses organiques nettement plus élevées que les structures présentes sur un axe dorso-ventral (Chapitre 4). Cette caractérisation conjointe permettrait ainsi une confrontation aux composés présents dans l'endolymphe et la caractérisation de leurs processus d'intégration dans l'otolithe. Une exploitation conjointe des techniques d'immuno-marquage, permettant la localisation des protéines spécifiques sur des sections d'otolithe, semble être pertinente dans ce contexte.

La modélisation de l'otolithe, un outil pour la compréhension du processus de biominéralisation ?

Les mécanismes associés à la régulation et au contrôle de la croissance de l'otolithe et des variations d'opacité par les paramètres environnementaux et métaboliques restent mal compris. Des facteurs associés à la saisonnalité tels que la température, le régime alimentaire, la photopériode ont été corrélés aux changements d'opacité (Beckman and Wilson 1995) de même que des facteurs métabolique tels que la croissance somatique, l'âge, la reproduction (Mina 1968; Hoff and Fuiman 1993; Beckman and Wilson 1995; Hüssy *et al.* 2004; Høie and Folkvord 2006). Mais les interactions entre ces facteurs ainsi que les effets sur les caractéristiques physico-chimiques des structures sont peu documentés. A notre connaissance seuls Hüssy *et al.* (Hüssy *et al.* 2004) ont développé un modèle permettant d'associer l'opacité aux variations de température, de composition en fraction soluble et de la croissance du poisson (à travers le poids). Un tel modèle pourrait constituer un outil permettant l'analyse de la formation de l'otolithe suivant ces différents paramètres.

Dans notre étude, à partir du modèle biologique choisi, l'expérimentation en milieu contrôlé a permis à la fois la caractérisation de la croissance de l'otolithe mais aussi de l'opacité dans des conditions métaboliques variables liées à la prise alimentaire (*ad libitum* ou réduite), ou l'état de maturation (poisson immature ou présentant des gonades en développement) et pour une gamme de température donnée sur deux classes de tailles considérées (Chapitre 4). Ainsi une relation forte entre les croissances somatique et de l'otolithe a pu être établie, qui est applicable aux différentes situations rencontrées et en particulier aux périodes de faible croissance. De même l'opacité a pu être définie comme une

fonction de deux composantes de la croissance de l'otolithe : la première corrélée à la croissance somatique et la seconde indépendante de la croissance somatique.

Ce modèle demande à être développé sur la base d'autres expérimentations faisant intervenir d'autres facteurs environnementaux et métaboliques tels qu'une plus large gamme de température ou de stades de développement (allant de la larve à l'adulte). Néanmoins, cette relation applicable aux différents scénarios rencontrés au cours de l'expérimentation met en évidence un processus générique impliquant deux contributions pouvant être associées à des flux énergétiques : un flux lié à la croissance et un flux lié à des coûts de maintenance concernant par exemple la synthèse et la dégradation des protéines impliquées dans le contrôle de la formation de l'otolithe.

D'autre part, ce modèle peut à partir de l'opacité observée sur l'otolithe et de la croissance de l'otolithe permettre une estimation de la croissance somatique. Ainsi il fournirait un outil d'estimation de la croissance complétant les modèles de rétro-calculs actuels (Morita and Matsuishi 2001; Finstad 2003) peu adaptés pour prendre en compte les périodes de périodes de faibles croissance. Le bénéfice attendu est celui d'une diminution de l'incertitude sur l'estimation de la croissance somatique (estimée à hauteur de 10-15%) (Campana 2005) et de ses effets sur les études de dynamique des populations et d'écologie halieutique.

En parallèle, l'opacité a pu être définie comme une fonction de différentes signatures Raman de fractions minérales et organiques. Ce modèle a été appliqué pour prédire l'opacité d'otolithes de merlu et de lieu noir. L'utilisation de ces deux modèles biologiques a été motivée par l'intérêt de confronter une espèce pour laquelle l'interprétation et le rythme de dépôt des macrostructures sont controversés (de Pontual *et al.* 2006) avec une espèce pour laquelle le caractère saisonnier des macrostructures a été validé (Andrade and Smith 1988).

Le modèle d'opacité proposé met en évidence un processus de contrôle de l'opacité des macrostructures par leurs caractéristiques physico-chimiques. Cependant, l'utilisation de deux résolutions différentes pour les analyses a mis en évidence une composition plus complexe des structures de l'otolithe de merlu. Ainsi, une caractérisation plus approfondie de ces structures pourraient déboucher sur une typologie des macrostructures (saisonnières *vs*. secondaires), les signatures Raman se comportant alors comme de nouveaux marqueurs de l'otolithe.

Comment la caractérisation des structures en fonction des facteurs métabolique et environnementaux permet-elle de calibrer l'otolithe?

L'exploitation des modèles précédemment présentés, basés sur les caractéristiques physico-chimiques des structures et leurs relations avec des facteurs environnementaux et métaboliques, nécessite la validation de ces marqueurs et leur calibration. Cette étude nécessite des expérimentations en milieu contrôlé permettant de manipuler les principaux facteurs et leurs interactions.

Dans notre étude, une expérimentation a permis d'analyser les effets de la croissance, du métabolisme et de la température sur l'opacité observée (Chapitre 2). Cette analyse a mis en évidence de nombreuses causes de formation des zones translucides (faible croissance, développement des gonades, hausse de température) et a conduit à les hiérarchiser. Ainsi la température, dans la gamme de variations choisie dans cette expérience, a montré des effets sur l'opacité mineurs vis-à-vis de la croissance et du métabolisme. La micro-spectrométrie Raman n'a pu être appliquée sur les échantillons issus de cette expérimentation du fait de la présence du marquage à l'oxytétracycline. En effet le protocole défini pour l'analyse des otolithes et en particulier la longueur d'onde utilisée induit une réponse par luminescence de

la tétracycline masquant un grand nombre de signatures organiques. Ces résultats sont donc une première étape sur l'analyse des interactions entre facteurs métaboliques et environnementaux qui devra complétée en milieu contrôlé et confrontée à des échantillons du milieu naturel.

Calibration des facteurs environnementaux et métaboliques

L'approche considérée (choix du modèle biologique et gamme de variations de la température) dans cette étude a montré ses limites de par le manque de connaissances à la fois sur les conditions d'élevages du merlu et sur sa biologie. De nouvelles expérimentations en milieu contrôlé pourraient permettre non seulement d'approfondir les effets des facteurs environnementaux par des études monofactorielles (gamme de température plus large, photopériode) puis multifactorielles permettant la caractérisation d'interactions entre des facteurs tels que température et alimentation sur la formation des macrostructures. Un élargissement de l'étude aux différents stades de vie du poisson (larves à l'adulte) permettrait d'une part de prendre en compte l'effet des facteurs environnementaux fonction de l'âge (e.g. déplacement des preferendum thermiques observé pour la morue) et d'autre part de distinguer les effets du métabolisme tels que les effets de métamorphose, maturation et de reproduction.

Les résultats des expérimentations en milieu contrôlé doivent être couplés à ceux d'expérimentation en milieu naturel et notamment ceux de campagnes de marquages-recaptures. De telles campagnes ont été effectuées sur le merlu à la fois dans le golfe de Gascogne entre 2002 et 2007 ainsi qu'en Méditerranée entre 2004 et 2006. Ces échantillons marqués issus de deux populations différentes constituent une base pouvant être utilisée pour évaluer l'impact des facteurs environnementaux et endogènes (e.g. génétique) sur la formation des structures. L'utilisation de marques électroniques permettant l'enregistrement de

paramètres environnementaux tels que la température et la profondeur doit permettre de compléter les approches multifactorielles en milieu contrôlé. Une telle opération a été tentée sur le merlu sur la base des résultats d'une expérimentation en milieu contrôlé mettant en évidence un effet comparable sur la mortalité vis à vis d'un marquage classique et définissant les conditions d'utilisations (Chapitre 1). Les recaptures obtenues ont permis la caractérisation des migrations verticales effectuées et les gammes de température pouvant être rencontrées par le merlu au cours de ces mouvements (Annexe 2).

Calibration physico-chimique

La caractérisation des compositions physico-chimiques à l'aide de la micro-spectrométrie demandent une modification des protocoles expérimentaux en milieu contrôlé. Plusieurs modifications pourraient être envisagées : l'allongement des temps d'exposition, la modification du protocole de marquage (autres marqueurs fluorescents ou marquages thermiques) ou une modification du protocole d'analyse à la micro-spectrométrie Raman et en particulier de la longueur d'onde du laser monochromatique utilisé. Ces protocoles pourraient être ainsi appliqués sur les structures formées au cours des expérimentations en milieu contrôlé afin d'associer composition physico-chimiques et conditions environnementales et / ou métaboliques.

La micro-spectrométrie Raman permettrait ainsi de dresser une base associant à la fois caractéristiques physico-chimiques et paramètres environnementaux. Cette base pourrait être complétée par l'identification de marqueurs individuels mis en évidence à travers la caractérisation de structures tels que le nucleus ou les marques de stress environnementaux, checks, mais pourrait être étendus aux stress types métaboliques liés par exemple à l'ontogénèse. Cette base constituerait un outil d'analyse robuste de l'otolithe permettant

d'affiner les reconstructions des traits de vie des poissons. Par exemple, lors de l'extraction des signatures chimiques tels que le Sr/Ca qui varierait en fonction de la température, la croissance et la salinité (Eldson and Gillanders 2002; Rooker *et al.* 2003; Bath Martin *et al.* 2004). Une analyse de poissons amphihalins présentant une grande variation du rapport Sr/Ca permettrait une caractérisation de cette signature et en particulier une probable signature de strontianite sur les spectres Raman dans les cas de fortes concentrations en strontium. Du fait de la haute résolution de la micro-spectrométrie Raman, l'analyse de structures saisonnières sur des poissons de grandes profondeurs pourrait aussi être envisageable. Ces poissons de grandes profondeurs sont souvent caractérisés par une longue durée de vie et une faible croissance et les stocks sont donc sensibles à la surexploitation. L'interprétation de leurs otolithes et la validation des rythmes de dépôt des macrostructures est connue pour être particulièrement difficile du fait de l'impossibilité de faire des marquages (profondeur) et de leur faible croissance induisant un grand nombre de marques sur le bord des otolithes. Ainsi serait-il envisageable de pouvoir caractériser ces structures à l'aide d'une analyse à l'échelle du micron par la micro-spectrométrie Raman en vue de l'interprétation de ces otolithes ?

Références bibliographiques

Références Bibliographiques

Adams, N.S., Rondorf, D.W., Evans, S.D., Kelly, J.E., and Perry, R.W. 1998. Effects of surgically and gastrically implanted radio transmitters on swimming performance and predator avoidance of juvenile chinook salmon (*Oncorhynchus tshawytscha*). Can. J. Fish. Aquat. Sci. **55**(4): 781-787.

Admassu, D., and Casselman, J.M. 2000. Otolith age determination for adult tilapia *Oreochromis niloticus* L. from Lake Awassa (Ethiopian Rift Valley) by interpreting biannual and differentiating biannual recruitment. Hydrobiologia **418**: 15-24.

Alemany, F., and Oliver, P. 1995. Growth of female hake in the Balearic Sea: a proposal of new growth model with higher growth rates. Cahiers Options Méditerranéennes **10**: 51-52.

Alheit, J., and Pitcher, T.J. 1995. Hake: biology, fisheries and markets. Chapman and Hall, London.

Ali, M., Nicieza, A.G., and Wootton, R.J. 2003. Compensatory growth in fishes: a response to growth depression. Fish. Fish. **4**(2): 147-190.

Alldredge, A.L., Passow, U., and Logan, B.E. 1993. The abundance and significance of a class of large, transparent organic particles in the ocean. Deep. Sea Res. I **40**(6): 1131-1140.

Allemand, D., Mayer-Gostan, N., de Pontual, H., Boeuf, G., and Payan, P. 2007. Fish otolith calcification in relation to endolymph chemistry. *In* Handbook of Biomineralization. Vol 1: Biological aspects and structure formation. *Edited by* E. Baeuerlein. Wiley - VCH, Weinheim. pp. 291-308.

Alvarez, P., and Cotano, U. 2005. Growth, mortality and hatch-date distributions of European hake larvae, *Merluccius merluccius* (L.), in the Bay of Biscay. Fish. Res. **76**(3): 379-391.

Alvarez, P., Fives, J., Motos, L., and Santos, M. 2004. Distribution and abundance of European hake *Merluccius merluccius* (L.), eggs and larvae in the North East Atlantic waters in 1995 and 1998 in relation to hydrographic conditions. Journal of Plankton Research **26**(7): 811-826.

Alvarez, P., Motos, L., Uriarte, A., and Egana, J. 2001. Spatial and temporal distribution of European hake, Merluccius merluccius (L.) eggs and larvae in relation to hydrographical conditions in the Bay of Biscay. Fish. Res. **50**: 111-128.

Andrade, K.G., and Smith, C.P. 1988. Pollock *Pollachius virens*. *In* Age determination methods for Northwest atlantic species. *Edited by* P. J. and D. L.M. NOAA Techn Report NMFS. pp. 37-40.

Arai, T., Otake, T., and Tsukamoto, K. 1997. Drastic changes in otolith microstructure and microchemistry in the Japanese eel *Anguilla japonica*. Mar. Ecol. Progr. Ser. **161**: 17-22.

Arneri, E., and Morales-Nin, B. 2000. Aspects of the early life history of European hake from the central Adriatic. J. Fish. Biol. **56**(6): 1368-1380.

Asano, M., and Mugiya, Y. 1993. Biochemical and calcium-binding properties of water-soluble proteins isolated from otoliths of the tilapia *Oreochromis niloticus*. Comp. Biochem. Physiol. **104**: 201-205.

Baba, K., Shimizu, M., Mugiya, Y., and Yamada, J. 1991. Otolith matrix proteins of walley pollock: biochemical properties and immunohistochemical localization in the saccular tissue. *In* Mechanisms and phylogeny of mineralization in biological systems. *Edited by* S. Suga and H. Nakahara. Springer Verlag, Tokyo. pp. 57-61.

Bagenal, T.B. 1954. Growth rate of the hake (Merluccius merluccius L.) in the Clyde and other Scottish areas. Journal of the Marine Biological Association of the U.K. **33**: 69-95.

Barber, M.C., and Jenkins, G.P. 2001. Differential effects of food and temperature lead to decoupling of short-term otolith and somatic growth rates in juvenile King George whiting. J. Fish. Biol. **58**(5): 1320-1330.

Barnard, W., and de Waal, D. 2006. Raman investigations of pigmentary molecules in the molluscan biogenic matrix. Journal of Raman Spectroscopy **37**: 342-352.

Bath Martin, G., Thorrold, S.R., and Jones, C.M. 2004. Temperature and salinity effects on strontium incorporation in otoliths of larval spot (*Leiostomus xanthurus*). Can. J. Fish. Aquat. Sci. **61**: 34-42.

Baumann, H., Peck, M.A., and Herrmann, J.P. 2005. Short-term decoupling otolith and somatic growth induced by food level changes in postlarval Baltic sprat, *Sprattus sprattus*. Mar. Freshwat. Res. **56**: 539-547.

Beamish, F.W.H. 1966. Vertical migration of demersal fish in the northwest Atlantic. J. Fish. Res. Bd. Can. **23**: 109-139.

Beckman, D.W., and Wilson, C.A. 1995. Seasonal timing of opaque zone formation in fish otoliths. *In* Recent developments in fish otolith research. *Edited by* D.H. Secor, J.M. Dean and S.E. Campana. University of South Carolina Press, Columbia, SC. pp. 27-44.

Bégout Anras, M.L., Covès, D., Dutto, G., Laffargue, P., and Lagardère, F. 2003. Tagging juvenile seabass and sole with telemetry transmitters: medium-term effects on growth. ICES J. Mar. Sci. **60**(6): 1328-1334.

Belcari, P., Ligas, A., and Viva, C. 2006. Age determination and growth of juveniles of the European hake, *Merluccius merluccius* (L., 1758), in the northern Tyrrhenian Sea (NW Mediterranean). Fish. Res. **78**(2-3): 211-217.

Belloc, G. 1935. Etude monographique du merlu *Merluccius merluccius* L., 3ème partie. Revue des Travaux de l'Office des Pêches Maritimes **8**: 145-202.

Bertignac, M., and de Pontual, H. 2007. Consequences of bias in age estimation on assessment of the northern stock of European hake (*Merluccius merluccius*) and on management advice. ICES J. Mar. Sci. **64**(5): 981-988.

Beverton, R.J.H., and Holt, S.J. 1957. On the dynamics of exploited fish populations, London.

Bez, N., Rivoirard, J., and Poulard, J.-C. 1995. Approche transitive et densité de poissons. Comptes-rendus des journées de Géostatistiques, Fontainebleau, France, pp. 161-177.

Bjelland, R.M., and Skiftesvik, A.B. 2006. Larval development in European hake (*Merluccius merluccius* L.) reared in a semi-intensive culture system. Aquacult. Res. **37**(11): 1117-1129.

Björnsson, B. 1994. Effects of stocking density on growth rate of halibut (*Hippoglossus hippoglossus* L.) reared in large circular tanks for three years. Aquaculture **123**(3-4): 259-270.

Björnsson, B., Steinarsson, A., and Arnason, T. 2007. Growth model for Atlantic cod (*Gadus morhua*): Effects of temperature and body weight on growth rate. Aquaculture **271**(1-4): 216-226.

Björnsson, B., Steinarsson, A., and Oddgeirsson, M. 2001. Optimal temperature for growth and feed conversion of immature cod (*Gadus morhua* L.). ICES J. Mar. Sci. **58**(1): 29-38.

Bodiguel, X., Maury, O., Mellon-Duval, C., Roupsard, F., Le Guellec, A.-M., and Loizeau, V. submitted. A dynamic and mechanistic model of PCB bioaccumulation in the European hake (*Merluccius merluccius*) J. Sea Res.

Borelli, G., Guibbolini, M.E., Mayer-Gostan, N., Priouzeau, F., de Pontual, H., Allemand, D., Puverel, S., Tambutte, E., and Payan, P. 2003a. Daily variations of endolymph composition: relationship with the otolith calcification process in trout. J. Exp. Biol. **206**: 2685-2692.

Borelli, G., Mayer-Gostan, N., de Pontual, H., Boeuf, G., and Payan, P. 2001. Biochemical relationships between endolymph and otolith matrix in the trout (*Oncorhynchus mykiss*) and turbot (*Psetta maxima*). Calcif. Tissue. Int. **69**: 356-364.

Borelli, G., Mayer-Gostan, N., Merle, P.L., De Pontual, H., Boeuf, G., Allemand, D., and Payan, P. 2003b. Composition of Biomineral Organic Matrices with Special Emphasis on Turbot (Psetta maxima) Otolith and Endolymph. Calcif. Tissue. Int. **72**: 717-725.

Bowman, R.E., and Bowman, E.W. 1980. Diurnal variation in the feeding intensity and catchability of the silver hake (*Merluccius bilinearis*). Can. J. Fish. Aquat. Sci. **37**: 1562-1572.

Brander, K.M. 1994. Patterns of distribution, spawning, and growth in North Atlantic cod: the utility of inter-regional comparisons. ICES Mar. Sci. Symp. **198**: 406-413.

Brattey, J., and Cadigan, N. 2004. Estimation of short-term tagging mortality of adult Atlantic cod (*Gadus morhua*). Fish. Res. **66**(2-3): 223-233.

Briget Mary, M., and Ramakrishnan, V. 2005. Infrared and laser Raman spectral studies of bis(DL-aspartic acid) sulfate. Spectrochim Acta A **62**: 164-170.

Buckley, L.J., Smigielski, A.S., Halavik, T.A., Burns, B.R., and Laurence, G.C. 1993. Growth and survival of the larvae of three temperate marine fish species at discrete prey densities. II. Cod (*Gadus morhua*), winter flounder (*Pseudopleuronectes americanus*), and silver hake (*Merluccius bilinearis*). *In* Physiological and Biochemical Aspects of Fish Development. *Edited by* B.T. Walter and H.J. Fyhn. University of Bergen, Bergen. pp. 183-195.

Bustos, C.A., Landaeta, M.F., Bay-Schmith, E., Lewis, R., and Moraga, X. 2007. Effects of temperature and lipid droplet adherence on mortality of hatchery-reared southern hake *Merluccius australis* larvae. Aquaculture **270**: 535-540.

Campana, D.K., and Neilson, J.D. 1985. Microstructures of fish otoliths. Can. J. Fish. Aquat. Sci. **42**(5): 1014-1032.

Campana, S.E. 1983a. Calcium deposition and otolith check formation during periods of stress in coho salmon, *Oncorhynchus kisutch*. Comp. Biochem. Physiol. A. Physiol **75**(2): 215-220.

Campana, S.E. 1983b. Feeding periodicity and the production of daily growth increments in otoliths of steelhead trout (*Salmo gairdneri*) and starry flounder (*Platichthys stellatus*). Can. J. Zool. **61**(7): 1591-1597.

Campana, S.E. 1996. Year-class strength and growth rate in young Atlantic cod *Gadus morhua*. Mar. Ecol. Progr. Ser. **135**(1-3): 21-26.

Campana, S.E. 1999. Chemistry and composition of fish otoliths: pathways, mechanisms and applications. Mar. Ecol. Progr. Ser. **188**: 263-297.

Campana, S.E. 2001. Accuracy, precision and quality control in age determination, including a review of the use and abuse of age validation methods. J. Fish. Biol. **59**(2): 197-242.

Campana, S.E. 2005. Otolith science entering the 21st century. Mar. Freshwat. Res. **56**: 485-495.

Campana, S.E., and Thorrold, S.R. 2001. Otoliths, increments, and elements: keys to a comprehensive understanding of fish populations? Can. J. Fish. Aquat. Sci. **58**(1): 30-38.

Careche, M., Herrero, A.M., Rodriguez-Casado, A., Del Mazo, M.L., and Carmona, P. 1999. Structural changes of hake (*Merluccius merluccius* L.) fillets: effects of freezing and frozen storage. J. Agr. Food. Chem. **47**: 952-959.

Casey, J., and Pereiro, J. 1995. European hake (*M. merluccius*) in the northeast Atlantic. *In* Hake: Biology, Fisheries and Markets. *Edited by* J. Alheit and T.J. Pitcher. Chapman & Hall, London. pp. 125-147.

Castillo, A.G.F., Martinez, J.L., and Garcia-Vasquez, E. 2004. Fine spatial structure of Atlantic hake (*Merluccius merluccius*) stocks revealed by variation at microsatellite loci. Mar Biotechnol **6**: 299-306.

Christiansen, J.S., Svendsen, Y.S., and Jobling, M. 1992. The combined effects of stocking density and sustained exercise on the behaviour, food intake, and growth of juvenile Arctic char (*Salvelinus alpinus* L.). Can. J. Zool. **70**(1): 115-122.

Cimmaruta, R., Bondanelli, P., and Nascetti, G. 2005. Genetic structure and environmental heterogeneity in the European hake (*Merluccius merluccius*). Molecular Ecology **14**: 2577-2591.

Clarke, L.M., and Friedland, K.D. 2004. Influence of growth and temperature on strontium deposition in the otoliths of Atlantic salmon. J. Fish. Biol. **65**: 744-759.

Cohen, D.M., Inada, T., Iwamoto, T., and Scialabba, N. 1990. FAO species catalogue. Vol. 10. Gadiform fishes of the world (Order Gadiformes). An annotated and illustrated catalogue of cods, hakes, grenadiers and other gadiform fishes known to date. FAO, Rome.

Colloca, F., Cardinale, M., Marcello, A., and Ardizzone, G.D. 2003. Tracing the life history of red gurnard (*Aspitrigla cuculus*) using validated otolith annual rings. J. Appl. Ichthyol. **19**(1): 1-9.

Cote, D., Scruton, D.A., Cole, L., and McKinley, R.S. 1999. Swimming performance and growth rates of juvenile Atlantic cod intraperitoneally implanted with dummy acoustic transmitters. N. Am. J. Fish. Manage. **19**(4): 1137-1141.

Courbin, N., Fablet, R., Mellon, C., and de Pontual, H. 2007. Ere hake otolith macrostructures randomly deposited? Insights from an unsupervised statistical and quantitative approach applied to Mediterranean hake otoliths ICES J. Mar. Sci. **64**(6): 1191-1201.

Crozier, W.W., and Kennedy, G.J.A. 2002. Impact of tagging with coded wire tags on marine survival of wild Atlantic salmon (*Salmo salar*, L.) migrating from the R. Bush, Northern Ireland. Fish. Res. **59**(1-2): 209-215.

Dannevig, E.H. 1956. Chemical composition of the zones in cod otoliths. J. Cons. Int. Explor. Mer **21**: 156-159.

Dardignac, J. 1988. Les pêcheries du Golfe de Gascogne - Bilan des connaissances, Paris.

Dauphin, Y., and Dufour, E. 2003. Composition and properties of the soluble organic matrix of the otolith of a marine fish: *Gadus morhua* Linne, 1758 (Teleostei, Gadidae). Comp. Biochem. Physiol. A. Physiol **134A**: 551-561.

Dauphin, Y., and Dufour, E. 2008. Nanostructures of the aragonitic otolith of cod (*Gadus morhua*). Micron **39**: 891-896.

Davie, A., de Quero, C.M., Bromage, N., Treasurer, J., and Migaud, H. 2007. Inhibition of sexual maturation in tank reared haddock (*Melanogrammus aeglefinus*) through the use of constant light photoperiods. Aquaculture **270**(1-4): 379-389.

Davis, J.G., Oberholtzer, J.C., Burns, F.R., and Greene, M.I. 1995. Molecular cloning and characterization of an inner ear-specific structural protein. Science (Wash., D.C.) **267**: 1031-1034.

de Pontual, H., Bertignac, M., Battaglia, A., Bavouzet, G., Moguedet, P., and Groison, A. 2003a. A pilot tagging experiment on European hake (*Merluccius merluccius*): methodology and preliminary results. ICES J. Mar. Sci. **60**(6): 1318-1327.

de Pontual, H., and Geffen, A.J. 2002. Otolith microchemistry. *In* Manual of Fish Sclerochronology. *Edited by* J. Panfili, H. de Pontual, H. Troadec and P.J. Wright. Coedition Ifremer-IRD, Brest, France. pp. 243-303.

de Pontual, H., Groison, A., Pineiro, C., and Bertignac, M. 2006. Evidence of underestimation of European hake growth in the Bay of Biscay, and its relationship with bias in the agreed method of age estimation. ICES J. Mar. Sci. **63**(9): 1674-1681.

de Pontual, H., Lagardère, F., Amara, R., Bohn, M., and Ogor, A. 2003b. Influence of ontogenetic and environmental changes in the otolith microchemistry of juvenile sole (*Solea solea*). J. Sea Res. **50**(2-3): 199-210.

de Pontual, H., Lagardère, F., Troadec, H., Batel, A., Désaunay, Y., and Koutsikopoulos, C. 2000. Otoliths imprinting of sole (*Solea solea*) from the Bay of biscay : a tool to discriminate individuals from nursery origins? Oceanol Acta **23**(4): 497-513.

Degens, E.T., Deuser, W.G., and Haedrich, R.L. 1969. Molecular structure and composition of fish otoliths. Mar. Biol. **2**: 105-113.

Descamps, P., and Labastie, J. 1978. Note sur la lecture et l'interprétation des otolithes du merlu.

Dorel, D. 1986. Poissons de l'Atlantique Nord-Est : relations taille-poids DRV.86.001, Ifremer, Nantes.

Du Buit, M.H. 1996. Diet of hake (Merluccius merluccius) in the Celtic Sea. Fish. Res. **28**: 381-394.

Dunkelberger, D.G., Dean, J.M., and Watabe, N. 1980. The ultrastructure of the otolithic membrane and otolith in the juvenile mummichog, *Fundulus heteroclitus*. J. Morphol. **163**(3): 367-377.

Dussault, C., and Rodrìguez, M.A. 1997. Field trials of marking stream salmonids by dye injection and coded-wire-tagging. N. Am. J. Fish. Manage. **17**(2): 451-456.

Dutil, J.D., Godbout, G., Blier, P.U., and Groman, D. 2006. The effect of energetic condition on growth dynamics and health of Atlantic cod (*Gadus morhua*). J. Appl. Ichthyol. **22**(2): 138-144.

Edeyer, A. 1999. Caractérisation du comportement chimique du complexe otosac-otolithe et réaction à des perturbations induites, Département des Ressources Halieutiques, Ifremer, Université de bretagne Occidentale, Brest.

Edeyer, A., de Pontual, H., Payan, P., Troadec, H., Sévère, A., and Mayer-Gostan, N. 2000. Daily variations of the saccular endolymph and plasma compositions in the turbot *Psetta maxima*: relationship with the diurnal rythm in otolith formation. Mar. Ecol. Progr. Ser. **192**: 287-294.

Eldson, T.S., and Gillanders, B.M. 2002. Interactive effects of temperature and salinity on otolith chemistry : challenges for determining environmental histories of fish. Can. J. Fish. Aquat. Sci. **59**: 1796-1808.

Falini, G., Fermani, S., Vanzo, S., Miletic, M., and Zaffino, G. 2005. Influence on the formation of aragonite or vaterite by otolith macromolecules. European Journal of Inorganic Chemistry **2005**(1): 162-167.

Fay, R.R. 1984. The goldfish ear codes the axis of acoustic particle motion in three dimensions. Science **225**(4665): 951-954.

Finstad, A.G. 2003. Growth back-calculations based on otoliths incorporating an age effect : adding an interaction term. J. Fish. Biol. **62**: 1222-1225.

Folkvord, A., and Otterå, H. 1993. Effects of initial size distribution, day length and feeding frequency on growth, survival and cannibalism in juvenile Atlantic cod (*Gadus morhua* L.). Aquaculture **114**: 243-260.

Francis, R.I.C.C. 1990. Back-calculation of fish length: a critical review. J. Fish. Biol. **36**(6): 883-902.

Gallahar, N.K., and Kingsford, M.J. 1996. Factors influencing Sr/Ca ratios in otoliths of *Girella elevata* : an experimental investigation. J. Fish. Biol. **48**: 174-186.

Gauldie, R.W. 1986. Vaterite otoliths from chinook salmon (*Oncorhynchus tshawytscha*). New Zeal J Mar Freshwat Res **20**: 209-217.

Gauldie, R.W. 1999. Ultrastructure of lamellae, mineral and matrix components of fish otolith twinned aragonite crystals implications for estimating age in fish. Tissue Cell **31**(2): 138-153.

Gauldie, R.W., Sharma, S.K., and Volk, E. 1997. Micro-Raman spectral study of vaterite and aragonite otoliths of the Coho Salmon, *Oncorhynchus kisutch*. Comp. Biochem. Physiol. **118A**(3): 753-757.

Gauldie, R.W., and Xhie, J. 1995. atomic-Force Microscopy of the morphology of the matrix and mineral components of the otolith of *Hyperoglyphe antarctica*. J. Morphol. **223**(2): 203-214.

Goni, R. 1983. Growth studies of European hake (Merluccius merluccius L.) from the northwest African shelf.

Goni, R., and Pineiro, C. 1988. Study of the growth pattern of European hake (Merluccius merluccius L.) from the southern stock: ICES Divisions VIIIc and IXa.

Greenstreet, S.P.R., and Morgan, R.I.G. 1989. The effect of ultrasonic tags on the growth rates of Atlantic salmon, *Salmo salar* L., parr of varying size just prior to smolting. J. Fish. Biol. **35**(2): 301-309.

Grima, L., Quillet, E., Boujard, T., Robert-Granié, C., Chatain, B., and Mambrini, M. 2008. Genetic variability in residual feed intake in rainbow trout clones and testing of indirect selection criteria. Genet. Sel. Evol. **40**(6): 607-624.

Guibbolini, M., Borelli, G., Mayer-Gostan, N., Priouzeau, F., De Pontual, H., Allemand, D., and Payan, P. 2006. Characterization and variations of organic parameters in teleost fish endolymph during day-night cycle, starvation and stress conditions. Comp. Biochem. Physiol. **145A**: 99-107.

Guichet, R. 1995. The diet of the European hake (*Merluccius merluccius*) in the northern part of the Bay of Biscay. ICES J. Mar. Sci. **52**: 21-31.

Guichet, R., Quero, J.C., and Labastie, J. 1973. Estimation de la composition du stock du merlu au nord et à l'ouest de l'Irlande.

Hale, R.S., and Gray, J.H. 1998. Retention and detection of coded wire tags and elastomer tags in trout. N. Am. J. Fish. Manage. **18**(1): 197-201.

Hansen, L.P. 1988. Effects of carlin tagging and fin-clipping on survival of Atlantic salmon (*Salmo salar*, L.) released as smolts. Aquaculture **70**(4): 391-394.

Hansen, L.P., and Johnson, B. 1988. Salmon ranching experiments in River Imsa: effects of dip-netting, transport and chlorobutanol anaesthesia on survival. Aquaculture **74**(3-4): 301-305.

Hansen, T., Karlsen, Ø., Taranger, G.L., Hemre, G.I., Holm, J.C., and Kjesbu, O.S. 2001. Growth, gonadal development and spawning time of Atlantic cod (*Gadus morhua*) reared under different photoperiods. Aquaculture **203**(1-2): 51-67.

Hedegaard, C., Bardeau, J.-F., and Chateigner, D. 2006. Molluscan shell pigments: an *in situ* resonance raman study. J. Mollus. Stud. **72**(2): 157-162.

Hickling, C.F. 1927. The natural history of the hake. Parts I and II. *In* Fishery Investigations of Ministry of Agriculture and Fisheries. Series II. p. 112 pp.

Hickling, C.F. 1933. The natural life history of hake. Part IV. Age determination and growth rate. . *In* Fishery Investigations of Ministry of Agriculture and Fisheries. Series II. p. 120 pp.

Hoff, G.R., and Fuiman, L.A. 1993. Morphometry and composition of red drum otoliths : changes associated with temperature, somatic growth rate, and age. Comp. Biochem. Physiol. A. Physiol **106**(2): 209-219.

Høie, H., Andersson, C., Folkvord, A., and Karlsen, O. 2004. Precision and accuracy of stable isotope signals in otoliths of pen-reared cod (Gadus morhua) when sampled with a high-resolution micromill. Mar. Biol. **2004**: 1039-1049.

Høie, H., and Folkvord, A. 2006. Estimating the timing of growth rings in Atlantic cod otoliths using stable oxygen isotopes. J. Fish. Biol. **68**(3): 826-837.

Høie, H., Folkvord, A., Mosegaard, H., Li, L., Clausen, L.A.W., Norberg, B., and Geffen, A.J. 2008. Restricted fish feeding reduces cod otolith opacity. J. Appl. Ichthyol. **24**(2): 138-143.

Holm, J.C., Refstie, T., and Bo, S. 1990. The effect of fish density and feeding regimes on individual growth rate and mortality in rainbow trout (*Oncorhynchus mykiss*). Aquaculture **89**(3-4): 225-232.

Houde, E.D., and Schekter, R.C. 1981. Growth rates, rations and cohort consumption of marine fish larvae in relation to prey concentrations. 2. ICES Symposium on the Early Life History of Fish, Woods Hole, MA (USA).

Hüssy, K. 2008. Otolith accretion rates: Does size really matter? J. Exp. Mar. Biol. Ecol. **362**(2): 131-136.

Hüssy, K., and Mosegaard, H. 2004. Atlantic cod (*Gadus morhua*) growth and otolith accretion characteristics modelled in a bioenergetics context. Can. J. Fish. Aquat. Sci. **61**(6): 1021-1031.

Hüssy, K., Mosegaard, H., and Jessen, F. 2004. Effect of age and temperature on amino acid composition and the content of different protein types of juvenile Atlantic cod (*Gadus morhua*) otoliths. Can. J. Fish. Aquat. Sci. **61**(6): 1012-1020.

ICES. 1993. Report of the Working Group on the Assessment of Southern Shelf Demersal Stocks.

ICES. 2005. Report of the Working Group on the Assessment of Southern Stocks of Hake, Monk, and Megrim (WGHMM).

ICES. 2006. Report of the Working Group on the Assessment of Hake; Monk and Megrim (WGHMM).

ICES. 2007. Report of the Working Group on the Assessment of Hake, Monk and Megrim (WGHMM).

Iglesia, S., and Dery, L. 1981. Age and growth of hake (Merluccius merluccius L.) from ICES Divisions VIIIc and IXa.

Ikoma, T., Kobayashi, H., Tanaka, J., Walsh, D., and Mann, S. 2003. Physical properties of type I collagen extracted from fish scales of *Pagrus major* and *Oreochromis niloticas*. Int. J. Biol. Macromol. **32**(3-5): 199-204.

Imsland, A.K., Foss, A., Alvseike, T., Folkvord, A., Stefansson, S.O., and Jonassen, T.M. 2007. Interaction between temperature and photoperiod on growth and feeding of Atlantic cod (*Gadus morhua*): possible secondary effects. Can. J. Fish. Aquat. Sci. **64**(2): 239-248.

Imsland, A.K., Foss, A., Folkvord, A., Stefansson, S.O., and Jonassen, T.M. 2005. The interrelation between temperature regimes and fish size in juvenile Atlantic cod (*Gadus morhua*): effects on growth and feed conversion efficiency. Fish Physiol. Biochem. **31**(4): 347-361.

Isaksson, A., and Bergman, P.K. 1978. An evaluation of two tagging methods and survival rates of different age and treatment groups of hatchery-reared Atlantic salmon smolts. J Agric Res Icel **10**(2): 74-99.

Iversen, M., Finstad, B., McKinley, R.S., and Eliassen, R.A. 2003. The efficacy of metomidate, clove oil, Aqui-S registered and Benzoak as anaesthetics in Atlantic salmon (*Salmo salar* L.) smolts, and their potential stress-reducing capacity. Aquaculture **221**(1-4): 549-566.

Iwama, G.K., McGeer, J.C., and Pawluck, M.P. 1989. The effects of five fish anaesthetics on acid-base balance, hematocrit, blood gases, cortisol and adrenaline in rainbow trout. Can. J. Zool. **67**(8): 2065-2073.

Jensen, A.C. 1967. Effects of tagging on the growth of cod. Trans. Am. Fish. Soc. **96**: 37-41.

Jepsen, N., Schreck, C., Clements, S., and Thorstad, E.B. 2005. A brief discussion on the 2% tag/bodymass rule of thumb. *In* Aquatic telemetry: advances and applications. *Edited by* M.T. Spedicato, G. Lembo and G. Marmulla. FAO/COISPA, Rome. pp. 255-261.

Jobling, M. 1988. A review of the physiological and nutritional energetics of cod, *Gadus morhua* L., with particular reference to growth under farmed conditions. Aquaculture **70**(1-2): 1-19.

Jobling, M., Covès, D., Damsgård, B., Kristiansen, H.R., Koskela, J., Petursdottir, T.E., Kadri, S., and Gudmundsson, O. 2001. Techniques for measuring feed intake. *In* Food intake in Fish. *Edited by* D. Houliham, T. Boujard and M. Jobling. Blackwell, Oxford, UK. pp. 49-87.

Johnson, J.B., and Belk, M.C. 2004. Temperate Utha chub form valid otolith annuli in the abscence of fluctuating water temperature. J. Fish. Biol. **65**(1): 293-298.

Jolivet, A., Bardeau, J.-F., Fablet, R., Paulet, Y.-M., and de Pontual, H. 2008. Understanding otolith biomineralization processes: new insights into microscale spatial distribution of organic and mineral fractions from Raman micro-spectrometry. Anal. Bioanal. Chem. **392**: 551-560.

Jolivet, A., de Pontual, H., Garren, F., and Bégout Anras, M.L. in press. Effects of T-bar and DST tagging on survival and growth of European hake. Rev. Fish Biol. Fish.

Jolivet, A., de Pontual, H., Hervy, M., Garren, F., Paulet, Y.-M., and Fablet, R. submitted. Towards domestication of European hake: relationships of growth with dietary and temperature. Aquaculture.

Kacher, M., and Amara, R. 2005. Distribution and growth of 0-group European hake in the Bay of Biscay and Celtic Sea: a spatial and inter-annual analyses. Fish. Res. **71**: 373-378.

Kaczorowska, B., Hacura, A., Kupka, T., Wrzalik, R., Talik, E., Pasterny, G., and Matuszewska, A. 2003. Spectroscopic characterization of natural corals. Anal. Bioanal. Chem. **377**: 1032-1037.

Kalish, J.M. 1991. Determinants of otolith chemistry: seasonal variation in the composition of blood plasma, endolymph and otoliths of bearded rock cod *Pseudophycis barbatus*. Mar. Ecol. Progr. Ser. **74**(2-3): 137-159.

Karlsen, Ø., Norberg, B., Kjesbu, O.S., and Taranger, G.L. 2006. Effects of photoperiod and exercise on growth, liver size, and age at puberty in farmed Atlantic cod (*Gadus morhua* L.). ICES J. Mar. Sci. **63**: 355-364.

Lambert, Y., and Dutil, J.D. 2001. Food intake and growth of adult Atlantic cod (*Gadus morhua* L.) reared under different conditions of stocking density, feeding frequency and size-grading. Aquaculture **192**(2-4): 233-247.

Lin, C.-C., and Liu, L.-G. 1997. Post-Aragonite phase transitions in strontianite and cerussite - a high pressure Raman spectroscopic study. J Phys Chem Solids **58**(6): 977-987.

Lucio, P., Murua, H., and Santurtun, M. 2000. growth and reproduction of hake (*Merluccius merluccius*) in the Bay of Biscayduring the period 1996-1997. Ozeanografika **3**: 325-354.

Lundy, C.J., Rico, C., and Hewitt, G.M. 2000. Temporal and spatial genetic variation in spawning grounds of European hake (*Merluccius merluccius*) in the Bay of Biscay. Molecular Ecology **9**: 2067-2079.

Mahe, K., Amara, R., Bryckaert, T., Kacher, M., and Brylinski, J.M. 2007. Ontogenetic and spatial variation in the diet of hake (*Merluccius merluccius*) in the Bay of Biscay and the Celtic Sea. ICES J. Mar. Sci. **64**(6): 1210-1219.

Martin, I. 1991. A preliminary analysis of some biological aspects of hake (*Merluccius merluccius*) in the Bay of Biscay.

Marty, G.D., and Summerfelt, R.C. 1986. Pathways and mechanisms for expulsion of surgically implanted dummy transmitters from channel catfish. Trans. Am. Fish. Soc. **115**(4): 577-589.

Marxen, J.C., Hammer, M., Gehrke, T., and Becker, W. 1998. Carbohydrates of the organic shell matrix and the shell-forming tissue of the snail *Biomphalaria glabrata* (Say). Biol. Bull. **194**(2): 231-240.

Mayer-Gostan, N., Kossmann, H., Watrin, A., Payan, P., and Boeuf, G. 1997. Distribution of ionocytes in the saccular epithelium of the inner ear of two teleosts (*Oncorhynchus mykiss* and *Scophthalmus maximus*). Cell. Tissue Res. **289**: 53-61.

McCreadie, B.R., Morris, M.D., Chen, T.-C., Rao, D.S., Finney, W.F., Widjaja, E., and Goldstein, S.A. 2006. Bone tissue compositional differences in women with and without osteoporotic fracture. Bone **39**(6): 1190-1195.

Melancon, S., Fryer, B.J., Ludsin, S.A., Gagnon, J.E., and Yang, Z.P. 2005. Effects of crystal structure on the uptake of metals by lake trout (*Salvelinus namaycush*) otoliths. Can. J. Fish. Aquat. Sci. **62**(11): 2609-2619.

Mellon, C., de Pontual, H., Metral, L., and Quémener, L. submitted. Growth of European hake (*Merluccius merluccius* L.) in the Gulf of Lions based on conventional tagging. ICES J. Mar. Sci.

Millner, R.S., Whiting, C.L., and Howlett, G.J. 1993. Estimation of discard mortality of plaice from small otter trawlers using tagging and cage survival studies, ICES, Copenhagen (Denmark).

Mina, M.V. 1968. A note on a problem in the visual qualitative evaluation of otolith zones. J. Cons. Int. Explor. Mer **32**: 93-97.

Moffett, I.J.J., Crozier, W.W., and Kennedy, G.J.A. 1997. A comparison of five external marks for Atlantic salmon, *Salmo salar* L. Fish. Manage. Ecol. **4**(1): 49-53.

Morales-Nin, B. 1986a. Chemical composition of the otoliths of the sea bass (*Dicentrarchus labrax* Linnaeus, 1758) (Pisces, Serranidae). Cybium **10**: 115-120.

Morales-Nin, B. 1986b. Structure and composition of otoliths of Cape hake *Merluccius capensis*. South African Journal of Marine Science **4**: 3-10.

Morales-Nin, B. 1987. Ultrastructure of the organic and inorganic constituents of the otoliths of the sea bass. *In* The Age and Growth of Fish. *Edited by* R.C. Summerfeld and G.E. Hall. The Iowa State University Press, Ames, Iowa. pp. 331-343.

Morales-Nin, B., and Aldebert, Y. 1997. Growth of juvenile Merluccius merluccius in the Gulf of lions (NW Mediterranean) based on otolith microstructure and length-frequency analysis. Fish. Res. **30**: 77-85.

Morales-Nin, B., Bjelland, R.M., and Moksness, E. 2005. Otolith microstructure of a hatchery reared European hake (Merluccius merluccius). Fish. Res. **74**: 300-305.

Morales-Nin, B., and Moranta, J. 2004. Recruitment and post-settlement growth of juvenile Merluccius merluccius on the western Mediterranean shelf. Scientia Marina **68**(3): 399-409.

Morales-Nin, B., Torres, G.J., Lombarte, A., and Recasens, L. 1998. Otolith growth and age estimation in the European hake. J. Fish. Biol. **53**: 1155-1168.

Morita, K., and Matsuishi, T. 2001. A new model of growth back-calculation incorporating age effect based on otoliths. Can. J. Fish. Aquat. Sci. **58**(9): 1805-1811.

Mosegaard, H., Svedang, H., and Taberman, K. 1988. Uncoupling of somatic and otolith growth rates in Arctic charr (*Salvelinus alpinus*) as an effect of differences in temperature response. Can. J. Fish. Aquat. Sci. **45**(9): 1514-1524.

Mosegaard, H., and Titus, R. 1987. Daily growth rates of otoliths in yolk sac fry of two salmonid species at five different temperatures. Proceedings of the V congress of European Ichthyology, Stockholm, Sueden, pp. 221-227.

Mugiya, Y. 1965. Calcification in fish and shell-fish. IV. The differences in nitrogen content between the translucent and opaque zones of otolith in some fish. Bulletin of the Japanese Society of the Scientific Fisheries **31**(11): 896-901.

Mugiya, Y. 1974. Calcium-45 behavior at the level of otolithic organs of rainbow trout. Bulletin of the Japanese Society of the Scientific Fisheries **40**(5): 457-463.

Mugiya, Y. 1984. Diurnal rhythm in otolith formation in the rainbow trout, *Salmo gairdneri*, seasonal reversal of the rhythm in relation to plasma calcium concentration. Comp. Biochem. Physiol. A. Physiol **78**(2): 289-293.

Mugiya, Y. 1987. Phase difference between calcification and organic matrix formation in the diurnal growth of otoliths in the rainbow rout, *Salmo gairdneri*. Fish. Bull. **85**(3): 395-401.

Mugiya, Y., and Takahashi, T. 1985. Chemical properties of the saccular endolymph in the rainbow trout, *Salmo gairdneri*. Bulletin of the Faculty of Fisheries, Hokkaido University **36**(2): 57-63.

Murayama, E., Herbomel, P., Kawakami, Y., Takeda, H., and Nagasawa, H. 2005. Otolith matrix proteins OMP-1 and Otolin-1 are necessary for normal growth and their correct anchoring onto the sensory maculae. Mech Dev **122**(6): 791-803.

Murayama, E., Okuno, A., Ohira, T., Takagi, Y., and Nagasawa, H. 2000. Molecular cloning and expression of an otolith matrix protein cDNA from the rainbow trout, *Oncorhynchus mykiss*. Comp. Biochem. Physiol. **126**(4): 511-520.

Murayama, E., and Takagi, Y. 2004. Immunohistochemical localization of two otolith matrix proteins in the otolith and inner ear of rainbow trout, Oncorhynchus mykiss: comparative

aspects between the adults inner ear and embryonic otocysts. Histochem Cell Biol **121**(2): 155-166.

Murayama, E., Takagi, Y., Ohira, T., Davis, J.G., Greene, M.I., and Nagasawa, H. 2002. Fish otolith contains a unique structural protein, otolin-1. Eur. J. Biochem. **269**(2): 688-696.

Murphy, H. 2002. Status of cod grow-out in Newfoundland. Bull. Aquacult. Assoc. Can. **102**(1): 18-22.

Murua, H., Lucio, P., Santurtun, M., and Motos, L. 2006. Seasonal variation in egg production and batch fecundity of European hake *Merluccius merluccius* (L.) in the Bay of Biscay. J. Fish. Biol. **69**(5): 1304-1316.

Murua, H., and Motos, L. 2006. Reproductive strategy and spawning activity of the European hake *Merluccius merluccius* (L.) in the Bay of Biscay. J. Fish. Biol. **69**(5): 1288-1303.

Neilson, J.D., and Geen, G.H. 1985. Effects of feeding regimes and diel temperature cycles on otolith increment formation in juvenile Chinook salmon, *Oncorhyncus tshawytscha*. Fish. Bull. **83**(1): 91-101.

Nordgarden, U., Oppedal, F., Taranger, G.L., Hemre, G.I., and Hansen, T. 2003. Seasonally changing metabolism in Atlantic salmon (*Salmo salar*, L.) I- Growth and feed conversion ratio. Aquacult. Nutr. **9**(5): 287-293.

Otterlei, E., Folkvord, A., and Nyhammer, G. 2000. Temperature dependent otolith growth of larval and early juvenile Atlantic cod (*Gadus morhua*), Department of Fisheries and Marine Biology, University of Bergen, Bergen, Norway.

Otterlei, E., Folkvord, A., and Nyhammer, G. 2002. Temperature dependent otolith growth of larval and early juvenile Atlantic cod (*Gadus morhua*). ICES J. Mar. Sci. **59**(4): 850-860.

Palomera, I., Olivar, M.P., and Morales-Nin, B. 2005. Larval development and growth of the European hake Merluccius merluccius in the northwestern Mediterranean. Scientia Marina **69**(2): 251-258.

Panfili, J., de Pontual, H., Troadec, H., and Wright, P.J. 2002a. Manual of fish Sclerochronology. Ifremer-IRD Coeditions, Brest, France.

Panfili, J., Meunier, F.J., Mosegaard, H., Troadec, H., Wright, P.J., and Geffen, A.J. 2002b. Glossary. *In* Manual of fish Sclerochronology. *Edited by* C. Ifremer-IRD. Ifremer-IRD Coeditions, Brest, France. pp. 373-384.

Pannela, G. 1971. Fish otoliths : daily growth layers and periodical patterns. Science **173**: 1124-1127.

Pannela, G. 1980. Growth patterns in fish sagittae. *In* Skeletal Growth of Aquatic Organisms : Biological Records of environmental change. *Edited by* D.C. Rhoads and R.A. Lutz. Plenum Press, New York. pp. 519-560.

Pannella, G. 1971. Fish otoliths: daily growth layers and periodical patterns. Science **173**(4002): 1124-1127.

Payan, P., Borelli, G., Priouzeau, F., de Pontual, H., Boeuf, G., and Mayer-Gostan, N. 2002. Otolith growth in trout *Oncorhynchus mykiss*: supply of Ca^{2+} and Sr^{2+} to the saccular endolymph. J. Exp. Biol. **205**(17): 2687-2695.

Payan, P., de Pontual, H., Boeuf, G., and Mayer-Gostan, N. 2004a. Endolymph chemistry and otolith growth in fish. C. R. Palevol. **3**(6-7): 535-547.

Payan, P., De Pontual, H., Edeyer, A., Borelli, G., Boeuf, G., and Mayer-Gostan, N. 2004b. Effects of stress on plasma homeostasis, endolymph chemistry, and check formation during otolith growth in rainbow trout (Oncorhynchus mykiss). Can. J. Fish. Aquat. Sci. **61**(7): 1247-1255.

Payan, P., Edeyer, A., de Pontual, H., Borelli, G., Boeuf, G., and Mayer-Gostan, N. 1999. Chemical composition of saccular endolymph and otolith in fish inner ear: lack of spatial uniformity. The American Journal of Physiology - Regulatory, Integrative and Comparative Biology **277**(1): 123-131.

Payan, P., Kossmann, H., Watrin, A., Mayer-Gostan, N., and Boeuf, G. 1997. Ionic composition of endolymph in teleosts: origin and importance of endolymph alkalinity. J. Exp. Biol. **200**(13): 1905-1912.

Peake, S., McKinley, R.S., Scruton, D.A., and Moccia, R. 1997. Influence of transmitter attachment procedures on swimming performance of wild and hatchery-reared Atlantic salmon smolts. Trans. Am. Fish. Soc. **126**(4): 707-714.

Perrin, C., and Smith, D.C. 2007. Decay of skeletal organic matrices and early diagenesis in coral skeletons. C. R. Palevol. **6**(4): 253-260.

Pierce, R.B., and Tomcko, C.M. 1993. Tag loss and handling mortality for northern pike marked with plastic anchor tags. N. Am. J. Fish. Manage. **13**(3): 613-615.

Pineiro, C., and Pereiro, J. 1993. Study on juvenile growth pattern of European hake (Merluccius merluccius L.) using whole otoliths and length frequency distributions from commercial catches and fish surveys.

Piñeiro, C., Rey, J., de Pontual, H., and Garcìa, A. 2008. Growth of Northwest Iberian juvenile hake estimated by combining sagittal and transversal otolith microstructure analyses. Fish. Res. **93**(1-2): 173-178.

Piñeiro, C., Rey, J., de Pontual, H., and Goni, R. 2007. Tag and recapture of European hake (*Merluccius merluccius* L.) off the Northwest Iberian Peninsula: first results support fast growth hypothesis. Fish. Res. **88**(1-3): 150-154.

Piñeiro, C., and Sainza, M. 2003. Age estimation, growth and maturity of the European hake (*Merluccius merluccius* (Linneaus, 1758)) from Iberian Atlantic waters. ICES J. Mar. Sci. **60**(5): 1086-1102.

Pineiro, C., Sainza, M., Mogado, C., de Pontual, H., Hoey, S., Beattie, S., Lucio, P., Afonso, M.H., Marin, M., Labastie, J., Warnes, S., Easey, M., Dores, S., Maceira, A., Maertens,

B., Hansen, F., Rey, J., Perez, J.L., and Latrouite, A. 2004. Report of the 3rd Workshop on European hake readings. Centro Oceanografico de Vigo, Spain.

Piot, O., Autran, J.-C., and Manfait, M. 2000. Spatial distribution of protein and phenolic constituents in wheat grain as probed by confocal Raman microspectroscopy. J. Cereal. Sci. **32**(1): 57-71.

Pisam, M., Jammet, C., and Laurent, D. 2002. First steps of otolith formation of the zebrafish: role of glycogen? Cell. Tissue Res. **310**(2): 163-168.

Pisam, M., Payan, P., LeMoal, C., Edeyer, A., Boeuf, G., and Mayer-Gostan, N. 1998. Ultrastructural study of the saccular epithelium of the inner ear of two teleosts, *Oncorhynchus mykiss* and *Psetta maxima*. Cell. Tissue Res. **294**(2): 261-270.

Platt, C., and Popper, A.N. 1981. Fine structure and function of the ear. *In* Hearing and Communication in Fishes. *Edited by* W.N. Tavolga, A.N. Popper and R.R. Fay. Springer-Verlag, New York. pp. 1-36.

Poulard, J.C. 2001. Distribution of hake (*Merluccius merluccius*, Linneaus, 1758) in the Bay of Biscay and the Celtic Sea from the analysis of french commercial data. Fish. Res. **50**(1-2): 173-187.

Quémener, L., Suquet, M., Mero, D., and Gaignon, J.-L. 2002. Selection method of new candidates for finfish aquaculture: the case of the French Atlantic, the Channel and the North Sea coasts. Aquat. Living Resour. **15**(5): 293-302.

Quero, J.C., and Vayne, J.J. 1997. Les poissons de mer des pêches françaises. Delachaux et Niestlé, Lausanne-paris.

Righton, D., Kjesbu, O.S., and Metcalfe, J. 2006. A field and experimental evaluation on the effect of data storage tags on the growth of cod. J. Fish. Biol. **68**(2): 385-400.

Robles, R., Periero, J.A., Fernandez, A.M., and Garcia, J.M. 1975. Estudios de cartografia, selectividad y marcado de merluza europea, Merluccius merluccius L., frente al litoral Gallego. Boletin del Instituto Espanol de Oceanografia **190**: 39 pp.

Roldan, M.I., Martin, J.L.G., Utter, F.M., and Pla, C. 1998. Population genetic structure of European hake, *Merluccius merluccius*. Heredity **81**: 327-334.

Romanek, C.S., and Gauldie, R.W. 1996. A predictive model of otolith growth in fish based on the chemistry of the endolymph. Comp. Biochem. Physiol. A. Physiol **114**(1): 71-79.

Rooker, J.R., Kraus, R.T., and Secor, D.H. 2004. Dispersive behaviors of black drum and red drum: Is otolith Sr:Ca a reliable indicator of salinity history? Estuaries **27**(2): 334-341.

Rooker, J.R., Secor, D.H., Zdanowicz, V.S., de Metrio, G., and Orsi Relini, L. 2003. Identification of Atlantic bluefin tuna (Thunnus thynnus) stocks from putative nurseries using otolith chemistry. Fish Oceanogr **12**(2): 75-84.

Rosenlund, G., and Skretting, M. 2006. Worldwide status and perspective on gadoid culture. ICES J. Mar. Sci. **63**(2): 194-197.

Rutecki, T.L., and Meyers, T.R. 1992. Mortality of juvenile sablefish captured by hand-jigging and traps. N. Am. J. Fish. Manage. **12**(4): 836-837.

Saether, B.S., and Jobling, M. 1999. The effects of ration level on feed intake and growth, and compensatory growth after restricted feeding, in turbot *Scophthalmus maximus* L. Aquacult. Res. **30**(9): 647-653.

Sasagawa, T., and Mugiya, Y. 1996. Biochemical properties of water-soluble otolith proteins and the immunohistochemical detection of the proteins in serum and various tissues in the tilapia *Oreochromis niloticus*. Fish Sci **62**(6): 970-976.

Saunders, R.L., and Allen, K.R. 1967. Effects of tagging and of fin-clipping on the survival and growth of Atlantic salmon between smolt and adult stages. J. Fish. Res. Bd. Can. **24**(12): 2595-2611.

Schöne, B.R., Dunca, E., Fiebig, J., and Pfeiffer, M. 2005. Mutvei's solution: An ideal agent for resolving microgrowth structures of biogenic carbonates. Palaeogeogr., Palaeoclimatol., Palaeoecol. **228**(1-2): 149-166.

Secor, D.H., and Dean, J.M. 1989. Somatic growth effects on the otolith - fish size relationship in young pond - reared striped bass, *Morone saxatilis*. Can. J. Fish. Aquat. Sci. **46**: 113-121.

Secor, D.H., Dean, J.M., and Laban, E.H. 1992. Otolith removal and preparation for microstructural examination. *In* Otolith microstructure examination and analysis. *Edited by* D.K. Stevenson and D.K. Campana. Can Spec Publ Fish Aquat Sci. pp. 19-57.

Secor, D.H., Rooker, J.R., Zlokovitz, E., and Zdanowicz, V.S. 2001. Identification of riverine, estuarine and coastal contingents of Hudson River striped bass based upon otolith elemental fingerprints. Mar. Ecol. Progr. Ser. **211**: 245-253.

Seyama, H., Edmonds, J.S., Moran, M.J., Shibata, Y., Soma, M., and Morita, M. 1991. Periodicity in fish otolith Sr, Na, K corresponds with visual banding. Experientia **47**: 1193-1196.

Simon, J., and Dorner, H. 2005. Marking the European eel with oxytetracycline, alizarin red and coded wire tags: an evaluation of methods. J. Fish. Biol. **67**(5): 1486-1491.

Soivio, A., Nyholm, K., and Huhti, M. 1977. Effects of anaesthesia with MS-222, neutralized MS-222 and benzocaine on the blood constituents of rainbow trout, *Salmo gairdneri*. J. Fish. Biol. **10**(1): 91-101.

Solbakken, V.A., Hansen, T., and Stefansson, S.O. 1994. Effects of photoperiod and temperature on growth and parr-smolt transformation in Atlantic salmon (*Salmo salar* L.) and subsequent performance in seawater. Aquaculture **121**(1-3): 13-27.

Söllner, C., Burghammer, M., Busch-Nentwich, E., Berger, J., Schwarz, H., Riekel, C., and Nicolson, T. 2003. Control of crystal size and lattice formation by starmaker in otolith biomineralization. Science **302**(5643): 282-286.

Stasko, A.B., and Pincock, D.G. 1977. Review of underwater biotelemetry, with emphasis on ultrasonic techniques. J. Fish. Res. Bd. Can. **34**(9): 1261-1285.

Stefansson, S.O., Nævdal, G., and Hansen, T. 1989. The influence of three unchanging photoperiods on growth and parr-smolt transformation in Atlantic salmon, *Salmo salar* L. J. Fish. Biol. **35**(2): 237-247.

Svåsand, T., Jørstad, K.E., and Kristiansen, T.S. 1990. Enhancement studies of coastal cod in western Norway. Part I. Recruitment of wild and reared cod to a local spawning stock. ICES J. Mar. Sci. **47**(1): 5-12.

Swan, S.C., Geffen, A.J., Morales-Nin, B., Gordon, J.D.M., Shimmield, T., Sawyer, T., and Massuti, E. 2006. Otolith chemistry: an aid to stock separation of *Helicolenus dactylopterus* (bluemouth) and *Merluccius merluccius* (European hake) in the Northeast Atlantic and Mediterranean. ICES J. Mar. Sci. **63**(3): 504-513.

Takagi, Y., and Takahashi, T. 1999. Characterization of Ootolith soluble matrix producing cells in the saccular epithelium of rainbow trout (Oncorhynchus mykiss) Inner ear. Anat Rec **254**(3): 322-329.

Takagi, Y., Tohse, H., Murayama, E., Ohira, T., and Nagasawa, H. 2005. Diel changes in endolymph aragonite saturation rate and mRNA expression of otolith matrix proteins in the trout otolith organ. Mar. Ecol. Progr. Ser. **294**: 249-256.

Taranger, G.L., Aardal, L., Hansen, T., and Kjesbu, O.S. 2006. Continuous light delays sexual maturation and increases growth of Atlantic cod (*Gadus morhua* L.) in sea cages. ICES J. Mar. Sci. **63**: 365-375.

Thomassen, S., Pedersen, M.I., and Holdensgaard, G. 2000. Tagging the European eel *Anguilla anguilla* (L.) with coded wire tags. Aquaculture **185**(1-2): 57-61.

Thorsteinsson, V. 2002. Tagging methods for stock assessment and research in fisheries.

Thresher, R.E. 1999. Elemental composition of otoliths as a stock delineator in fishes. Fish. Res. **43**: 165-204.

Tohse, H., and Mugiya, Y. 2001. Effects of enzyme and anion transport inhibitors on in vitro incorporation of inorganic carbon and calcium into endolymph and otoliths in salmon *Oncorhynchus masou*. Comp. Biochem. Physiol. A. Physiol **128**(1): 177-184.

Tohse, H., and Mugiya, Y. 2008. Source of otolith carbonate: experimental determination of carbon incorporation rates from water and metabolic CO_2, and their diel variations. Aquatic Biology **1**(3): 259-268.

Tohse, H., Takagi, Y., and Nagasawa, H. 2008. Identification of a novel matrix protein contained in a protein aggregate associated with collagen in fish otoliths. FEBS Journal **275**: 2512-2523.

Tomás, J., and Geffen, A.J. 2003. Morphometry and composition of aragonite and vaterite otoliths of deformed laboratory reared juvenile herring from two populations. J. Fish. Biol. **63**(6): 1383-1401.

Tomás, J., Geffen, A.J., Allen, I.S., and Berges, J. 2004. Analysis of the soluble matrix of vaterite otoliths of juvenile herring (*Clupea harengus*): do crystalline otoliths have less protein? Comp. Biochem. Physiol. A: Mol. Integr. Physiol. **139**(3): 301-308.

Tomás, J., Geffen, A.J., Millner, R.S., Pineiro, C.G., and Tserpes, G. 2006. Elemental composition of otolith growth marks in three geographically separated populations of European hake (*Merluccius merluccius*). Mar. Biol. **148**(6): 1399-1413.

Toole, C.L., Markle, D.F., and Harris, P.M. 1993. Relationships between otolith microstructure, microchemistry, and early lifs history events in Dover sole, *Microstomus pacificus*. Fish. Bull. **91**: 732-753.

Tranquilli, J.A., and Childers, W.F. 1982. Growth and survival of largemouth bass tagged with Floy anchor tags. N. Am. J. Fish. Manage. **2**(2): 184-187.

Tzeng, W.N., Chang, C.W., Wang, C.H., Shiao, J.C., Iizuka, Y., Yang, Y.J., You, C.F., and Ložys, L. 2007. Misidentification of the migratory history of anguillid eels by Sr/Ca ratios of vaterite otoliths. Mar. Ecol. Progr. Ser. **348**: 285-295.

Tzeng, W.N., Iizuka, Y., Shiao, J.C., Yamada, Y., and Oka, H.P. 2003. Identification and growth rates comparison of divergent migratory contingents of Japanese eel (Anguilla japonica). Aquaculture **216**(1-4): 77-86.

Urmos, J., Sharma, S.K., and Mackenzie, F.T. 1991. Characterization of some biogenic carbonates with Raman spectroscopy. Am. Miner. **76**(3-4): 641-646.

Valencia, V., Motos, L., and Urrutia, J. 1989. Estudio de la variacion de la hidrografia y el plancton en la zona neritica frente a San Sebastian. p. 80 pp.

Van der Meeren, T., and Ivannikov, V.P. 2006. Seasonal shift in spawning of Atlantic cod (*Gadus morhua* L.) by photoperiod manipulation: egg quality in relation to temperature and intensive larval rearing. Aquacult. Res. **37**(9): 898-913.

Volk, E.C., Schroder, S.L., and Fresh, K.L. 1990. Inducement of unique otolith banding patterns as a pratical means to mass-mark juvenile Pacific salmon. Am. Fish. Soc. Symp. **7**: 203-215.

Wege, G.J., and Anderson, R.O. 1978. Relative weight (W_r); a new index of condition for largemouth bass. *In* New approaches to the management of small impoundments. *Edited by* G.D. Novinger and J.G. Dillard. American Fisheries Society, North Central Division, Special Publication 5, Bethesda, Maryland. pp. 79-91.

Weidman, C.R., and Millner, R. 2000. High-resolution stable isotope records from North Atlantic cod. Fish. Res. **46**(1-3): 327-342.

Winter, J.D. 1983. Underwater biotelemetry. *In* Fisheries Techniques. *Edited by* L.A. Nielsen and D.L. Johnson. American Fisheries Society, Bethesda, MD. pp. 371-395.

Woillez, M., Poulard, J.-C., Rivoirard, J., Petitgas, P., and Bez, N. 2007. Indices for capturing spatial patterns and their evolution in time, with application to European hake (*Merluccius merluccius*) in the Bay of Biscay. ICES J. Mar. Sci. **64**(3): 537-550.

Wright, P.J. 1991a. Calcium-binding by soluble matrix of the otoliths of Atlantic salmon, *Samo salar* L. J. Fish. Biol. **38**(4): 625-627.

Wright, P.J. 1991b. The influence of metabolic rate on otolith increment width in Atlantic salmon parr, *Salmo salar* L. J. Fish. Biol. **38**(6): 929-933.

Wright, P.J., Fallon-Cousins, P., and Armstrong, J.D. 2001. The relationship between otolith accretion and resting metabolic rate in juvenile Atlantic salmon during a change in temperature. J. Fish. Biol. **59**(3): 657-666.

Wright, P.J., Metcalfe, N.B., and Thorpe, J.E. 1990. Otolith and somatic growth rates in atlantic salmon parr, *Salmo salar L*: evidence against coupling. J. Fish. Biol. **36**(2): 241-249.

Wright, P.J., Panfili, J., Folkvord, A., Mosegaard, H., and Meunier, F.J. 2002a. Validation and verification methods. A. Direct validation. *In* Manuel of fish sclerochronology. *Edited by* J. Panfili, H. de Pontual, H. Troadec and P.J. Wright. Ifremer-IRD Coédition, Brest, France. pp. 114-128.

Wright, P.J., Panfili, J., Morales-Nin, B., and Geffen, A.J. 2002b. Types of calcified structures. A. Otoliths. *In* Manual of Fish Sclerochronology. *Edited by* J. Panfili, H. De Pontual, H. Troadec and P.J. Wright. Ifremer-IRD Coédition, Brest, France. pp. 31-57.

Wurster, C.M., and Patterson, W.P. 2003. Metabolic rate of late Holocene freshwater fish: evidence from δ13C values of otoliths. Paleobiology **29**: 492-505.

Zhang, F., Cai, W., Sun, Z., and Zhang, J. 2008. Regular variations in organic matrix composition of small yellow croaker (*Pseudociaena polyactis*) otoliths: an *in situ* Raman microspectrometry and mapping study. Anal. Bioanal. Chem. **390**(2): 777-782.

Annexes

Annexe 1

Annexe 1

Microscopie AFM et caractérisation physico-chimique des otolithes

Objectif :

- évaluation du potentiel de l'AFM pour la caractérisation à nano- / micro-échelle des microstructures.

Premiers résultats obtenus en octobre 2006 sur des otolithes de merlus

Collaboration LASAA/Paris XI/Univ. Cath. Louvain

Modalités analytiques :

- Sections d'otolithe de merlu polies avec des solutions colloïdales (5/25 nm)
- Analyse AFM en mode tapping
- Analyse des microstructures L et D
- Différentes tailles de scan (500x500nm, 3x3µm, 10x10µm)

Microstructures L et D : Observation d'un microrelief (bande haute : zone L)

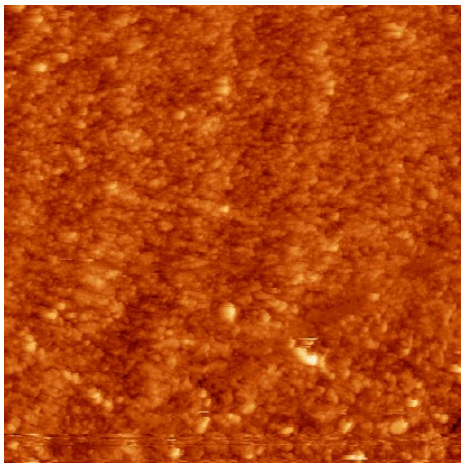

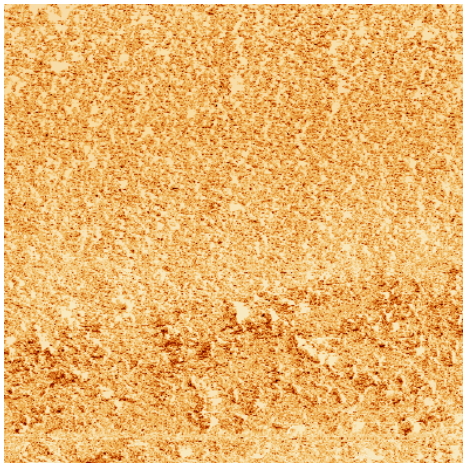

10x10 µm

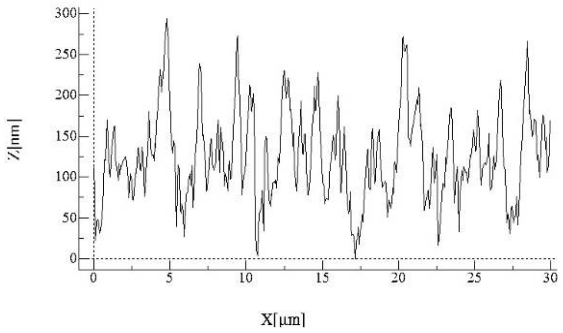

Profil relief

Image de phase

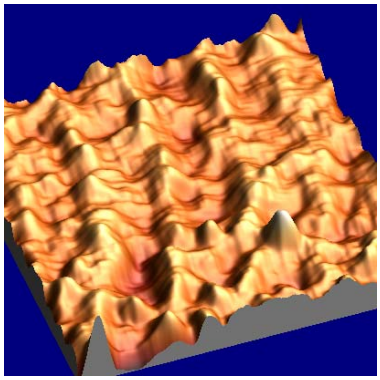

Représentation du relief 3D

Analyse structurelle : Structures morphologiques différentes (taille des cristaux) avec des lamelles pour les zones basses et des grains pour les zones hautes.

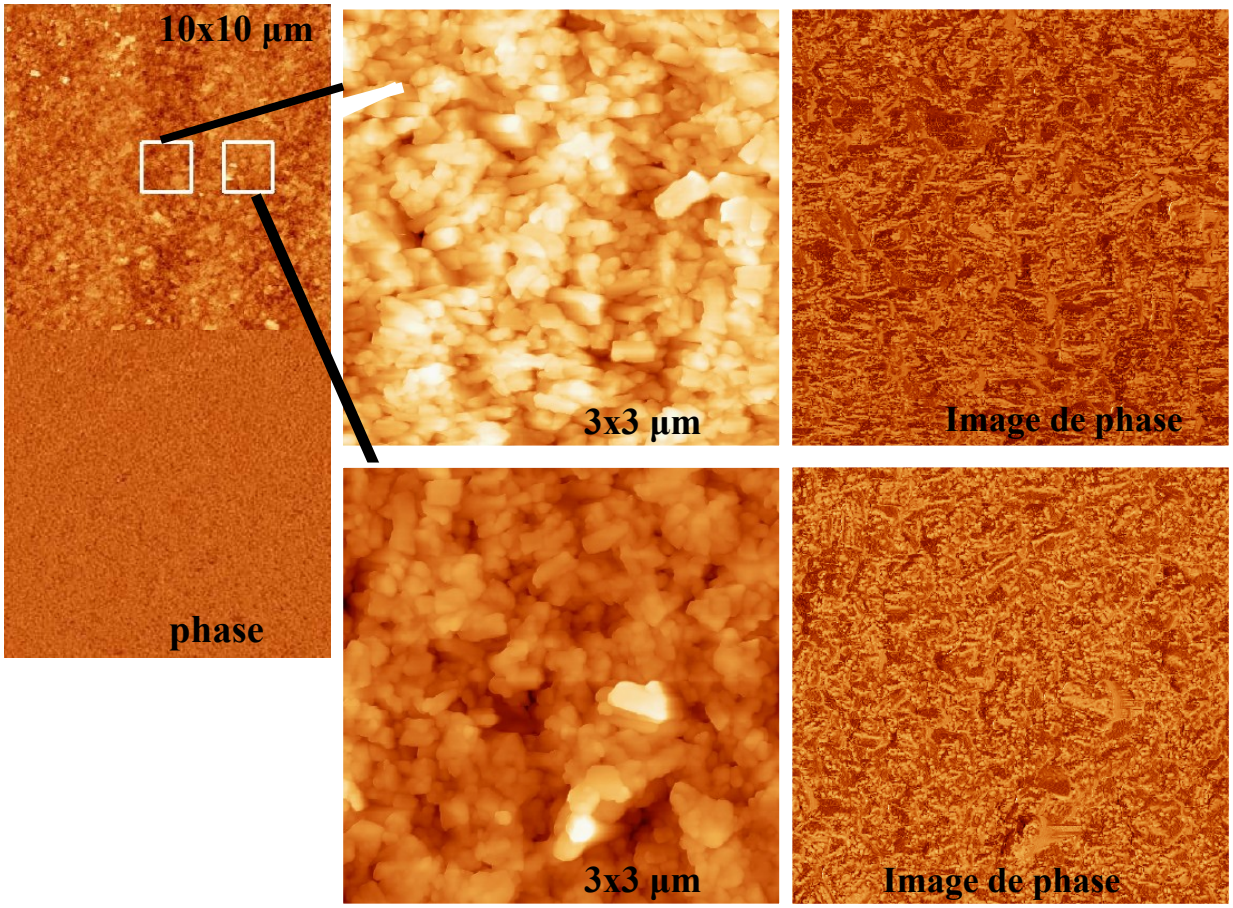

Annexe 2

Annexe 2

First archival tagging on European hake: what have we learnt?

Hélène de Pontual[1], *Aurélie Jolivet*[1], *François Garren*[1],

Michel Bertignac[2] *and Ronan Fablet*[1,3,4]

Introduction

Thanks to an innovative capture methodology, conventional tagging recently opened new avenues for a better knowledge on the biology of European hake (de Pontual *et al.* 2003a). It provided evidence of growth underestimation due to age overestimation (de Pontual *et al.* 2006) and thus challenged the internationally agreed age estimation method. More tagging efforts, both off the Northwest Iberian Peninsula (Pineiro *et al.* 2007) and the Mediterranean Sea (Mellon *et al.* submitted), have since proved that growth underestimation was not a regional (Bay of Biscay) issue: hake does grow much faster than previously thought. Experiments in controlled conditions have also confirmed field observations and revealed a growth potential close to that of cod (Jolivet *et al.* submitted). Despite these advances, the complex otolith macrostructural pattern of the species, responsible for age estimation issues, remains misunderstood. It might well result from specific temperature histories as temperature and food are thought to be the main driving factors of otolith growth and opacity (Hoie *et al.* 2008). Electronic tagging using data storage tags (DSTs) recently appeared as a powerful mean to address such issues. Additionally, providing that suitable geolocation models are

available to reconstruct individual trajectories, DSTs also supply invaluable information on movements and migrations. It has been recognized that the current separation of European hake in two different stocks for assessment and management may not be biologically sound and that the actual population structure is unknown (ICES 2008). This critical issue was a second strong argument in favour of a pilot archival tagging experiment for this species, which results are presented below.

Feasibility

Because of the high cost of DST tagging experiments, we first assessed its feasibility using dummy tags in an experimental work carried out on hake successfully maintained in aquaculture facilities. Hake is not domesticated yet and zootechnical guidelines were totally missing prior to this experiment. Despite this limiting factor, our results indicated that DST tagging should not drastically affect survival and growth compared to conventional tagging (Jolivet *et al.* in press).

Tagging survey and DST records

The pilot experiment was carried out in the northern Bay of Biscay during a conventional tagging survey (26 May - 2 July 2006) on board the 25m trawler RV "Gwen-Drez. Out of the 115 fish (size range 31-40 cm TL) that were released with DSTs surgically implanted in the peritoneal cavity, 4 fish have been recovered to date. Only 3 fish were returned with the DSTs. Time at liberty ranged from 18 to 80 days. The corresponding high resolution environmental records (pressure and temperature data at 30 minutes interval, Figure 1) provide evidence of a general behaviour characterised by two features:

1) Extended periods spent near the seabed during the day, such that some portions of the recorded pressure signals reveal the tidal signal;

2) Vertical movements (VMs) at night probably related to foraging. Such VMs occur within the whole water column, from the seabed up to the surface. All 3 records suggested that fish recovered rapidly from tagging as the VM behaviour was observed as early as the first night at liberty. This suggests that, like Pacific cod (Nichol and Chilton 2006) and Atlantic cod (van der Kooij *et al.* 2007) hake have very efficient swimbladder-repair mechanisms. However, depth profiles did not reveal any post-release equilibration behaviour as depicted on some cod populations by the latter authors. A more thorough analysis of the available records was conducted to address the two main issues:

1) What are the main characteristics of the VM behaviour in terms of rhythm, amplitude, temperature variation and tidal effects?

2) Can we learn something about horizontal movements?

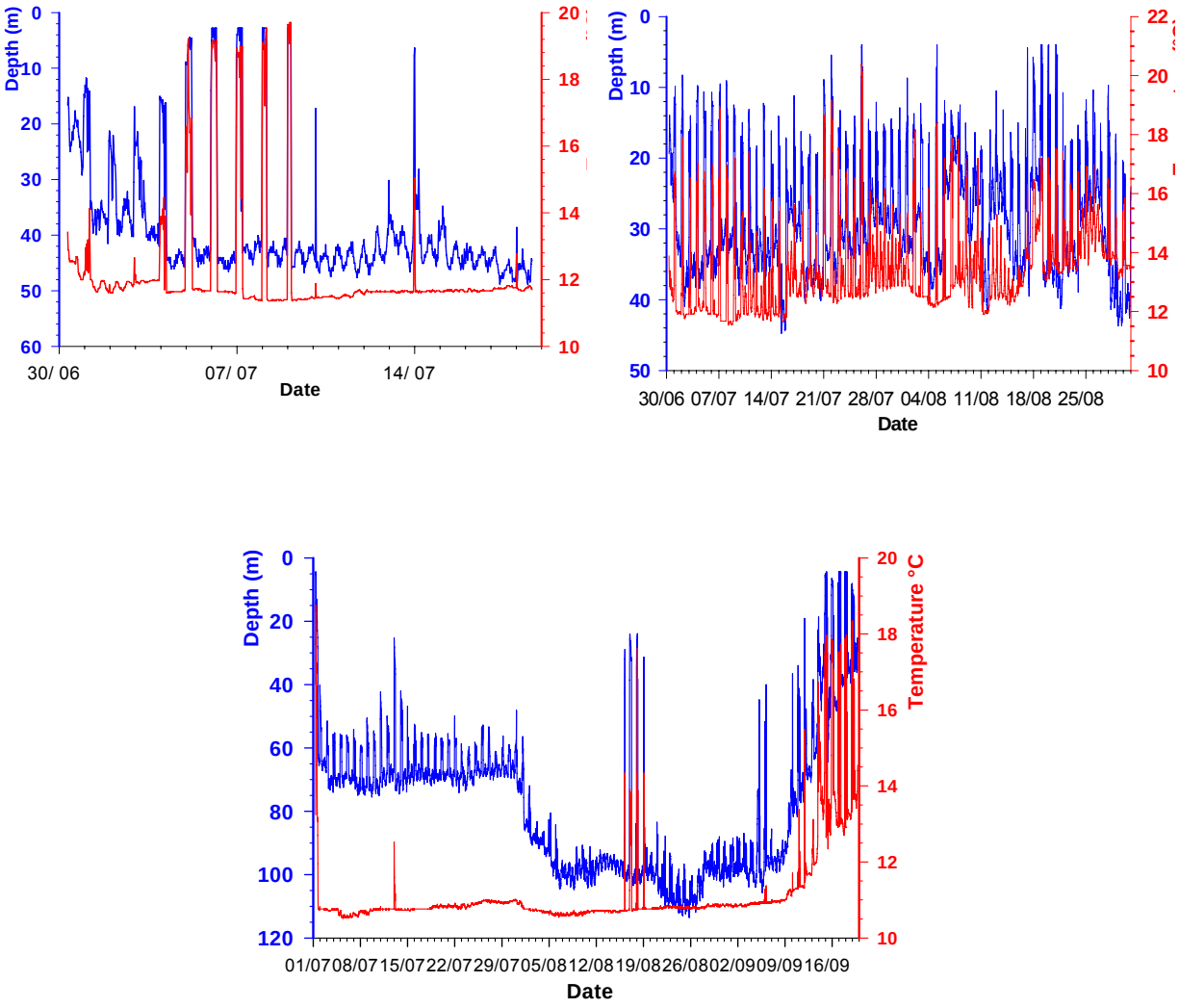

Fig 1. Depth (blue) and temperature(red) histories of the 3 fish recovered with DSTs. From left to right and up to bottom, respective fish characteristics (sex, total length (TL) at capture → recapture, number of days at liberty): ♀, TL 34 → 34 cm, 18 days; ♂, TL 31 → 32.5 cm, 62 days; ♀, TL 34.5 → 35.1 cm, 80 days.

Vertical movement characterisation

In order to quantitatively characterize and analyze VMs, a bathymetric signal processing method was developed to automatically separate the three signal components of the DST depth signal namely seabed, VM and tidal-related components. In the subsequent, the tidal-related component is referred to as the ~tidal signal. The developed method as well as the corresponding result for one of the 3 available records is explained in Figure 2.

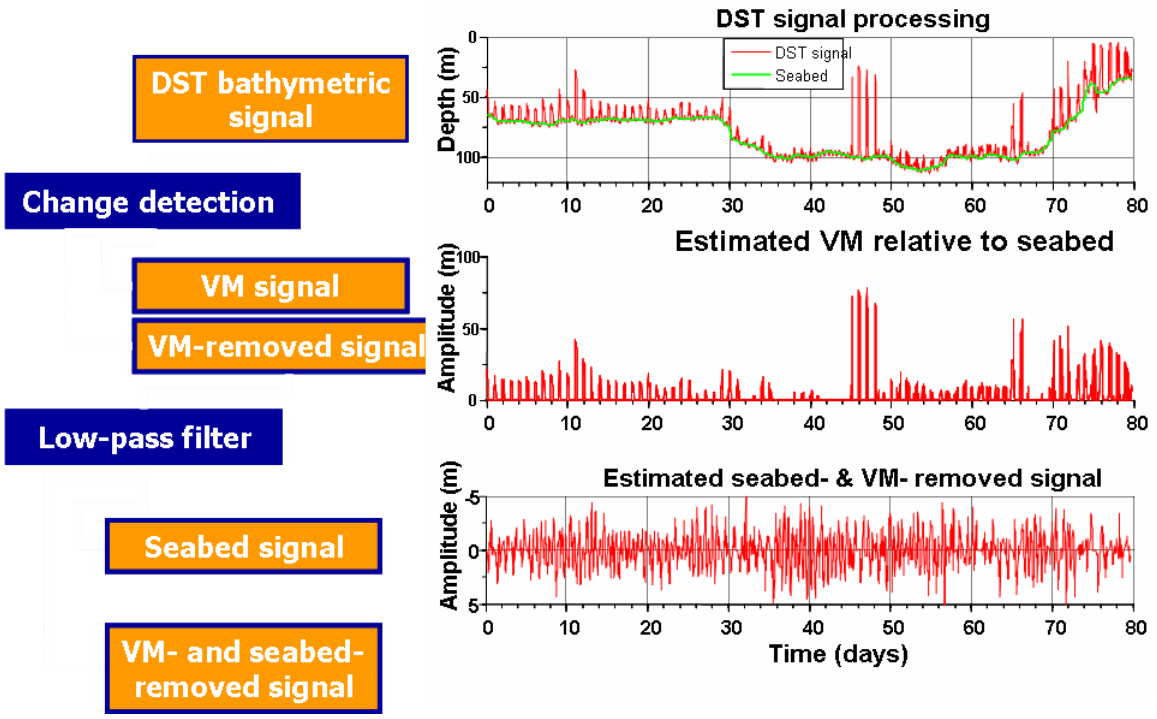

Fig. 2. Automatic extraction of the 3 components of a DST bathymetric signal (in red on the right upper graph). VMs are detected (middle graph) and removed from the original signal. A low pass filter applied on the VM-removed signal extracts the seabed component (green on the right upper graph). The residual signal (VM- and seabed-removed signals) consists in a tidal signal + noise subsequently referred as "~tidal signal"

With a view to analyzing the frequency content of the extracted signals, a time-frequency analysis is applied (Flandrin 1999). Time frequency analyses (Figure 3) performed on the ~tidal component clearly revealed, on the 3 available records, the principal lunar semidiurnal constituent also called M2 tidal constituent (Hicks 2006), which presented greater intensities during spring tide periods. This result constitutes an indirect validation of the method developed to automatically extract the VM component.

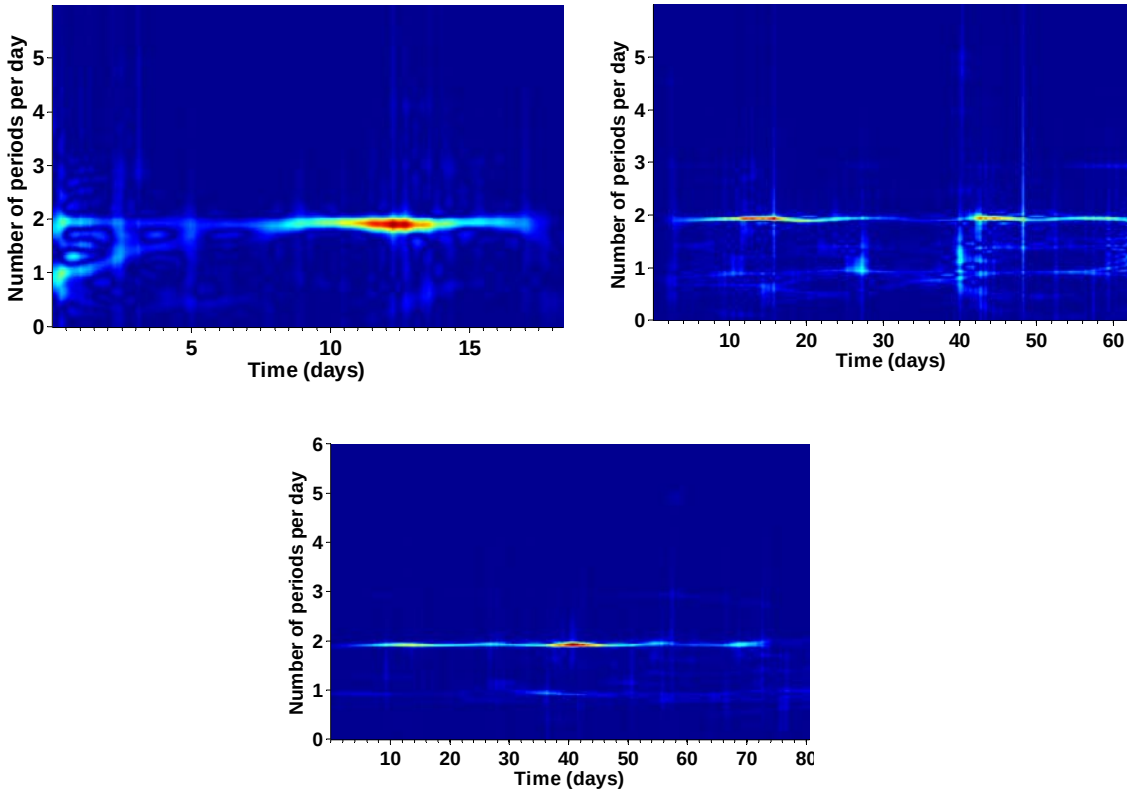

Fig. 3 Results of time frequency analyses performed on the ~tidal component of each available record. Image intensities (min= blue; max = red) are the highest at about 2 periods per day wich actually corresponds to the M2 tidal constituent.

Once the VM component was isolated, the characteristics of the VMs could be statistically analyzed. Results indicate that:

- Nocturnal VMs broadly initiate at sunset times. However, no correlation could be observed between activity and night durations. Interestingly, such rhythms could be observed even at high depth (>100 m);
- Vertical amplitude can be high (observed maximum of 80 m). Daily activity could either consist in a single event (upward movement, stay at a given depth, then downward movement) or successive up and down movements during the same night. In the latter case, cumulative vertical distances greater than 400 m per night could be observed;

- VMs were not constrained by the position of the thermocline. The maximum thermal gradient (SST- seabed temperature) was greater than 7°C. No correlation was found between the duration of the VM and the temperature gradient that fish could experienced. These results provide evidence of the high tolerance of the species to thermal variations which constitutes an unexpected finding;
- Tide amplitude had a direct effect on the amplitude of the VM, normalized VM amplitude being negatively correlated with the tidal coefficient. This behaviour can be thought to be aimed at avoiding strong current layers.

Horizontal movements

The lack of an appropriate geolocation model has not permitted the reconstruction of individual horizontal movements yet. However an interesting finding came out from the joint analyses of 1) capture, release and recapture positions and 2) depth information. All three fish had been caught in the same area (Bay of Vilaine). Two fish were released and recaptured close to the area where they came from. The third one was released SW of Groix but did not stay in this region yet known to be a good habitat for hake as it was actually among our favourite tagging spots. The fish probably moved southward according to depth record depicting a sequence at depth greater than 100 m. It then moved eastward back to its original area. This observation strongly suggests a homing behaviour.

Conclusion and prospects

Although still being an emergent technology, electronic tagging has already provided invaluable information for underpinning fisheries to biology. Migratory behaviour, depth and

thermal preferences etc. have been described for emblematic species such as for instance, Atlantic bluefin tuna (Block *et al.* 2001), cod (Svedang *et al.* 2007) and plaice (Hunter *et al.* 2004). Our results on hake seem equally promising. Although still scarce, data provides new information for the understanding of both the somatic growth of the species and the complex structural otolith patterns. However, firm conclusions would require longer sequences (greater time at liberty) as well as a greater number of fish to account for the variability at the population level. Reported results also suggest that hake may present a homing behaviour. Whether or not this is a general characteristic has to be addressed as well as the issue of seasonal migrations which remains poorly understood. On a more general point of view, the spatio-temporal structure of the population remains virtually unknown although two stocks are managed separately. Joint analyses of traditional and electronic tagging as well as natural tags such as otolith chemical fingerprint and/or genetic markers should provide clues to this critical issue. Such information is decisive for a sustainable exploitation of the resource which status remains fragile despite two different recovery plans implemented by the EU commission in 2004 for the northern stock and in 2006 for the southern stock (ICES 2008).

References

Block, B.A., Dewar, H., Blackwell, S.B., Williams, T.D., Prince, E.D., Farwell, C.J., Boustany, A., Teo, S.L.H., Seitz, A., Walli, A., and Fudge, D. 2001. Migratory movements, depth preferences, and thermal biology of Atlantic bluefin tuna. Science 293(5533): 1310-1314.

de Pontual, H., Bertignac, M., Battaglia, A., Bavouzet, G., Moguedet, P., and Groison, A.L. 2003. A pilot tagging experiment on European hake (Merluccius merluccius): methodology and preliminary results. ICES J. Mar. Sci. 60(6): 1318-1327.

de Pontual, H., Groison, A.L., Pineiro, C., and Bertignac, M. 2006. Evidence of underestimation of European hake growth in the Bay of Biscay, and its relationship with bias in the agreed method of age estimation. ICES J. Mar. Sci. 63(9): 1674-1681.

Flandrin, P. 1999. Time-Frequency/Time-Scale Analysis. Academic Press.

Hicks, S.D. 2006. Understanding tides http://tidesandcurrents.noaa.gov/publications/Understanding_Tides_by_Steacy_finalFINAL11_30.pdf.

Hoie, H., Folkvord, A., Mosegaard, H., Li, L., Clausen, L.A.W., Norberg, B., and Geffen, A.J. 2008. Restricted fish feeding reduces cod otolith opacity. J. Appl. Ichthyol. 24(2): 138-143.

Hunter, E., Metcalfe, J.D., Arnold, G.P., and Reynolds, J.D. 2004. Impacts of migratory behaviour on population structure in North Sea plaice. J. Anim. Ecol. 73(2): 377-385.

ICES. 2008. Report of the Working Group on the Assessment of Southern Shelf Stocks of Hake, Monk and Megrim. ICES Document CM 2008/ACOM:07.

Jolivet, A., de Pontual, H., Fablet, R., Hervy, M., Garren, F., and Paulet, Y.M. submitted. Domestication of European hake: growth and relationships with dietary and temperature. Aquaculture.

Jolivet, A., de Pontual, H., Garren, F., and Begout, M.L. in press. Effects of T-bar and DST tagging on survival and growth of European hake. Reviews in Fish Biology and Fisheries.

Mellon, C., de Pontual, H., Metral, L., and Quemener, L. submitted. Growth of European hake (Merluccius merluccius L.) in the Gulf of Lions based on conventional tagging. ICES Journal of Marine Sciences

Nichol, D.G., and Chilton, E.A. 2006. Recuperation and behaviour of Pacific cod after barotrauma. ICES J. Mar. Sci. 63(1): 83-94.

Pineiro, C., Rey, J., de Pontual, H., and Goni, R. 2007. Tag and recapture of European hake (Merluccius merluccius L.) off the Northwest Iberian Peninsula: First results support fast growth hypothesis. Fish Res. 88(1-3): 150-154.

Svedang, H., Righton, D., and Jonsson, P. 2007. Migratory behaviour of Atlantic cod Gadus morhua: natal homing is the prime stock-separating mechanism. Mar. Ecol.-Prog. Ser. 345: 1-12.

van der Kooij, J., Righton, D., Strand, E., Michalsen, K., Thorsteinsson, V., Svedang, H., Neat, F.C., and Neuenfeldt, S. 2007. Life under pressure: insights from electronic data-storage tags into cod swimbladder function. ICES J. Mar. Sci. 64: 1293-1301.

Malgré un grand nombre d'études relatives à l'utilisation des otolithes, les connaissances sur les mécanismes de formation de l'otolithe et leur modulation par les facteurs environnementaux et physiologiques restent parcellaires. En particulier, la caractérisation des fractions minérale et organique des structures de l'otolithe et l'influence de leurs propriétés qualitatives et quantitatives sur l'opacité restent peu documentées. Pourtant ces informations sont d'importance en vue d'une calibration robuste de l'archive « otolithe ». Le premier axe de recherche s'est concentré sur l'opacité et les effets de la température, la croissance et du métabolisme à partir d'expérimentation en milieu contrôlé. L'opacité a ainsi été définie comme une fonction de deux contributions énergétiques : l'une relative à la croissance somatique et l'autre indépendante de la croissance somatique et associée à des mécanismes de maintenance. Le second axe de recherche s'est focalisé sur l'analyse des propriétés physico-chimiques des structures de l'otolithe. Le développement d'une approche en micro-spectrométrie Raman, non destructive, nous a permis de discriminer de manière quantitative des signatures organique et minérale à une très haute résolution. La caractérisation de micro et macrostructures a permis la construction d'un modèle de prédiction de l'opacité en fonction des signatures de ces deux fractions. Si la relation entre facteurs modulant la biominéralisation et caractéristiques physico-chimiques des structures reste à établir, les résultats obtenus dans cette thèse ouvrent de pistes prometteuses pour une meilleure compréhension des mécanismes de formation de l'otolithe.

Despite numerous applications on the use of otoliths at both population and individual levels, knowledge regarding the mechanisms of the otolith and their variations with environmental and physiological factors has to be improved. In particular, the characterization of mineral and organic fractions of the otolith structures and the influence of their qualitative and quantitative composition on the opacity remain poorly documented. Yet this information is of key interest for the calibration of the archive "otolith" allowing a robust analysis of information. The first issue of this study focused on the analysis of the opacity and the effects of temperature, growth and metabolism through experiments in controlled conditions. Results led to the modelling of opacity as a function of two energetic contributions: one related to somatic growth and the other independent of somatic growth and associated to maintenance mechanisms. The second issue dealt with the physico-chemical characterization of otolith structures. The development of an approach based on micro-spectrometry Raman, non-destructive, has allowed to quantitatively discriminating organic and mineral signatures at very high resolution. It has led to the characterization of microstructures (L and D zones) and macrostructures (translucent and opaque zones) led to the development of a predictive model of opacity from the signatures of these two fractions. The relationship between the environmental and metabolic factors and the chemical composition of structural features has still to be established but our results promising perspectives for a better understanding of the mechanisms of otolith biomineralisation.